MEASUREMENT-BASED STUDIES ON GREENHOUSE GASES IN NATURE AND IN THE INDUSTRIAL SECTOR IN CANADA

By © Judith Vogt

A thesis submitted to the School of Graduate Studies in partial fulfillment of the requirements for the degree of

Doctor of Philosophy

Environmental Sciences

Memorial University of Newfoundland

June 2023

St. John's, Newfoundland and Labrador

Abstract

Persistent emissions of anthropogenic greenhouse gases are causing the Earth to warm at an increasingly fast pace. Nitrous oxide (N_2O) and methane (CH_4) are two well-mixed greenhouse gases with high global warming potential. This thesis investigates both the impacts provoked by human-induced climatic disturbances on natural ecosystems, and anthropogenic emissions from the industrial and agricultural sectors, the root cause of global warming.

Results show that peatland disturbance in eastern Canada did not alter emissions of N_2O despite distinct features of the studied sites located in Newfoundland, Canada. Even though a combination of land-use change did not increase N_2O emissions, the degradation of peatlands may intensify the emission of other greenhouse gases, especially of carbon compounds.

The Arctic Ocean constitutes a negligible source of CH_4 to the atmosphere but warming temperatures may increase emissions. During a measurement cruise off the coast of north-eastern Canada, low sea-air CH_4 fluxes and super-saturated CH_4 concentrations within the water column originating from persistent seeps were found. The ocean is another ecosystem that naturally exchanges greenhouse gases with the atmosphere.

The investigation of CH_4 emissions from the oil and gas industry in different regions of western Canada revealed several “super-emitters”, and overall significant contributions of suspended and abandoned sites to emissions. Compared to previous studies, oil and gas-related emissions decreased in recent years, possibly in response to federal regulations and the transition towards net-zero emissions.

Lastly, in a regional cross-sectoral study in Canada’s west, CH_4 emissions from livestock and waste significantly contributed to total regional emissions dominated by oil and gas. The

emissions from agriculture were comparable with those from oil and gas production, and results suggested high emissions from a landfill.

This thesis provides insight into greenhouse gas exchange processes in vulnerable natural ecosystems and advances the knowledge about anthropogenic emission patterns from various sectors targeted under the Emissions Reduction Plan in Canada. To limit global warming in the future, continued measurements of greenhouse gases are crucial for adequate emission management and mitigation. The findings of this thesis contribute to a better understanding of recent emissions in nature and the industrial sector.

Acknowledgements

First and foremost, I would like to thank my current supervisor Dr. David Risk for your encouragement and support, your kindness and positive attitude during the completion of my PhD. The whole FluxLab team was very supportive at all times, be it during project planning, fieldwork, data processing or interpretation of results, and I am very thankful for that. Particularly, Dr. Evelise Bourlon and Dr. Martin Lavoie provided guidance and valuable input. I thank Justin Laforest, Mark Argento, Sarah Kennedy, and Gilles Perrine for their assistance during data collection. I would have not made it to the FluxLab without the help of Dr. Evan N. Edinger. You helped me transition smoothly from my former lab to the FluxLab as I changed my supervisor and re-oriented my research foci in difficult times affected by the pandemic. I would like to thank you for your support when I needed it. Despite pandemic-driven limitations, this transition offered me the opportunity to learn about novel and exciting areas of research, measurement methods and scientific challenges in a new environment, the FluxLab. In the course of my supervisory change, the originally intended path of my thesis topic was no longer pursuable, and I was stretched to find my place in new research projects. Therefore, I am thankful that the FluxLab could smoothly provide these opportunities. At the same time, I was able to make new connections that I am very grateful for, for example with Dr. Owen A. Sherwood who offered me the opportunity to participate in an unforgettable expedition to the Arctic which became part of my thesis. Moreover, I am grateful for the contributions from Dr. Kumiko Azetsu-Scott and colleagues, and lively discussions with Dr. Evan N. Edinger. I would also like to thank my initial supervisor, Dr. Jianghua Wu, and former colleagues Dr. Thuong Ba Le and Dr. Yu Gong, for your help and support, as well as Dr. Daniel Altdorff for your contributions and guidance. I particularly appreciate the positivity from my supervisory committee members, Dr.

Penny Morrill, who also took on the co-supervision of my PhD, Dr. Rebecca Fisher, and Dr. Owen A. Sherwood, and would like to thank you for stepping into this role, for your time and support.

This research was financially supported by a Natural Sciences and Engineering Research Council of Canada (NSERC) Discovery Grant, the Canada Foundation for Innovation's John R. Evans Leaders Fund, as well as grants from the Research & Development Corporation of Newfoundland and Labrador and the Humber River Basin Research Initiative of Newfoundland awarded to Dr. Jianghua Wu. Furthermore, funding was provided by a NSERC ship time grant to Dr. Owen Sherwood and others, and a NSERC Discovery Grant awarded to Dr. Owen Sherwood. Funders also included Environment and Climate Change Canada, the Alberta Energy Regulator, Geoverra and Mitacs. Finally, Memorial University of Newfoundland provided funding throughout my PhD.

Table of Contents

List of Figures

List of Tables

Chapter 1: Introduction

The increasing abundance of greenhouse gases in the atmosphere has caused the Earth to warm by 1−2°C since the pre-industrial era (IPCC, 2021). Aside from carbon dioxide (CO_2), methane (CH_4) and nitrous oxide (N_2O) are potent greenhouse gases driving climate change. Global averages of greenhouse gas mixing ratios in the atmosphere amounted to 412 ppmv CO_2, 1879 ppbv CH_4 and 333 ppbv N_2O in 2020 (Dlugokencky and Tans, 2022), which implicate approximately 50%, 150% and 20% increases, respectively, since pre-industrial times. These increases are largely of anthropogenic origin from agriculture, fossil fuel use, and waste, whereas natural wetlands contribute a significant share of natural global CH_4 emissions (Friedlingstein et al., 2022; Saunois et al., 2020; Tian et al., 2020). Although CH_4 and N_2O may reside in the atmosphere for a shorter time than CO_2, their capacity to absorb solar radiation and trap the energy over 20 years in the atmosphere is around 80 and 273 times higher, respectively (Forster et al., 2021). As a result, mitigation of CH_4 and N_2O emissions to the atmosphere prove to be an effective fast-track option of climate action (Nisbet et al., 2021). The 2015 Paris Agreement targeted joint efforts of 196 parties to limit the global average temperature rise to 1.5°C above pre-industrial levels. This global treaty was most recently reaffirmed at the Conference of the Parties 26 (UK Government, 2021), stressing the urgent need to reduce greenhouse gas emissions to stay on track of set temperature goals. Effectively, greenhouse gas emissions would have to reach their peak within this decade and decrease to net-zero by 2050. The principle of net-zero encompasses a sustained reduction of greenhouse gas emissions to close-to-zero, while offsetting the residual net emissions by removal into sinks (Fankhauser et al., 2022). In support of that, the Global Methane Pledge was signed to curb CH_4 emissions by 30% of 2020 levels until 2030

(European Commission, 2021). However, a comparable multi-national commitment with set reduction targets for N_2O emissions does not exist to date.

In recent years, anthropogenic CH_4 emissions contributed between 50−70% to the global CH_4 budget, with main contributions from the energy sector (predominantly from oil and gas), the agricultural and waste sector, while wetlands were responsible for the largest natural CH_4 sources (Jackson et al., 2020; Rosentreter et al., 2021; Saunois et al., 2020). Other natural CH_4 sources with overall small contributions include inland water systems, permafrost thaw and other oceanic sources, for example seafloor gas seeps (Saunois et al., 2020). In regard to the global N_2O budget, natural emissions from soils and oceans (57%) exceeded anthropogenic emissions (43%) between 2006 and 2017, whereas recent increases of anthropogenic N_2O emissions were mostly caused by the enrichment of agricultural soils with nitrogen fertilizers (Tian et al., 2020).

Uncertainties in global greenhouse gas budgets arise where the approaches used to measure, manage, and report greenhouse gases show large discrepancies when cross-validated. For example, bottom-up approaches entail data collection from reports and inventories ("bottom"), complimented with models to derive greenhouse gas sinks and sources on a larger spatial scale ("up"). As such, national greenhouse gas inventories in the industrial sector summarize emissions reported by different entities and resulting emission estimates can thus be prone to reporting errors or model limitations. For top-down approaches, atmospheric greenhouse gas mixing ratios are directly measured ("top") to infer sinks and sources ("down"), for example by atmospheric inversion models. Since the top-down approach is based on direct atmospheric ground- or airborne observations, its accuracy is limited by the availability of measurement data and model complexity. According to the most recent Global Methane Budget, the emission estimate for the exploitation, transportation, and use of fossil fuels in the decade 2008−2017 based on the bottom-

up approach yields 128 Tg CH_4 yr^{-1}, while the top-down approach amounts to 111 Tg CH_4 yr^{-1} of emissions (Saunois et al., 2020). Largest discrepancies between bottom-up and top-down approaches occur for wetlands (149 Tg CH_4 yr^{-1} vs. 181 Tg CH_4 yr^{-1}) and other natural sources (222 Tg CH_4 yr^{-1} vs. 37 Tg CH_4 yr^{-1}) in the CH_4 budget (Saunois et al., 2020), and the quantification of emissions remains a huge challenge to date (Peng et al., 2022). To aid with closing these quantification gaps, a better understanding of emission drivers is needed to advance process-based models. Similarly, more accurate landcover maps of wetlands and other natural sources at fine resolution are necessary to decrease uncertainties in greenhouse gas budgets. In addition, higher accuracy of activity data (for example, oil and gas site activity data) is crucial to improve inventory estimates in the anthropogenic sector. On common ground, a larger abundance of observational data on various temporal and spatial scales are needed to address shortcomings of process understanding and model complexity, to improve both bottom-up and top-down approaches (Saunois et al., 2020; Tian et al., 2020), and to help with net-zero pledges.

In addition to improvements in activity data, better understanding of measurement methods and potential blindspots, is urgently required because inter-method differences can also contribute to discrepancies. Vast opportunities to measure greenhouse gas mixing ratios in the atmosphere and their derivative exchange with adjoining spheres exist, from widely used low-cost static chamber measurements to high-end remote sensing technologies. Measurement techniques are applicable across various scales. Soil chambers can be used to determine instantaneous greenhouse gas fluxes locally (Subke et al., 2021), whereas micrometeorological techniques such as eddy covariance towers deliver continuous flux estimates valid for an approximate landscape footprint (Zaman et al., 2021). Networks of stationary sensors are employed to monitor mixing ratios of atmospheric greenhouse gases over extended periods of time in regions affected by large

emissions, for example from industry (Penza et al., 2017). Mobile laboratories that involve these or similar techniques are commonly used to detect and quantify snapshots of air pollutants from the ground with the possibility to extend spatial coverage to regional scales (Brantley et al., 2014; Jakober et al., 2015; Xia et al., 2020). Emissions that may not be detected on the ground could possibly be captured with airborne techniques using drones on a local scale (Shaw et al., 2021) or aircrafts on a regional scale (Schwietzke et al., 2017). In addition, satellite-based techniques are powerful tools that can localize high emitters from space on a global scale (Jacob et al., 2016). Advantages and disadvantages of these and further techniques are outlined in previous studies (Denmead, 2008; Fox et al., 2019).

Greenhouse gas measurements making use of these and similar methods across various sectors serve the purpose to inform policymakers about necessary emission reduction goals to stay on track to net-zero, and are thus much needed to avoid a temperature rise beyond 1.5°C. Within the scope of this thesis, a set of greenhouse gas measurement-based studies conducted in different parts of Canada across the natural and anthropogenic sectors is presented in manuscript style. Together the thesis chapters illustrate the range of approaches needed to reach net-zero, and the four main studies of this thesis produced urgently needed observational data on greenhouse gas emissions and present a significant contribution to the field of climate mitigation research. Chapters 2, 3 and 4 are published in peer review journals, and Chapter 5 is in preparation for submission to a peer review journal. Whereas the first part of my PhD focused on N_2O fluxes in a boreal peatland affected by land-use change, later chapters focus on CH_4 emissions from natural sources, the oil and gas industry, as well as other anthropogenic sources. In the following, a brief introduction to each subtopic is given, also outlining the context of research within the discipline of environmental science.

1.1 Nitrous oxide fluxes in boreal peatlands

Peatlands are ecosystems covered by a peat layer and are strongly driven by waterlogged conditions. While peatlands only cover about 3% of the Earth's terrestrial area, they act as net carbon sinks storing 415±150 TgC (Hugelius et al., 2020), supply rivers and lakes with freshwater, and provide habitat for flora and fauna adapted to waterlogged conditions. Peatlands can be subdivided into two main types dependent on their water sources. Bog-type peatlands receive water from precipitation and are characterized as acidic and ombrotrophic (nutrient-poor) peatlands dominated by peat moss (*Sphagnum* species) whose recalcitrant litter (Malmer et al., 2003) contributes to low pH and slow decomposition rates. Fens are often populated with brown moss, which draws nutrients directly from the groundwater and surrounding mineral terrain. Fen-type peatlands tend to be more alkaline, and minerotrophic (nutrient-rich), where in the upper peat layer, free oxygen is abundant and living plant material is decomposed aerobically. Conditions become anoxic with depth, which slows down decomposition rates (Ingram, 1978). The main microbial processes that lead to N_2O production are nitrification and denitrification. Atmospheric nitrogen is fixed by soil bacteria and archaea and is further processed to animal and plant-available nitrogen compounds. As these compounds are nitrified aerobically by soil microbes, N_2O can be produced as a by-product. Where nitrogen compounds leach to the anaerobic peat layer, denitrification may occur. How much N_2O ultimately diffuses into the atmosphere depends on nitrification and denitrification rates, which are affected by climate change and human disturbance, for example by drainage and nutrient input via soil fertilization, but also on features of the peatland including, but not limited to vegetation cover, water table level and peat density (Liimatainen et al., 2018; Liu et al., 2019; Maljanen et al., 2003; Minkkinen et al., 2020; Regina et al., 1996). Globally, pristine peatlands feature low emissions of

N_2O (Frolking et al., 2011), but because they are the largest natural terrestrial carbon store, their preservation plays an important role on the road to net-zero. Nonetheless, peatlands are often drained or otherwise destroyed due to increasing demand of land for agriculture, forestry, and peat extraction. Where nutrients are scarce, drainage only has a fractional effect on N_2O emissions, but the impact in nutrient-rich peatlands is usually significant compared to undisturbed peatlands (Minkkinen et al., 2020; Regina et al., 1996). Application of fertilizer on peatland soils affects not only nutrient levels, but also the vegetation composition (Nykänen et al., 2002). These anthropogenic disturbance factors tend to increase N_2O fluxes in boreal peatlands (Frolking et al., 2011), whereas the summed effect of multiple disturbance factors can be complex (McCarter et al., 2021). To shed light on the effect of multiple disturbance factors on N_2O fluxes in a boreal peatland, the study of two contrasting sites in Newfoundland, Canada, was addressed as a first objective of this thesis: an undisturbed bog and a peatland formerly affected by a chain of land-use changes including drainage and fertilization.

Canada holds about 25% of global peatlands covering roughly 1.1 million km² of the country (Hugelius et al., 2021), and thus can take the role of a global player to protect these climate cooling ecosystems in support of net-zero by 2050, since degradation may not only affect N_2O flux patterns, but more severely those of CO_2 and CH_4 (Lai, 2009).

1.2 Methane in the Arctic Ocean

Methane in the ocean may be generated through biogenic, abiogenic, or thermogenic processes, by gas hydrates or permafrost. Biogenic CH_4 production by microbes, or methanogenesis, occurs in oxygen-depleted ocean waters and sediments (Barnes and Goldberg, 1976), within micro-environments linking methanogens with sinking particles (Marty et al., 1997), or in well-aerated

surface waters with high abundance of other substrates suitable for strictly anaerobic methanogens, for example those released by sea ice (Damm et al., 2015, 2008). The less common process of abiogenic CH_4 production occurs through chemical reactions absent of organic matter, under specific geological and thermal conditions (Etiope and Sherwood Lollar, 2013). Methane can also be produced thermogenically at depth where fossil organic matter is degraded by pressure and heat. Due to overpressure, submarine CH_4 reservoirs that have accumulated over long time spans may seep slowly due to incomplete geologic trapping, or burst as a result of geologic change, causing CH_4 release to the water column as hydrothermal vents, mud volcanoes or cold seeps, which can most often be found along continental margins (Suess, 2014). Many processes are unique to the polar oceans due to the presence of permafrost, CH_4 hydrates, sea ice, and substantial concomitant seasonal variations. Methane hydrates are CH_4 molecules trapped within an ice-like structure. They can form under cold or high-pressure conditions and cause CH_4 release to the water column upon dissociation, for example due to warming (Ruppel and Kessler, 2017). CH_4 hydrates often co-occur with submarine permafrost, which also stores large amounts of CH_4 susceptible to degradation with ongoing climate change (Chuvilin et al., 2020; Miner et al., 2022; Streletskaya et al., 2018). As CH_4 is released to the water column through different processes, most of it is aerobically oxidized to CO_2 so that only a fraction reaches the water surface, or none at all if the water is deep enough. Compared to atmospheric levels, dissolved CH_4 concentrations in the surface water in different regions of the Arctic Ocean range from slight under- to super-saturation (Damm et al., 2015; Fenwick et al., 2017; Kitidis et al., 2010; Li et al., 2021; Rees et al., 2022). Sea ice often acts as a buffer of diffusive fluxes into the atmosphere, but with accelerated sea ice retreat under global warming (Fox-Kemper et al., 2021) this effect is dampened (He et al., 2013). Global oceans contribute negligibly (~1−3%) to CH_4 budgets (Saunois et al., 2020). However, the impact of climate change on the Arctic CH_4 cycle creates

concerns due to its potential role in climate change feedback loops. Currently, the Arctic Ocean constitutes a small source of CH_4 to the atmosphere (Manning et al., 2022; Rees et al., 2022), but as global warming proceeds, changes in CH_4 levels over the ocean and within the water column require careful monitoring. Therefore, the second objective of this thesis was to investigate CH_4 levels in and over the Arctic Ocean of eastern Canada to determine potential impacts of cold seeps on the CH_4 cycle, and to obtain a baseline of atmospheric CH_4 levels. The mitigation of greenhouse gas emissions to the atmosphere is necessary, particularly to avoid increased loss of sea ice cover (Sun et al., 2021) to keep maintaining the potent role of the ocean as CO_2 sink (DeGrandpre et al., 2020; Friedlingstein et al., 2022). The needed mitigation can most effectively be achieved by a reduction of anthropogenic CH_4 emissions.

1.3 Mitigation of anthropogenic methane emissions

In support of the Global Methane Pledge, Canada has committed to reduce CH_4 emissions from the oil and gas sector, contributing 40% to national CH_4 emissions, by 75% below 2012 levels by 2030 (Environment and Climate Change Canada, 2022a). Methane emissions prevail in the upstream sector, which refers to the exploration and production of oil and gas, compared to the midstream and downstream sectors, responsible for the transportation, storage, processing, and marketing. Methane in the upstream sector is mostly released intentionally through venting, or unintentionally as fugitive emissions. Regulations of vented and fugitive emissions in Canada are evolving over time to meet the goal of net-zero emissions by 2050, and the government is making large investments (CAD 8 billion) to support new technologies and other mitigation efforts in the oil and gas industry. Apart from oil and gas, initiatives to curb emissions from agricultural sources while increasing productivity are planned (CAD 4 billion) (Environment and Climate Change Canada, 2021a), and regulations could theoretically be introduced in the near future. In

agriculture, CH_4 is mainly released via enteric fermentation in ruminants, through management of animal manure, but also through burning of residues, whereas emissions from rice paddies are a minor concern in Canada (Smith et al., 2021). The third sector of prevalent CH_4 emissions is the waste sector (Scarpelli et al., 2021), where both CO_2 and CH_4 are co-produced in approximately equal amounts as a result of microbial decomposition of organic waste components. Methane, the gas of greater concern, is released to the atmosphere through diffusion, gas migration, and fugitive and vented emissions. With increasing numbers of studies investigating landfill CH_4 emissions, the origin of problematic emission hotspots was investigated. Findings show that active waste cells were hotspots of CH_4 emissions (Maasakkers et al., 2022), as well as leachate collection systems (Fredenslund et al., 2010). While the efficiency of landfill gas collection systems could be improved (Duan et al., 2022), the recovery or combustion of the collected gas decreases landfill CH_4 emissions. Even though CH_4 regulations are currently not in place in the solid waste sector, knowledge and technology for mitigation exist (Nisbet et al., 2020), and the timely implementation of regulations is anticipated (Environment and Climate Change Canada, 2022b). The reduction of CH_4 emissions from one emitting sector, for example, the oil and gas industry in Canada, will result in a substantial relief of national CH_4 emissions, but in the long-term a holistic approach is needed that targets the emission reduction of all main sectors to reach net-zero by 2050. However, this holistic understanding of cross-sector emissions from different regions with high emission potential is often lacking, and there may not be a one-size-fits-all climate solution.

Within the third study, CH_4 emissions from understudied oil and gas producing regions in Saskatchewan, Canada, were investigated to advance the understanding of regional differences of CH_4 emissions within the oil and gas sector. And lastly, a single region was chosen to quantify

CH_4 emissions from oil and gas, agriculture, and the waste sector to rank the sectors with the highest emission reduction potential. This case study in Grande Prairie, Alberta, Canada, tied together measurements in the three main anthropogenic sectors covered in net-zero programs and represented the fourth objective of this thesis.

1.4 Multi-disciplinarity of greenhouse gas measurements

This thesis focuses on greenhouse gas measurements in various sectors to answer a range of research questions that evolve around the quantification of greenhouse gas emissions to the atmosphere. The increasing carbon input to the atmosphere concerns not only the scientific community, but more so humankind due to its many effects on climate, health, and economy. Holistically, greenhouse gas measurements are in high demand in multiple disciplines beyond science, such as the health and policy sectors, as we approach the 1.5°C threshold, but also for businesses and stakeholders. For instance, air pollution is directly associated with increased human mortality (Fang et al., 2013) and thus atmospheric measurements can be used to inform about air quality. Conversely, atmospheric measurements showed short-term decreases of greenhouse gases with the outbreak of the COVID-19 pandemic (Ray et al., 2022), outlining feedback processes between different systems. Furthermore, the reduction of fugitive emissions from the energy sector also benefits industrial operators economically if the gas is captured and re-purposed rather than wasted. On a larger scale, networks of observatories are used to inform both policy and society about current greenhouse gas levels (e.g. Heiskanen et al., 2022). Moreover, the measurement-based concept of the carbon footprint is widely implemented ranging from the individual to large scales and showcases the need to assess life cycle impacts of human action on the environment, particularly as we transition towards a low-carbon future. As portrayed by these examples, greenhouse gas measurements can be viewed from multiple

perspectives, provide a crucially needed service to a broad audience, strengthening the importance of multi-disciplinary research. Likewise, this thesis targets multiple disciplines and provides valuable data from natural environments and anthropogenic sectors.

1.5 Co-authorship statement

The present thesis is written in manuscript style and is based on four main research chapters covering greenhouse gas studies across natural ecosystems and the industrial sector.

Chapter 2. This chapter was published by Science of the Total Environment and follows the journal's submission guidelines:

Vogt, J., Wu, J., Altdorff, D., Le, T. B., Gong, Yu (2020). Nitrous oxide fluxes of a boreal abandoned pasture do not significantly differ from an adjacent natural bog despite distinct environmental conditions. Science of the Total Environment. https://doi.org/10.1016/j.scitotenv.2020.136648

As the first author, I conducted all research pertaining to the objective of this manuscript including the literature review, research methodology, sample collection and analysis (except where stated below) and manuscript writing. My initial supervisor, Dr. Jianghua Wu, was responsible for the initial design and identification of the research topic. Dr. Junwei Luan and Dr. Mei Wang collected gas and water samples during the summers of 2013–2015, Maryam Hajheidari, Asare Gymiah and Dr. Riad Eissa took gas and water samples during the summer of 2016, and Dr. Thuong Ba Le and Dr. Yu Gong assisted with the field work in 2019. Dr. Daniel Altdorff provided ground penetrating radar data together with respective methodological background and analysis of peat depth. I received helpful suggestions for the manuscript preparation by all co-authors.

Chapter 3. This chapter was published and follows the submission guidelines for the journal Biogeosciences:

Vogt, J., Risk, D., Azetsu-Scott, K., Edinger, E. N., Sherwood, O. A. (2023). Sea-air methane flux estimates derived from marine surface observations and instantaneous atmospheric measurements in the northern Labrador Sea and Baffin Bay.

https://doi.org/10.5194/bg-20-1773-2023

As the first author, I conducted all research pertaining to the objective of this manuscript including the literature review, research methodology, sample collection and analysis (except where stated below) and manuscript writing. The design and identification of the research question was supported by my current supervisor, Dr. David Risk, by Katlyn MacKay and Daniel Wesley, and the principal investigator of this project, Dr. Owen Sherwood at Dalhousie University, Halifax, Nova Scotia. Water samples were collected with assistance by various cruise participants, and the samples were analyzed by Dr. Kumiko Azetsu-Scott and Dr. Carrie-Ellen Gabriel at the Bedford Institute for Oceanography in Dartmouth, Nova Scotia. Dr. Evan Edinger provided support during the cruise including helpful discussions about water sampling locations. All co-authors provided valuable feedback during the manuscript preparation, which helped direct the research interpretations and substantially improved the quality of the manuscript.

Chapter 4. This chapter was published by Elementa: Science of the Anthropocene and follows the journal's submission guidelines:

Vogt, J., Laforest, J., Argento, M., Kennedy, S., Bourlon, E., Lavoie, M., Risk, D. (2022). Active and inactive oil and gas sites contribute to methane emissions in western Saskatchewan, Canada. Elementa: Science of the Anthropocene.

https://doi.org/10.1525/elementa.2022.00014

As the first author, I conducted all research pertaining to the objective of this manuscript including the literature review, research methodology, sample collection and analysis (except where stated below) and manuscript writing. My current supervisor, Dr. David Risk, as well as Dr. Martin Lavoie guided the design and identification of research questions. Justin Laforest, Mark Argento and Sarah Kennedy assisted in the field. Dr. Evelise Bourlon took on the data processing and modification of the method used for emission quantification based on stationary measurements. All co-authors provided valuable feedback during the manuscript preparation, which helped direct the research interpretations and substantially improved the quality of the manuscript.

Chapter 5. This chapter is in preparation for journal submission:

Vogt, J., Perrine, G., Bourlon, E., Lavoie, M., Risk D. (in prep): Cross-sector comparison of methane emissions from anthropogenic sources: A case study in Canada.

As the first author, I conducted all research pertaining to the objective of this manuscript including the literature review, research methodology, sample collection and analysis (except where stated below) and manuscript writing. My current supervisor, Dr. David Risk, as well as Dr. Martin Lavoie guided the design and identification of research questions. Gilles Perrine assisted in the field. Dr. Evelise Bourlon supported the data processing. All co-authors provided valuable feedback during the manuscript preparation, which helped direct the research interpretations and substantially improved the quality of the manuscript.

Chapter 2: Nitrous oxide fluxes of a boreal abandoned pasture do not significantly differ from an adjacent natural bog despite distinct environmental conditions

Preamble

This chapter was published in Science of the Total Environment. For this study, I organized, prepared, and conducted field measurements in 2019 and analyzed respective gas and water samples. Furthermore, I processed all collected data (excluding data related to ground penetrating radar), analyzed the data statistically, produced related figures and tables, and wrote the manuscript. This study was conducted under supervision of my initial supervisor, Jianghua Wu. The manuscript was co-authored with Jianghua Wu, Daniel Altdorff, Thuong Ba Le, and Yu Gong. Jianghua Wu was responsible for the initial design and identification of the research topic, and provided funding. Thuong Ba Le and Yu Gong assisted with the field work in 2019. Daniel Altdorff provided ground penetrating radar data together with respective methodological background and analysis of peat depth. All co-authors provided helpful comments for the preparation of the final manuscript.

2.0 Abstract

Land-use conversion of pristine boreal peatlands for agricultural purposes is an ongoing process and projected to become more intensive with rising population growth and increased demands for food production. However, agricultural use of peatlands affects the production and emission of nitrous oxide (N_2O), a very potent greenhouse gas currently gaining more attention in the global assessment of greenhouse gases. While the intensity of N_2O emissions depends on a range of environmental factors, including hydrological parameters, temperature and the availability of nitrogen in soils, key driving processes remain poorly understood. In order to understand the

effects of land-use change on the peatland ecosystem, we quantified N_2O fluxes under different land-use in a comparative study between a natural bog and an adjacent abandoned pasture in Newfoundland, Canada. We conducted in situ gas flux measurements using the static chamber method over five growing seasons. In addition, we measured photosynthetic rates and environmental parameters, namely soil temperature and moisture, water table and concentrations of total nitrogen and dissolved organic carbon in pore waters. According to previous studies, we hypothesized higher N_2O emissions from the abandoned pasture due to drainage compared to the natural bog. However, despite significant differences of environmental parameters and photosynthetic rates, we found no significant difference of N_2O fluxes between the two sites. We argue that N_2O production at the abandoned pasture was inhibited due to exhaustion of plant-available nitrogen as a result of increased gross primary production compared to the natural bog. We conclude that the effect of drainage and fertilization on N_2O fluxes during the growing season was superposed by vegetation composition change effects at the abandoned pasture, leading to similar N_2O fluxes at both sites.

2.1 Introduction

Due to rising demands of agricultural production, around 15% of global peatlands are drained for agricultural purposes and thus contribute to at least 6% of global carbon dioxide emissions (Joosten, 2009) and may yield substantial nitrous oxide (N_2O) losses (Kasimir-Klemedtsson et al., 1997; Kroeze et al., 1999). Although N_2O is 265 times more potent in promoting global warming over a 100-year time horizon than carbon dioxide (Myhre et al., 2013), the impacts of anthropogenic disturbances in peatlands (drainage, fertilization, vegetation composition change) on the greenhouse gas N_2O remain poorly understood. Hence, it is important to quantify the

magnitude of N_2O emissions to the atmosphere as a result of anthropogenic peatland degradation, particularly to mitigate climate change.

Peatlands are commonly affected by anthropogenic land-use change through drainage, nutrient addition via fertilization and vegetation composition change (Bhatti and Tarnocai, 2009; Limpens et al., 2008). These changes cause shifts in N_2O production pathways and potentially increase N_2O fluxes, strongly depending on the nutrient status of the peatland.

Several studies investigating the impact of water table draw-down revealed increased N_2O emissions due to drainage (Dinsmore et al., 2008; Freeman et al., 1992; Nykänen et al., 1995; Tiemeyer et al., 2016), with a strong increase in nutrient-rich soils (fens) and a low or no considerable increase in nutrient-poor bogs (Aerts and Ludwig, 1997; Laine et al., 1996; Maljanen et al., 2010; Martikainen et al., 1993; Regina et al., 1996). In these studies, drainage triggered higher abundance of oxygen in the upper peat layer, enhancing mineralization of plant organic matter and soil microbial activity, further promoting losses of N_2O to the atmosphere (Freeman et al., 1992). N_2O emissions in a mesotrophic transition peatland complex in Germany were also found to be higher in a drained peatland than in a rewetted bog that showed near-zero emissions (Osterloh et al., 2017). Likewise, Salm et al. (2012) showed slightly higher N_2O emissions from drained transitional fens and ombrotrophic bogs than from pristine ecosystems. Apart from that, drainage can affect the soil physical properties resulting in a decline of peat thickness and subsidence (Ewing and Vepraskas, 2006; Maljanen et al., 2012; Wösten et al., 1997). The effect of nitrogen fertilization on N_2O fluxes in peatlands has been extensively studied. Among others, Regina et al. (1998), Van Beek et al. (2011), Cui et al. (2016) and Lozanovska et al. (2016) showed that nitrogen addition promoted N_2O emissions in peatlands due to higher soil nutrient availability, while Lund et al. (2009) and Nykänen et al. (2002) found no

significant increase. In addition, higher nutrient availability as a result of fertilization affects plant growth (Geisseler and Scow, 2014), potentially causing shifts in vegetation composition towards an invasion of vascular plants out-competing *Sphagnum* species (Nordbakken et al., 2003). Similarly, long-term drainage was found to shift the vegetation cover towards a dominance of vascular plants (Jukaine et al., 1995; Kokkonen et al., 2018; Laiho et al., 2003). Vascular plants in particular consume available nutrients for plant growth and thus decrease soil nutrient availability, potentially reducing N_2O production (Aerts et al., 1995; Silvan et al., 2005).

In order to better understand the effects of land-use change on N_2O fluxes in peatlands, it is crucial to determine factors that control N_2O dynamics. Previous studies revealed a broad range of main drivers of N_2O fluxes in peatlands: Water table was identified to correlate with N_2O fluxes (Lohila et al., 2010; Maljanen et al., 2012; Martikainen et al., 1993; Regina et al., 1996; Salm et al., 2012; Tiemeyer et al., 2016; Van Beek et al., 2010) as well as soil temperature (Lohila et al., 2010; Pärn et al., 2018), water content (Pärn et al., 2018), soil nitrate concentration (Maljanen et al., 2012; Pärn et al., 2018) or nitrogen content in the upper peat layer (Tiemeyer et al., 2016), carbon to nitrogen (C/N) ratio (Klemedtsson et al., 2005; Leppelt et al., 2014; Liimatainen et al., 2018; Maljanen et al., 2010), pH (Leppelt et al., 2014; Maljanen et al., 2012) and peat depth (Leppelt et al., 2014).

This study aims to investigate the impact of drainage, former fertilization, vegetation composition change and site abandonment on N_2O fluxes and potential drivers. We hypothesize that (1) N_2O emissions at the abandoned pasture are higher than at the natural bog due to land-use change effects, (2) environmental parameters − soil/water temperature and moisture, water table, concentrations of total nitrogen (TN) and dissolved organic carbon (DOC) in pore waters – as well as gross primary production (GPP) at the abandoned pasture show significant differences

compared to the natural bog and (3) hydrological parameters, in particular water table, drive N_2O fluxes.

2.2 Methods

2.2.1 Study area

The peatland complex is located in Robinsons, western Newfoundland, Canada (48.261°N, 58.664°W). The soil of the studied area can be classified as histosol according to the World Reference Base classification. The climate is maritime temperate with a mean annual air temperature of 5°C and total annual precipitation of 1340 mm for 1981-2010 (measured at the nearest weather station in Stephenville, around 30 km away from the study site).

The study area covers two adjacent sites: A natural bog (natural site) and an abandoned pasture (pasture site). The natural bog covers an area of approximately 36 ha and is characterized by bog mosses (*Sphagnum warnstorfii* Russow and *Sphagnum capillifolium* (Ehrhart) Hedwig). Dominant microlandforms at the natural site are hummocks, hollows and permanently inundated pools. While the hummocks are mainly covered by ericaceous shrubs (*Gaylussacia* spp. and *Rhododendron groenlandicum* (Oeder) Kron & Judd), sedges (*Trichophorum cespitosum* (L.) Schur) are most abundant in hollows (Wang et al., 2018). Besides, gray reindeer lichens (*Cladina* spp.) spread at the site. The natural bog remains unaffected by an important anthropogenic land-use change.

The pasture site used to be an undisturbed bog, but was drained by 50 cm deep and 30 cm wide ditches with an approximate distance of 20-30 m between the drains in the 1970's. The introduction of pasture forage grasses (reed canary grass, *Phalaris arundinacea* L.) happened around 1985. Consecutively, the site was fertilized (no lime added) and used to graze cattle. After

ten years of active pasture and fertilization, the site was abandoned (Figure 1), meaning it was left to regenerate naturally for over two decades without active management or grazing of livestock. Therefore, the pasture site constitutes a representative abandonment site. In the course of time, vegetation partially overgrew the drainage ditches. Nonetheless, sufficient drainage is still provided, resulting in a lower water table level at the pasture site compared to the natural site. The abandoned pasture is dominated by reed canary grass (*Phalaris arundinacea*), several lower herbaceous and graminoid species (*Carex* spp., *Ranunculus acris* L., *Ranunculus repens* L., *Hieracium* sp. L.) and low shrubs, for example sweet gale (*Myrica gale* L.), labrador tea (*Rhododendron groenlandicum*), mountain fly honeysuckle (*Lonicera villosa* (Michx.) Schult., rhodora (*Rhododendron canadense* (L.) Torrey), and chokeberry (*Photinia* sp. Lindley) (Luan and Wu, 2014). The abandoned pasture spreads over an area of approximately 20 ha. As a result of the forage grass introduction, the approximate canopy height during the growing season of the abandoned pasture (estimated average of 1 m) is higher than at the bog (0.2 m). Field measurements from 2013 confirm significantly higher aboveground biomass at the abandoned pasture than at the natural bog (Luan and Wu, 2015). Besides, surface water at the natural bog is more acid (pH ≈ 4) than at the abandoned pasture (pH ≈ 5; measured with an Oakton Eco Testr pH2 in 2019).

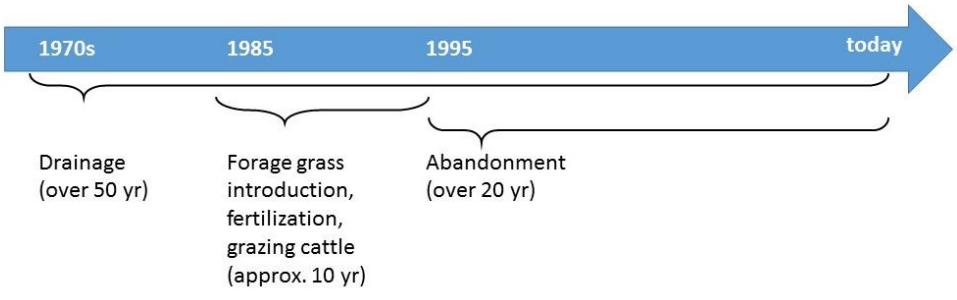

Figure 1: Land-use change history of the abandoned pasture site since the 1970s.

2.2.2 Experimental design

Measurements were obtained from the natural bog and the abandoned pasture during the snow-free period between May and October from 2013 to 2016, and in 2019. While the pasture site represented soils affected by land-use change, the pristine bog was used as a control site. In order to represent microtopography and ecological features of each site, three microlandforms with three replicates each were established (Figure 2). In the natural bog, microlandforms were represented by: hollow (NO), hummock (NU) and pool (NP). The spatial extent of the bog covered by hollows and hummocks amounted to roughly 45% each, while the pools covered the remaining 10% of the bog area. The pasture site was dominated by: lower herbaceous and graminoid species (PG), shrubs (PS) and drainage ditches (PD). Roughly 45% of the pasture site was covered by patches dominated by lower herbaceous and graminoid species, 45% by patches covered by shrubs, while ditches covered around 10% of the abandoned pasture. These spatial weights were used previously at these sites (Wang et al., 2019).

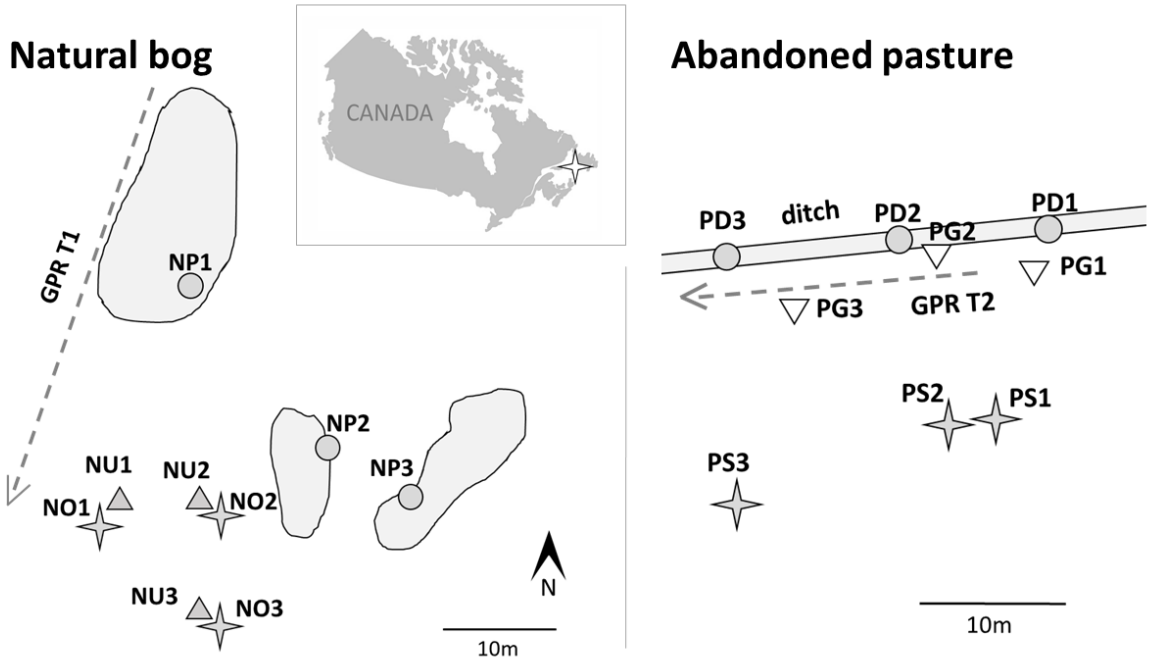

Figure 2: Experimental design at the peatland complex. Three microlandforms per site constitute dominant features of the natural bog and the abandoned pasture: Natural hollow (NO), hummock (NU) and pool (NP); Pasture grass (PG), shrub (PS) and ditch (PD). Each microlandform is represented by three replicates. In addition, transects of ground penetrating radar (GPR) measurements at both sites are indicated.

2.2.3 Chamber flux measurements

Diffusive N_2O and carbon dioxide (CO_2) samples were obtained separately and were taken *in situ* from cylindrical chambers with a height of 50 cm, a diameter of 26 cm, an open bottom and a fitted lid. In 2013, PVC (polyvinyl chloride polymer) collars with a groove were permanently inserted into the peat soil to a depth of 10 cm for all plots. The grooves were sealed with water shortly before each measurement in order to prevent gas leakage. For the static chamber measurements in the pools with permanently standing water, four ABS (Acrylonitrile butadiene styrene) pipes were inserted into the bottom of each pool to keep the chamber in place. At each

plot, measurements were conducted between 10:00 and 16:00 each sampling day. A capillary tube on the chamber lid maintained atmospheric pressure inside the chamber during the measurement.

In order to determine N_2O fluxes, gas samples were taken manually with a 30 ml syringe from an opaque chamber after repeated mixing of the headspace air. For each replicate, gas samples were drawn at minutes 0, 10, 20 and 30 after closing the chamber. The syringes were sealed with three-way stopcocks. The N_2O analysis was carried out injecting 5 ml of the collected sample into a gas chromatograph (Scion 456-GC, Bruker Ltd., Canada) equipped with an electron capture detector operating at 350°C. The change in N_2O (and CO_2) concentration over time ($\frac{dC}{dt}$, in µmol mol^{-1} s^{-1}) in the headspace of the chamber was obtained via linear regression. The gas flux (f, in µmol mol^{-1} s^{-1}) was estimated by the empirical closed chamber method (Holland et al., 1999):

$$f = \frac{dC}{dt} \cdot \frac{p}{R \cdot T} \cdot h, \qquad (1)$$

with standard atmospheric pressure (p = 101325 Pa), the ideal gas constant (R = 8.314 m³ Pa K^{-1} mol^{-1}), standard atmospheric temperature (T = 293.15 K) and the height of the chamber (h = 0.5 m). This approach relies on the ideal gas law. In order to obtain N_2O fluxes in nmol m^{-2} s^{-1}, the fluxes from Equation 1 were multiplied by 10³.

In addition, fluxes of CO_2 were determined from measurements with an Ultraportable Greenhouse Gas Analyzer (Los Gatos Research, USA) in 2013 and 2016. A transparent chamber equipped with a computer fan was used to measure net ecosystem exchange (NEE) and an opaque chamber for ecosystem respiration (R_{eco}). A 4 m long tubing connected the analyzer with the chambers. At each plot, 1 Hz measurements lasted between two and three minutes. Dry CO_2 molar fractions were used to obtain NEE and R_{eco} as shown in Equation 1. GPP as an indicator of

plant growth was derived from GPP = R_{eco} − NEE (Chapin et al., 2006). We assumed CO_2 release to the atmosphere for ecosystem respiration (R_{eco}) during measurements with the opaque chamber and excluded unreasonable, negative measurements (i.e. CO_2 uptake). Likewise, we excluded negative values for GPP. According to weather conditions, the measurements were conducted biweekly or monthly. Due to time restrictions, it was not always possible to take measurements of CO_2 and N_2O fluxes at the same sampling day.

2.2.4 Measurements of environmental parameters

Concurrently with N_2O flux sampling, environmental parameters were determined in the field. The water table was measured as distance from the peat soil surface to the water surface, to indicate the thickness of the aerobic peat layer inhabited by a high abundance of aerobic microorganisms. Water tables (WT) were negative, or zero if water was standing in the plot, for example in ditches (PD) and pools (NP). Soil and water temperatures were measured at 5 cm and 20 cm depth with a soil thermometer (Traceable Digital Thermometer, Fisher Scientific Inc., Canada). However, measurements of soil/water temperatures in 20 cm depth were lacking for the growing season of 2014. Soil moisture at 5 cm depth was measured with a soil moisture sensor (ProCheck, Decagon Devices Inc., USA), but were scarcely conducted depending on the availability of the soil moisture sensor.

TN comprises all forms of organic nitrogen (amino acids, proteins, etc.) as well as inorganic nitrogen (ammonium, dinitrogen, nitrite and nitrate). In 2013, 2016 and 2019, TN and DOC concentrations were obtained from soil pore water samples at the same time as the N_2O flux measurements were taken at each plot. Samples from approximately 10 cm depth were collected with a MacroRhizons (Rhizosphere Inc., Netherlands). Pore water samples from 40 cm depth were drawn with 60 ml syringes from a perforated 50 cm long PVC tube sealed at the bottom,

previously inserted into the soil. The top opening of the tubes was covered with a cap to prevent precipitation from entering. Water samples from the pools were taken from the water surface and from approximately 40 cm water depth. After filtering the samples through a 0.45 µm membrane, the pore water analysis was conducted with a Shimadzu TOC-LCPH/TN analyzer (Shimadzu Inc., Japan). Subsequently, we estimated the soil C/N ratio as DOC/TN ratio within the top 10 cm of the peat soil (as done by Luan et al., 2019).

2.2.5 Peat depth investigation

Since peat depth has previously been considered a potential driver of N_2O fluxes (Leppelt et al., 2014; Maljanen et al., 2012), we investigated the unknown peat depth for both sites. Ground penetrating radar (GPR) has been a widely used and established method for peat depth investigations for almost four decades (e.g. Bjelm, 1980; Pereira et al., 2017; Rosa et al., 2009; Warner et al., 1990). In this study, we used a PulseEkko System (Sensors and Software, Canada), with a center frequency of 100 MHz unshielded at the natural bog, and 250 MHz shielded at the pasture site. The 100 MHz antennas were placed and triggered manually with an offset of 100 cm and 25 cm step size, whereas the 250 MHz antennas were fixed to the sled provided by the manufacturer with a (default) offset of 38 cm, triggered by odometers at 2 cm intervals. GPR data from several transects between approximately 10 and 40 m were collected at both test sites, while the position of two selected transects are shown in Figure 2. Travel time-depth relations were analyzed by wide-angle reflection and refraction (WARR) survey for the natural bog, and by hyperbole analysis for the pasture site using EKKOProject (Sensors and Software, Canada). The application of a lower frequency and the WARR at the natural site were required due to low contrast in the radargrams and the lack of a proper reflector. GPR measurements were conducted in August 2019.

2.2.6 Statistical analysis

All statistical analyses were performed in R (Version 3.5.1; packages `dplyr`, `userfriendlyscience` and `Hmisc`). Throughout this paper, results were considered significantly different if $p < 0.05$. N_2O fluxes and environmental parameters (soil/water temperature, soil moisture, water table, DOC and TN concentrations) including GPP were non-normally distributed. Therefore, the non-parametric Kruskal-Wallis test was used to detect differences of median values for each variable between microlandforms, the two sites and years. In order to further examine mean differences of N_2O fluxes between years, the non-parametric Games-Howell post-hoc test was used to detect trigger years.

In order to identify potential drivers of N_2O fluxes, non-parametric Spearman's rank correlation coefficients and significance levels were determined for GPP and environmental parameters. Mean values are always given with standard errors. Spatial weights were applied for gas fluxes, TN and DOC concentrations on a site-level, assuming the respective cover ratios of each microlandform.

2.3 Results

2.3.1 N_2O fluxes

2.3.1.1 Temporal variation of N_2O fluxes

We observed low fluxes of N_2O, mostly fluctuating around zero (Figure 3). At the beginning of the growing season in 2019, we partly observed higher N_2O fluxes than in the remaining growing season. However, that was not the case in other years, so that we could not detect a repetitive seasonal pattern. We found significant differences of median N_2O fluxes between years ($p < 0.001$). According to a Games-Howell post-hoc test, mean N_2O fluxes in 2019 were significantly

higher (0.24 nmol m^{-2} s^{-1}) than in other years (2013: −0.05 nmol m^{-2} s^{-1}, 2014: −0.10 nmol m^{-2} s^{-1}, 2015: −0.15 nmol m^{-2} s^{-1}, 2016: −0.03 nmol m^{-2} s^{-1}; Figure 4a).

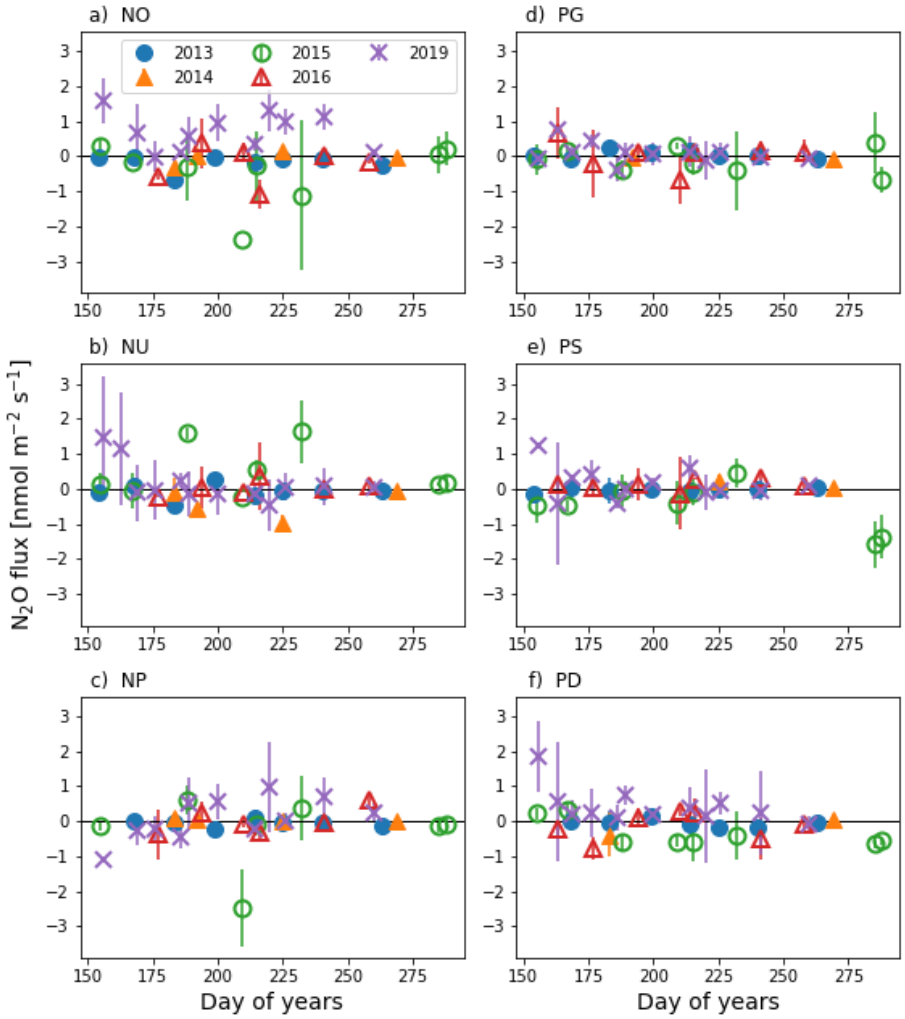

Figure 3: Daily mean N_2O fluxes over the growing seasons from 2013 to 2016 and 2019 for the different microlandforms at the natural bog (a-c) and the abandoned pasture (d-f). Each data point represents the mean of the three replicates and the bars indicate standard errors. Microlandforms: Natural hollow (NO), hummock (NU) and pool (NP); Pasture grass (PG), shrub (PS) and ditch (PD).

2.3.1.2 Comparison of N_2O fluxes between microlandforms

Fluxes ranged from −3.57 nmol m^{-2} s^{-1} to 3.23 nmol m^{-2} s^{-1} (Figure 4). While the mean N_2O fluxes for the bog amounted to 0.06±0.09 nmol m^{-2} s^{-1} (NO), 0.08±0.08 nmol m^{-2} s^{-1} (NU) and −0.00±0.07 nmol m^{-2} s^{-1} (NP), mean fluxes at the abandoned pasture were 0.00±0.06 nmol m^{-2} s^{-1} (PG), −0.04±0.07 nmol m^{-2} s^{-1} (PS) and 0.00±0.08 nmol m^{-2} s^{-1} (PD). For all microlandforms, the median and mean fluxes were close to zero (Figure 4b), and the median N_2O fluxes did not differ significantly between the microlandforms (p = 0.974).

2.3.1.3 Comparison of N_2O fluxes between sites

Accounting for spatial weights of the characteristic microlandforms at the natural bog and the pasture site, mean N_2O fluxes per site are shown in Figure 5. Both sites fluctuated between marginal N_2O release and slight N_2O consumption over the years. In this study, median N_2O fluxes did not differ significantly (p = 0.887) between the sites (natural bog: −0.03 nmol m^{-2} s^{-1}; abandoned pasture: 0.01 nmol m^{-2} s^{-1}). Spatially weighted mean N_2O fluxes at the natural bog amounted to 0.06±0.09 nmol m^{-2} s^{-1} and at the abandoned pasture to −0.01±0.07 nmol m^{-2} s^{-1} (Figure 6a).

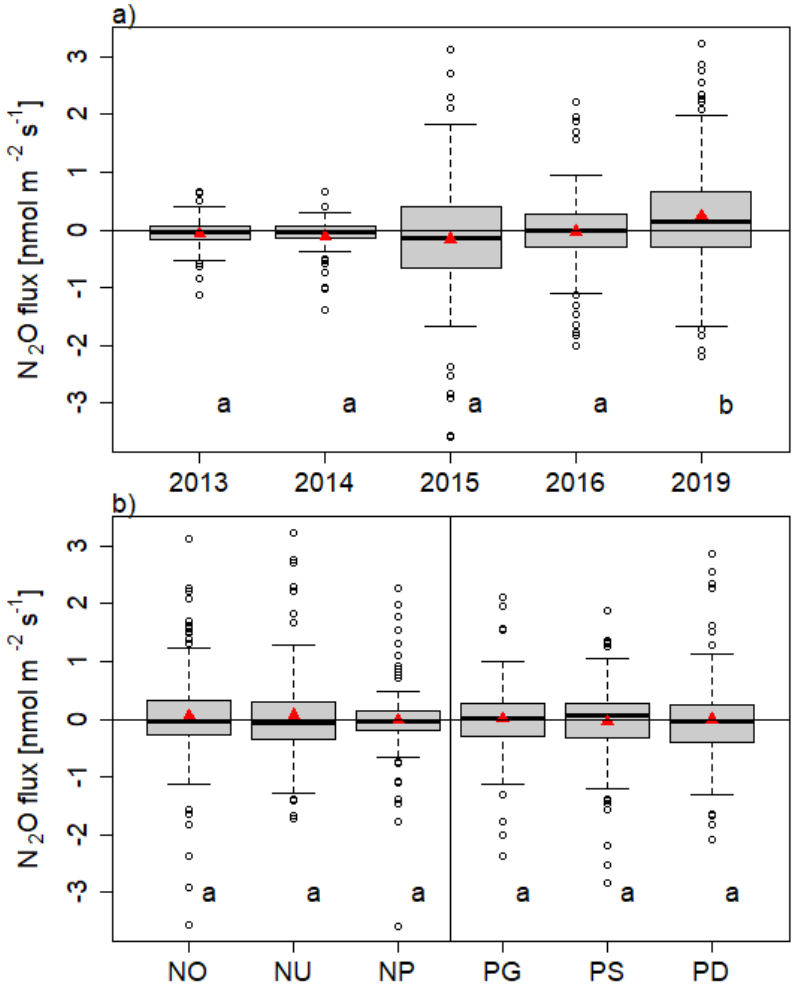

Figure 4: Individual daily N_2O fluxes per year (a) and microlandform (b). Years/microlandforms sharing a lowercase letter do not show significantly different N_2O fluxes. The black bold lines represent the median, the triangle the mean and the black circle outliers. Microlandforms: Natural hollow (NO), hummock (NU) and pool (NP); Pasture grass (PG), shrub (PS) and ditch (PD).

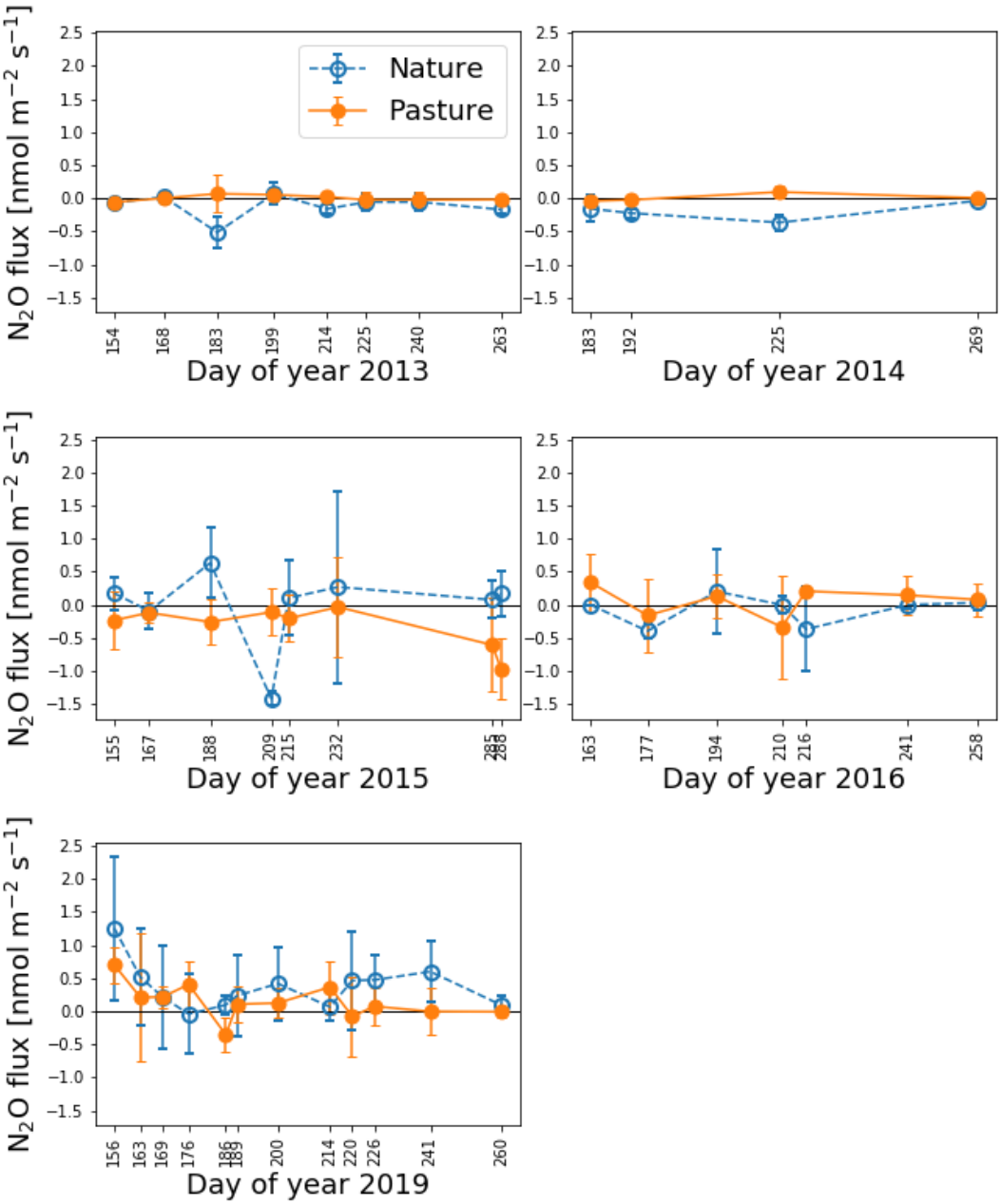

Figure 5: Spatially weighted mean N_2O fluxes and standard errors for each sampling day of the growing seasons from 2013 to 2016 and 2019 for the natural bog (hollow blue circles) and the abandoned pasture (orange circles).

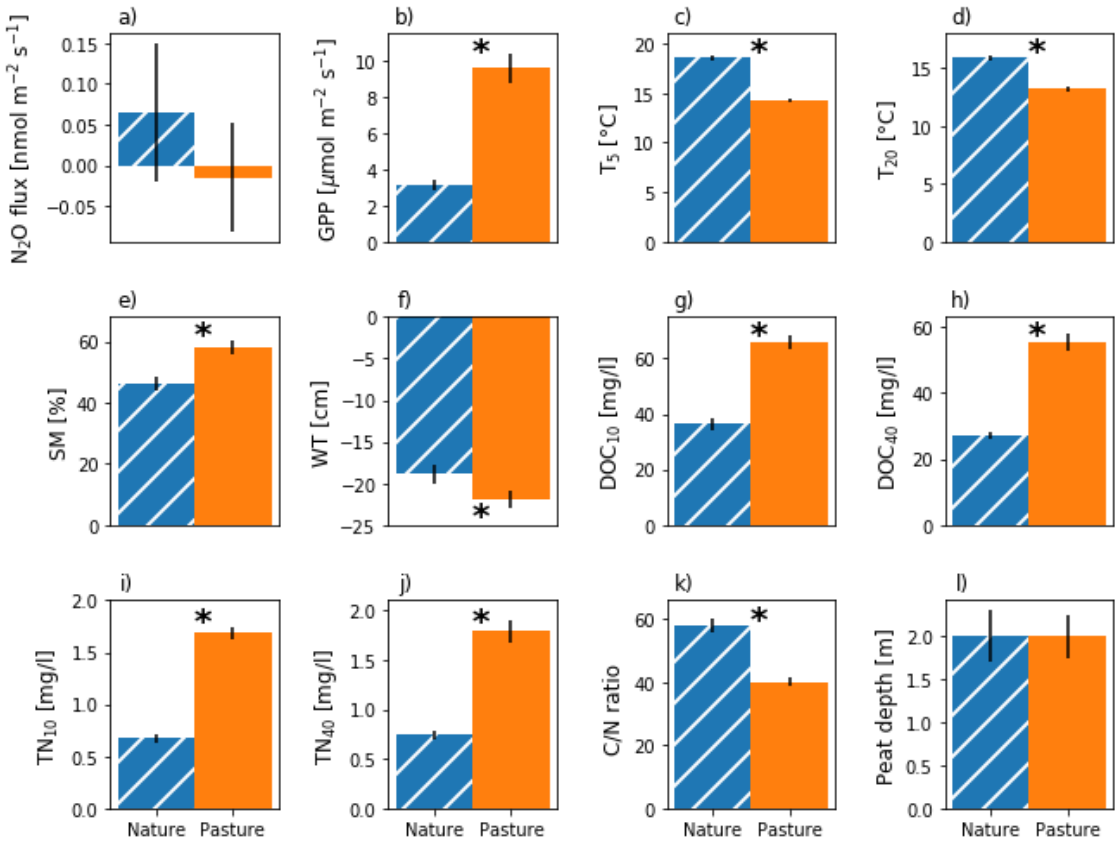

Figure 6: Site-level means and standard errors of N_2O flux (a), GPP (b), soil temperature (c-d), soil moisture (e), water table (f), DOC (g-h) and TN concentrations (i-j), C/N ratio (k) and peat depth (l). N_2O flux, GPP, DOC and TN concentrations are given as spatially weighted means, while the remaining parameters are given as conventional means. Asterisks (*) indicate significant differences ($p < 0.05$) between the natural bog (blue hatched) and the abandoned pasture (orange).

2.3.2 Potential drivers of N_2O fluxes

2.3.2.1 Temporal variation

All environmental parameters (soil temperature, soil moisture, water table, DOC and TN concentration) and GPP showed significant differences between the years ($p < 0.02$). Mean GPP was significantly higher in 2016 than in 2013 (Table 1; Figure 7). The warmest mean soil temperatures in 5 and 20 cm as well as the highest mean soil moisture were detected in the

growing season of 2013. The lowest water table was found in 2015, while TN and DOC concentrations were highest in 2016 (Table 1).

Table 1: Yearly mean GPP, soil/water temperature in 5 cm (T_5) and 20 cm depth (T_{20}), soil moisture (SM), water table (WT), DOC and TN concentrations from 10 cm (DOC_{10}, TN_{10}) and 40 cm (DOC_{40}, TN_{40}) deep pore water as well as the C/N ratio are shown. Negative values indicate water tables below the soil surface. Different lowercase letters indicate statistically significant differences.

Year	GPP	T_5	T_{20}	SM	WT	DOC_{10}	DOC_{40}	TN_{10}	TN_{40}	C/N
	$[\frac{\mu mol}{m^2\ s}]$	[°C]	[°C]	[%]	[cm]	[mg/l]	[mg/l]	[mg/l]	[mg/l]	[-]
2013	5.3±0.4^{a}	17.0±0.3^{a}	15.4±0.3^{a}	63±4^{a}	−21±2^{ab}	41±2^{a}	37±1^{a}	1.0±0.1^{a}	1.2±0.1^{a}	49.5±2.2^{a}
2014	-	12.4±0.5^{b}	-	-	−12±3^{c}	-	-	-	-	-
2015	-	16.1±0.4^{ac}	13.2±0.3^{b}	46±4^{b}	−26±2^{a}	-	-	-	-	-
2016	7.7±0.6^{b}	15.4±0.3^{c}	14.7±0.3^{ac}	-	−15±2^{bc}	72±3^{b}	58±3^{b}	1.3±0.1^{b}	1.6±0.2^{b}	58.1±1.6^{b}
2019	-	16.7±0.4^{ac}	14.2±0.3^{bc}	50±2^{b}	−20±1^{ab}	44±2^{a}	33±1^{c}	1.1±0.0^{ab}	1.1±0.1^{a}	44.1±0.9^{a}

2.3.2.2 Comparison of GPP between sites

GPP represents the total CO_2 gained by the ecosystem, going along with plant growth. Since plant growth is strongly linked to the production of N_2O in peatlands, we examined measurements of GPP on a site-level. Noticeably, Figure 7 shows a stronger seasonal cycle of GPP at the pasture site than at the natural bog. Figure 6b indicates significantly different ($p < 0.001$) and remarkably higher fixation of CO_2 at the pasture site (median: 8.6 nmol m^{-2} s^{-1}; mean: 9.6±0.8 µmol m^{-2} s^{-1}) than at the natural bog (median: 2.5 nmol m^{-2} s^{-1}; mean: 3.1±0.3 µmol m^{-2} s^{-1}).

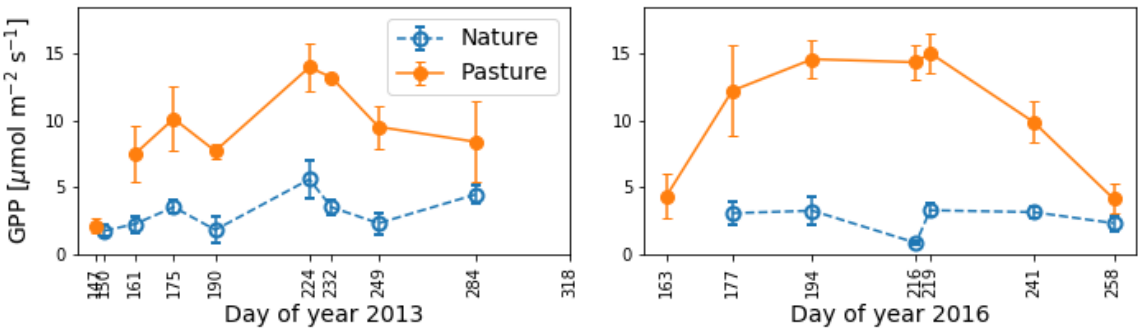

Figure 7: Spatially weighted mean gross primary production at the natural bog and the abandoned pasture. Points indicate spatially weighted mean CO_2 flux of the measurements on each sampling day in 2013 and 2016. Bars represent standard errors.

2.3.2.3 Comparison of environmental parameters between sites

On a site-level, significant differences ($p \leq 0.002$) were found between the abandoned pasture site and the natural bog for the median of all environmental parameters. Furthermore, mean soil/water temperatures were lower at the pasture (T_5 = 14.3±0.2°C and T_{20} = 13.2±0.2°C) than at the natural bog (T_5 = 18.6±0.3°C; T_{20} = 15.9±0.3°C; Figure 6c-d). Mean soil moisture was slightly higher at the pasture site (SM = 58±2%) than at the bog (SM = 46±3%; Figure 6e). However, the mean water table was lower at the abandoned pasture (WT = −22±1 cm) than at the bog (WT = −19±1 cm; Figure 6f). In this study, DOC concentrations ranged from 10-192 mg L^{-1} and TN concentrations from 0.2-7 mg L^{-1}. Throughout all measurements, mean DOC and TN concentrations in pore waters were about twice as high at the pasture site compared to the bog (Figure 6g-j). The C/N ratio at the natural bog ranged from 15 to 107, while the median amounted to 56 and the mean to 58±2. For the pasture site, the C/N ratio ranged from 14-74, with a median of 39 and a mean of 40±1. Median C/N ratios between the sites were significantly different ($p < 0.001$; Figure 6k). Peat depths were similar at both sites (Figure 6l), ranging around

2 m. For the natural bog, the peat depth varied from approximately 1.8 to 2.4 m and for the abandoned pasture from 1.7 to 2.2 m (Figure 8).

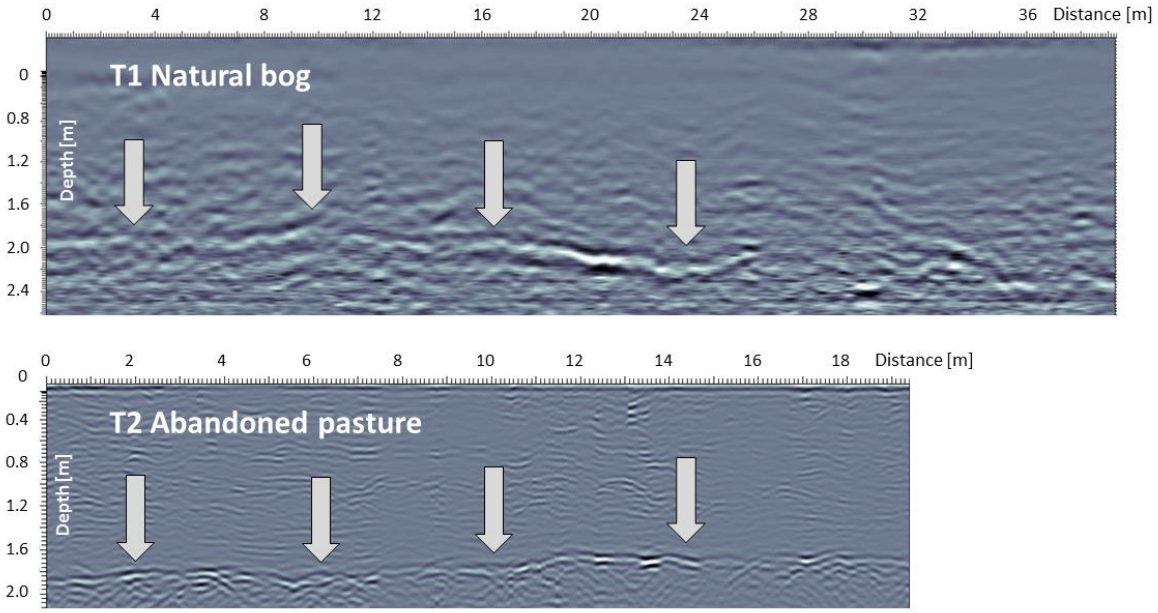

Figure 8: GPR measurements along the transects at the natural bog and the abandoned pasture, indicating the transition between the organic and mineral layer in a depth of approximately 2 m at both sites.

2.3.2.4 Relationships with N_2O fluxes

In order to identify possible biotic and abiotic drivers of N_2O fluxes in the boreal peatland complex, we conducted a non-parametric Spearman's rank correlation test with GPP, soil temperature, soil moisture, water table, DOC and TN concentrations as well as the C/N ratio as potential controls. As a result, a significant, but weak negative correlation was only found between the C/N ratio and N_2O fluxes (Table 2; Figure 9), explaining roughly 2% of N_2O flux variation. GPP showed significant positive correlations with DOC and TN concentrations (Table 2), but not with temperature and soil moisture.

Table 2: Spearman's rank correlation coefficients to evaluate the association between N_2O fluxes and environmental parameters including GPP and the C/N ratio. All available measurements from 2013 to 2016, and from 2019 were included. Sampling days of GPP measurements solely coincided with N_2O flux measurements in 2016. Soil/water temperature at 20 cm depth was not measured in 2014, neither was soil moisture in 2014 and 2016. Pore water samples were only collected in 2013, 2016 and 2019. Asterisks indicate statistically significant correlations ($p < 0.05$).

	N_2O	**GPP**	**T_5**	**T_{20}**	**SM**	**WT**	**DOC_{10}**	**DOC_{40}**	**TN_{10}**	**TN_{40}**	**C/N**
N_2O	1	0.21	−0.01	−0.06	−0.05	−0.07	0.00	0.08	0.09	0.05	−0.14**
GPP		1	−0.12	−0.06	-	−0.01	0.37**	0.53***	0.40***	0.56***	−0.43***
T_5			1	0.87***	−0.49***	−0.01	−0.32**	−0.40***	−0.41***	−0.34***	0.26***
T_{20}				1	−0.45***	0.03	−0.09	−0.18**	−0.19***	−0.16**	0.19***
SM					1	0.63***	−0.23**	0.33***	0.03	0.06	−0.36***
WT						1	−0.31***	0.01	−0.19***	−0.03	−0.13*
DOC_{10}							1	0.74***	0.81***	0.60***	−0.03
DOC_{40}								1	0.71***	0.75***	−0.17**
TN_{10}									1	0.73***	−0.58***
TN_{40}										1	−0.38***
C/N											1

Note: * $p < 0.05$; ** $p < 0.01$; *** $p < 0.001$

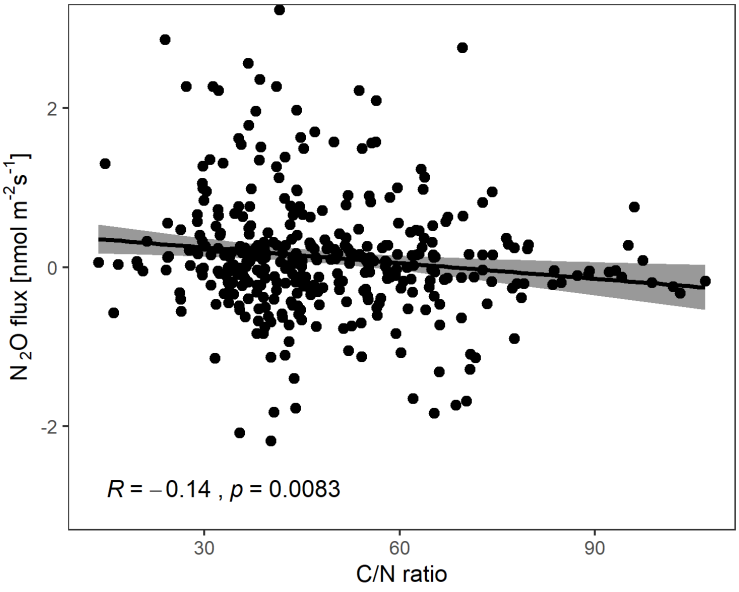

Figure 9: Scatter plot with regression line between all individual N_2O fluxes and C/N ratios determined in this study. The Spearman correlation coefficient (R), significance level (p) and 95% confidence interval (gray shaded area) are shown.

2.4 Discussion

2.4.1 N_2O fluxes

The broad range of individual N_2O emission and consumption rates found in this study (Figure 3 and Figure 4) is in line with previous findings (e.g. Maljanen et al., 2001; Mustamo et al., 2016; Regina et al., 1996). Emission rates lay within the scope of N_2O release found in a German mire by Tauchnitz et al. (2007), in an afforested Finish peatland by Maljanen et al. (2001) and drained and undrained Estonian peatlands by Salm et al. (2009), but exceeded their N_2O consumption rates. However, our results for N_2O consumption coincide with findings from Schlesinger (2013), who suggested high N_2O uptake potential for wetlands and peatlands. Accordingly, about half of the diffusive N_2O fluxes determined in this study were negative, revealing noticable N_2O consumption. This behaviour can be explained by a shortage of soil nitrate at our research site, so

that N_2O was consumed instead as electron acceptor in order to finish the formation of dinitrogen during denitrification (Chapuis-Lardy et al., 2007).

However, on a broader scale mean N_2O fluxes showed significant temporal variations only for the year 2019 (Figure 4a), possibly due to a slightly lower mean C/N ratio (Table 1) promoting emissions of N_2O (Klemedtsson et al., 2005). Spatially, median N_2O fluxes were not significantly different, neither on a microlandform-level (Figure 4b) nor on a site-level. As anticipated for pristine nutrient-poor peatlands (Martikainen et al., 1993), mean N_2O fluxes at the natural bog were low. Contrary to our expectations and several studies (Aerts and Ludwig, 1997; Cui et al., 2016; Freeman et al., 1992; Laine et al., 1996; Maljanen et al., 2010; Martikainen et al., 1993; Regina et al., 1998, 1996), mean N_2O fluxes at the abandoned pasture were similarly low (Figure 6a), so that our first hypothesis was rejected.

Relatively high C/N ratios at both sites may be responsible for the absence of these spatial differences, suggesting limiting soil nitrogen availability for N_2O production (Klemedtsson et al., 2005). In addition, the areal cover of vascular plants and accordingly the aboveground biomass was significantly higher at the abandoned pasture compared to the natural bog (Luan and Wu, 2015). Consequently, GPP (Figure 7) and thus soil nutrient consumption through plant growth at the pasture site were higher than at the natural bog, inhibiting N_2O emissions (Silvan et al., 2005). A combination of these factors presumably led to attenuated N_2O fluxes from the abandoned pasture.

2.4.2 Environmental parameters and GPP

In accordance with our second hypothesis, environmental parameters and GPP at the abandoned pasture showed significant differences compared to the natural bog, with the single exception of peat depth (Figure 6b-l). As a result of higher aboveground biomass at the pasture site (Luan and

Wu, 2015), the site was photosynthetically more active and yielded significantly higher GPP than the natural bog (Figure 7). Soil temperature was significantly higher at the natural bog, while soil moisture was higher at the abandoned pasture.

Since sampling days usually started with measurements at the pasture site in the cooler morning time, followed by the natural site in the afternoon, this finding seems reasonable. In addition, shading through plants at the pasture site likely provoked a decrease in soil temperature as well as an increase in surface soil moisture compared to the natural bog (Waddington et al., 2015). Furthermore, the water table was slightly deeper at the pasture site as a result of drainage.

In this study, DOC and TN concentrations in pore waters were significantly higher at the pasture site than at the natural bog (Figure 6g-j), partly exceeding the typical range of DOC concentrations from 20-60 mg L^{-1} for northern peatlands (Blodau, 2002) and TN concentrations determined in pristine and drained peatland forests in Finland (0.1-1.7 mg L^{-1}) (Nieminen et al., 2017). These higher concentrations of DOC and TN at the abandoned pasture may partly have resulted from past land-use changes going along with fertilization, grazing and drainage (Banaś and Gos, 2004; Glatzel et al., 2003; Moore and Clarkson, 2007; Wallage et al., 2006), but also due to internal cycling of the soil-plant system (Hättenschwiler and Vitousek, 2000; Hemond, 1983; Morris, 1991). The resulting C/N ratio was significantly lower at the pasture site than at the natural bog (Figure 6k), presumably as a result of land-use change (Kasimir-Klemedtsson et al., 1997; Klemedtsson et al., 2005).

Furthermore, we measured the peat depth and found no considerable difference between the two sites (Figure 6l). Most likely, the effect of a decreased peat thickness as a result of drainage was out-competed by high plant production rates at the pasture site, inhibiting a significant decrease of peat depth compared to the natural bog.

2.4.3 Biotic and abiotic drivers of N_2O fluxes

In this study, we did not find a significant correlation between any hydrological parameter and N_2O fluxes (Table 2), so that our third hypothesis was rejected. However, we detected a significant negative correlation between N_2O fluxes and the C/N ratio (Table 2, Figure 9), as found previously (Klemedtsson et al., 2005; Leppelt et al., 2014; Liimatainen et al., 2018; Maljanen et al., 2010). The C/N ratio at the natural bog and the abandoned pasture was relatively high, suggesting a lack of mineral nitrogen for soil microbial processes at both sites (Maljanen et al., 2012). Although differences between the site-level C/N ratios were significant (Figure 6k), we suppose that the threshold of C/N ratios (> 25) promoting significant N_2O emissions found by Klemedtsson et al. (2005) was mostly exceeded at both sites and therefore did not result in significantly different N_2O fluxes between the sites, but rather in generally low N_2O fluxes. However, only 2% of N_2O flux variation at our study site could be explained by the C/N ratio.

More importantly, we assumed the availability of inorganic nitrogen to be a limiting factor constraining N_2O fluxes in our peatland complex, as suggested previously (Kandel et al., 2018; Maljanen et al., 2012; Pärn et al., 2018), in particular as a result of increased plant growth at the pasture site. Especially fast growing herbaceous plant species were highly efficient in nutrient uptake and thus may be strong competitors for nutrients with soil microbes (Jingguo and Bakken, 1997; Korsaeth et al., 2001; Silvan et al., 2005). Since the pasture site in our study was dominated by lower herbaceous and graminoid species, we further attributed the homogeneity of N_2O fluxes between the two sites to the vegetation composition; in the case of the pasture site leading to increased nutrient competition under higher plant production rates. Considering a constraining effect of plant growth on N_2O fluxes, winter N_2O fluxes in our study area (not measured) may have been higher than during the growing season, as found in several studies

(Alm et al., 1999; Holtan-Hartwig et al., 2002; Kandel et al., 2018; Maljanen et al., 2007). Although peat depth was the only environmental parameter not revealing significant differences between the sites, we could not show a considerable influence of peat thickness on N_2O fluxes at our peatland complex.

2.5 Conclusion

In this study, we found no significant differences in growing season N_2O fluxes between a natural bog and a bog formerly drained and used as pasture, despite significantly different environmental parameters (soil temperature, moisture, water table, concentrations of total nitrogen and dissolved organic carbon) and gross primary production. The results of this study contradict previous findings that drained peatlands with higher nutrient availability emit significantly more N_2O than peatlands with lower nutrient availability.

None of the hydrological parameters were identified as responsible drivers for similar N_2O fluxes between the two land-use types. However, we found that the C/N ratio in the topsoil layer significantly affected the N_2O flux variation, although this relationship was weak. Further drivers could be the supply of plant-available nitrogen in the soil (not measured in this study) and the nutrient demand of dominant plant species of boreal bogs.

We conclude that a combination of drainage, former fertilization, grazing, plant community change and subsequent site abandonment does not necessarily result in higher N_2O emissions during the growing season, since the effects of drainage and fertilization may be superposed by vegetation composition change effects. Due to inter-annual variability, we recommend further research on the indicated plant species effects on N_2O fluxes over a longer time scale. Although land-use change might not affect N_2O fluxes, we emphasize the importance of other greenhouse

gases (CO_2 in particular) as contributors to global warming after peatland drainage (Freeman et al., 1992; Kasimir-Klemedtsson et al., 1997; Maljanen et al., 2010).

2.6 Acknowledgements

This study was made possible by the support of the following funding to J. Wu: Natural Sciences and Engineering Research Council of Canada (NSERC) Discovery Grant, Canada Foundation for Innovation-John R. Evans Leaders Fund, Research & Development Corporation of Newfoundland and Labrador (RDC, NL) – Leverage R&D, RDC-Ignite R&D, RDC-RCRI (Regional Collaborative Research Initiative), Humber River Basin Research Initiative of NL, Vice-President Research Fund, Seed Bridge Fund of Memorial University of Newfoundland, and the Graduate Student Stipend funding from the Institute for Biodiversity, Ecosystem Science, and Sustainability (IBES, NL). J. Vogt, T. B. Le and Y. Gong received a Graduate Student Baseline Fellowship from School of Graduate Studies, Memorial University. We would like to thank Dr. Junwei Luan and Dr. Mei Wang for their assistance in taking gas and water samples during the summers of 2013-2015, and Maryam Hajheidari for taking soil water samples during the summer of 2016. We thank Asare Gymiah and Riad Eissa for their assistance in taking gas samples during the summer of 2016.

Chapter 3: Sea-air methane flux estimates derived from marine surface observations and instantaneous atmospheric measurements in the northern Labrador Sea and Baffin Bay

Preamble

This chapter was published in Biogeosciences. For this study, I led the conceptualization of the study, I prepared, organized, and conducted field measurements of atmospheric data and assisted in the collection of water samples. Furthermore, I gathered external data, analyzed all measurements, produced figures and tables, and wrote the manuscript. As a result of the pandemic, proper testing and preparing of the measurement setup on the ship in advance of the cruise were not possible. In addition, uncertainties if the expedition could go ahead due to pandemic-related restrictions lasted until the departure of the ship. This study was conducted under supervision of my current supervisor, David Risk. The manuscript was co-authored with David Risk, Evelise Bourlon, Kumiko Azetsu-Scott, Evan N. Edinger and Owen A. Sherwood. David Risk supported the conceptualization of the study, supervised, and provided insights regarding the interpretation of the data. Evelise Bourlon processed raw data and helped interpret study results. Kumiko Azetsu-Scott provided the analysis of water samples. Evan N. Edinger provided insights and guided water-based measurements. Owen A. Sherwood provided the funding and helped conceptualize the study. All co-authors provided helpful comments for the preparation of the final manuscript.

3.0 Abstract

Vast amounts of methane (CH_4) stored in submarine sediments are susceptible to release in a warming Arctic, further exacerbating climate change in a positive feedback. It is therefore critical to monitor CH_4 over pan-regional scales to detect early signs of CH_4 release. However, our

ability to monitor CH_4 is hampered in remote northern regions by sampling and logistical constraints and few good baseline data exist in many areas. From high-resolution atmospheric CH_4 measurements and discrete surface water samples, we estimated instantaneous sea-air CH_4 fluxes at various locations. We also created a baseline study of current background levels of CH_4 in North Atlantic waters based on the atmospheric CH_4 data over 22 days in summer 2021 on a roughly 5100 km voyage in the northern Labrador Sea and Baffin Bay between 55 °N and 72 °N. In addition, we measured CH_4 concentrations across the water column at various stations. Measured atmospheric mixing ratios of CH_4 ranged from 1944 ppbv to 2012 ppbv, with a mean of 1966±8 ppbv and a baseline of 1954−1981 ppbv. Dissolved CH_4 concentrations in the near-surface water peaked at 5.3 nmol L^{-1} within 1 km down-current of a known cold seep at Scott Inlet and were consistently oversaturated throughout the water column in Southwind Fjord, which is an area recently affected by submarine landslides. Local sea-air CH_4 fluxes ranged from 0.003−0.119 μmol m^{-2} d^{-1} indicating that the ocean released only small amounts of CH_4 to the atmosphere at all stations. Atmospheric CH_4 levels were also driven by meteorological, spatial, and temporal variations, and both onshore and ocean-based contributions to atmospheric CH_4 mixing ratios are likely. Coupled high-resolution measurements of marine and atmospheric CH_4 data have the potential to provide ongoing monitoring in a region susceptible to CH_4 releases, as well as critical validation data for global-scale measurements and modelling.

3.1 Introduction

Global atmospheric methane (CH_4) levels have substantially increased in recent years, with the largest recorded yearly increase from 2020 to 2021 (Dlugokencky, 2016; Nisbet et al., 2019). Due to the high radiative forcing of the greenhouse gas CH_4, close observations of atmospheric levels are needed to immediately detect trends and impacts on the future climate. While Arctic

regions are subject to rapid warming (Meredith et al., 2019), measurements of atmospheric CH_4 levels in these regions are scarce, especially over the ocean. The Arctic Ocean contains large amounts of CH_4 in sediments along the continental margins (Kvenvolden, 1988; Mau et al., 2017; Shakhova et al., 2010). With ongoing climate change, permafrost thaw, destabilization of CH_4 hydrates and reduction of sea ice cover may make the Arctic Ocean susceptible to substantial CH_4 release further exacerbating global warming (James et al., 2016). Seafloor gas seeps releasing CH_4-rich bubbles into the water column are often found along continental margins. However, the contribution of seafloor gas seeps to atmospheric CH_4 entails large uncertainties (Saunois et al., 2016), mostly due to significant temporal and spatial differences of emissions (Boles et al., 2001; Cramm et al., 2021; Dølven et al., 2022; Leifer and Boles, 2005; Shakhova et al., 2014). Water depth and the abundance of methanotrophic bacteria influence the oxidation of CH_4, and the speed and strength of currents affect the distribution of the gas in surface waters and in the water column (Leonte et al., 2017; McGinnis et al., 2006; Reeburgh, 2007; Silyakova et al., 2020). Among others, these factors determine how much of the gas escapes to the atmosphere.

While the East Siberian Arctic Shelf overall releases up to 4.5 Tg CH_4 yr^{-1} of mostly thermogenic, but also biogenic origin (Berchet et al., 2020) with large temporal and spatial variability (Shakhova et al., 2014, 2010; Thornton et al., 2020, 2016), prevailing thought suggests that the North American Arctic Ocean contributes relatively little CH_4 to the atmosphere (Manning et al., 2022). Increasing atmospheric concentrations of CH_4 have however been reported over the European Arctic Ocean and mostly attributed to land-based sources, but also marine point sources from active underwater seeps (Platt et al., 2018). While a few studies focused on dissolved CH_4 levels in northeastern Canadian Arctic waters (Punshon et al., 2019, 2014) where seep locations were suggested (Jauer and Budkewitsch, 2010; Punshon et al., 2019)

or confirmed (Cramm et al., 2021), continuous measurements of atmospheric CH_4 levels in this region are lacking and more measurements in this area are needed. To investigate how the identified seep areas affected atmospheric CH_4 levels, we conducted CH_4 monitoring onboard the icebreaker CCGS *Amundsen*. We collected measurements of CH_4 dissolved in the water column at various locations between the northern Labrador Sea to Baffin Bay adding to a small but growing body of data on water column CH_4 concentrations in the Arctic and sub-Arctic seas. We also tracked atmospheric CH_4 levels continuously along a north-south transect to establish a baseline study for above-ocean CH_4 mixing ratios in the area that can be used as a benchmark for further monitoring of CH_4 levels in Arctic regions.

3.2 Methods

3.2.1 Study area

Data for this study was collected during an expedition of the Canadian research icebreaker CCGS *Amundsen* starting on July 15, 2021, in St. John's, Newfoundland, Canada, and ending on August 12, 2021, in Iqaluit, Nunavut, Canada. The expedition transited the western Labrador Sea, Davis Strait, and Baffin Bay along the northeastern Canadian continental shelf (Figure 10). Along the shelf margins, seafloor gas seepage was previously localized at Scott Inlet, Baffin Bay (71° 22' 41.2" N, 70° 04' 28.3" W) (Cramm et al., 2021; Levy and MacIean, 1981; Loncarevic and Falconer, 1977), while further locations were suggested in the Saglek Basin in northern Labrador (60° 21' 03.6" N, 61° 51' 50.4" W) (Jauer and Budkewitsch, 2010; Punshon et al., 2019) and off the coast of Cape Dyer, Baffin Island (67° 26' 56.4" N, 61° 55' 08.4" W) (Punshon et al., 2019) also indicated in Figure 10. The studied region lies within the seasonal sea ice zone and partial sea ice cover was observed in the northernmost regions between July 30, 2021, and August 3, 2021. Hydrography in the studied area is dominated by the Baffin Island Current (BIC), the

integrated Arctic outflow through the Canadian Arctic Archipelago. The BIC flows southward along the Baffin Island coast and slope and becomes a component of the Labrador Current (Figure 10), being modified by the Hudson Strait overflow, and continues flowing southward, mainly confined to the shelf and upper slope (Azetsu-Scott et al., 2012). The West Greenland Current bifurcates at Davis Strait, with part of the flow entering Baffin Bay on the eastern side of Davis Strait and contributing to the cyclonic circulation in the Bay, and partly continuing westward as the Labrador Sea cyclonic circulation (Melling et al., 2001; Tang et al., 2004; Wu et al., 2013). The eastern coast of Baffin Island is characterized by the Baffin Mountains, with elevations up to 2147 m. With its location north of the tree line, the land is dominantly barren and sparsely vegetated, or covered with smaller waterbodies and wetland areas.

3.2.2 Atmospheric measurements

Instruments were mounted on the meteorological tower at the bow of the ship: A 2D heated anemometer (model 86004, RM Young, USA) at a height of 8.1 m above deck and about 14.1 m above sea level (considering a constant height of the deck), a temperature probe (model 107B, Campbell Scientific, USA) 7.6 m above the deck, a 1 Hz GPS puck (GPS 18x LVC, Garmin, USA), and an air inlet for gas sampling at 7.3 m (Appendix A, Figure 30). Roughly 30 m long Synflex tubing connected the air inlet with the greenhouse gas analyzer (Ultraportable Greenhouse Gas Analyzer, Los Gatos Research, USA), making high-resolution monitoring of atmospheric carbon dioxide (CO_2), methane (CH_4) and water vapour (H_2O) mixing ratios possible. In this study, all CH_4 and CO_2 measurements reflect dry mixing ratios. The analyzer is equipped with a built-in pump drawing the air from the inlet on the tower to the analyzer stored securely inside a laboratory on deck. By repeatedly breathing on the air inlet, we determined an average delay time of 90 seconds for the air samples to reach the analyzer and accounted for this

delay time during data processing. The greenhouse gas analyzer was calibrated in-lab on July 10, 2021 before deployment on the ship with certified calibration gas (calibrated by the AmeriFlux QA/QC team at the Lawrence Berkeley National Laboratory, Berkeley, CA, USA at 385.18±0.01 ppmv CO_2, 1810.6±0.1 ppbv CH_4, and 4.08±1.58 ppmv H_2O), and was benchmarked daily during the cruise (only starting on July 23, 2021, due to logistical issues) to assure proper functioning of the analyzer, determine precision and detect potential drift. The benchmarking gas was a standard gas mixture (from Praxair) balanced with air and certified for 450 ppmv CO_2 (mixing ratios for CH_4 were not specified by the supplier). Once the analyzer was connected to the benchmarking gas, it was left to stabilize for a few minutes, and we used a 100 s-window after stabilization for analysis of the daily benchmarking data. Mixing ratios measured by the gas analyzer during these 100 s-windows amounted to 451±1 ppmv CO_2 and 5056±9 ppbv CH_4 (mean ± standard deviation) throughout the cruise, which was well within the analyzer's measurement range (200−20,000 ppmv for CO_2 and 100−100,000 ppbv for CH_4). Based on the benchmarking data, we determined a standard error of 2 ppbv for CH_4 and 0.13 ppmv for CO_2, which can be considered the uncertainty of our measurements. Even though day-to-day differences between averaged benchmarks reached up to 34 ppbv for CH_4 and 2 ppmv for CO_2 under field conditions, we did not correct the measured mixing ratios since a post-expedition in-lab benchmark on August 30, 2021, revealed no significant drift from the initial calibration (1814.8 ppbv CH_4 and 384.81 ppmv CO_2) with the certified gas used prior to the expedition.

Once the setup was mounted and leak proof, we recorded atmospheric measurements between July 20, 2021, and August 10, 2021, on a datalogger (CR1000, Campbell Scientific, USA) at a frequency of 1 Hz. We processed wind measurement timeseries to exclude occasional erroneous values of direction and speed, and linearly interpolated across gaps before resampling onto the

datalogger's timestamp. Wind parameters were corrected for lateral ship motion when the ship was not in transit or not headed forward, using speed, track and heading from the ship's own navigation system (Amundsen Science Data Collection, 2021a).

To exclude data potentially contaminated by the ship's exhaust, we removed all measurements of CH_4 and CO_2, whenever the wind direction was 80°−280° relative to the bow of the ship, and when CO_2 levels were larger than 420 ppmv. As a result, 26 % of all 1 Hz CH_4 and CO_2 measurements were excluded on the account of potential contamination (see also Figure 31). To determine CH_4 baseline levels for the studied region, we applied a Savitzky-Golay filter (Savitzky and Golay, 1964) of second polynomial order with a 24-hour window size on the mixing ratios.

Maxima in atmospheric CH_4 measurements were further investigated using the online Real-time Environmental Applications and Display System (READY) for the Hybrid Single-Particle Lagrangian Integrated Trajectory (HYSPLIT) model (Rolph et al., 2017; Stein et al., 2015). Ensemble back-trajectories of air masses from the time and location where CH_4 maxima were measured (referred to as source) to the point of possible origin within the previous 12 hours were modelled. Two gridded meteorological data archives were used: the Global Data Assimilation System (GDAS) model (1° horizontal resolution) and the Global Forecast System (GFS) model (0.25° horizontal resolution). For the ensemble, the datapoints of the meteorological input model were offset by a fixed grid factor resulting in an output of 27 possible trajectories (Rolph et al., 2017).

Atmospheric pressure and dew point temperature measurements were recorded every two minutes with a digital barometer (PTB-210, Vaisala, Finland) and a humidity-temperature sensor (MP101A-T7, Rotronic, USA) located on the bridge of the ship (Amundsen Science Data

Collection, 2021b). For statistical analyses, we examined CH_4 measurements for linear Spearman rank correlations with available data and also fitted a simple Generalized Additive Model (Hou and Xu, 2022; GAM; used previously in air quality studies, e.g. Pearce et al., 2011) to hourly averaged CH_4 data in order to identify trends of inter-dependencies. The GAM was well suited due to its ability to describe the non-linear effects of non-normally distributed data using non-parametric smoothing functions. The respective analysis was performed in R (package: "mgcv", function: "gam"; Wood, 2011).

3.2.3 Water column measurements

Seawater was collected at 15 stations for measurements of dissolved CH_4: Makkovik in the Labrador Shelf, northeastern Labrador ("Kelp"), two locations at Saglek Bank (Figure 32), Hatton Sill, Davis Strait, Southwind Fjord, Disko Fan, six locations at Scott Inlet, and Clark Fiord (Figure 10). While exclusively surface samples were taken at Clark Fjord and at four co-located stations close to the Scott Inlet seep (SI1, SE-1K, NE-1K, NE-5K; Figure 32), we gathered water column profiles at the remaining ten locations. Collection and measurement protocols followed that of Punshon et al. (2014, 2019). Briefly, seawater samples were collected from 12 L Niskin bottles mounted on a Conductivity-Temperature-Depth (CTD)/Rosette system to 60 ml glass serum bottles (after triple rinsing with the sample water) to overfilling by 1.5 times the bottle volume, immediately fixed with mercuric chloride, capped with metal crimp seals and rubber septa, and stored at 4 °C. Replicates were not taken. Samples were analyzed for CH_4 at the Bedford Institute of Oceanography (Department of Fisheries and Oceans, Canada) using a single-phase batch headspace equilibration method with gas chromatography (similar to Neill et al., 1997). Marine CH_4 concentrations are given in nmol L^{-1}, abbreviated as nM hereinafter. Multiple measurements of standard gases show an analytical uncertainty of ±0.5−0.8 % or better for

dissolved CH_4 similar to previous studies (Punshon et al., 2019, 2014). Data from previous studies conducted in 2011, 2012 and 2016 (Punshon et al., 2019, 2014) were included here to examine regional patterns and temporal variations of dissolved CH_4 concentrations in the Baffin Bay. Potential temperature (θ) and potential density of seawater at atmospheric pressure (σ_θ) were calculated based on water temperature, pressure and salinity measured on the ship (SBE 911 CTD, Seabird Scientific, Canada) (Amundsen Science Data Collection, 2021c) using the package 'seawater' in Python (calculations based on Bryden, 1973; Fofonoff and Millard, 1983; Millero and Poisson, 1981). Water masses were defined following previous studies (Azetsu-Scott et al., 2012; Fratantoni and Pickart, 2007; Table 1 in Sherwood et al., 2021; Stramma et al., 2004). These water masses comprise Halocline Water ($\sigma_\theta \leq 27.30$ kg m^{-3}, $\theta \leq 0$ °C), Baffin Bay Water ($27.50 < \sigma_\theta \leq 27.80$ kg m^{-3}, $\theta \leq 2$ °C), Labrador Shelf Water ($\sigma_\theta \leq 27.40$ kg m^{-3}, $\theta \leq 2$ °C), Irminger Water ($27.30 < \sigma_\theta \leq 27.68$ kg m^{-3}, $\theta > 2$ °C), Labrador Sea Water ($27.68 < \sigma_\theta \leq 27.80$ kg m^{-3}, $\theta > 2$ °C), and to a lesser extent North East Atlantic Deep Water ($27.80 < \sigma_\theta \leq 27.88$ kg m^{-3}) and Denmark Strait Overflow Water ($\sigma_\theta > 27.88$ kg m^{-3}). It should be noted that surface waters (~2 m) did not necessarily match operational definitions of water masses as outlined in Sherwood et al. (2021) and were interpreted separately. We also used seawater density and oxygen data (not shown) from the CTD casts (Amundsen Science Data Collection, 2021c) and determined the mixed layer depth where the density change was higher than 0.125 kg m^{-3} compared to the density at 5 m depth. Continuous water temperature and salinity measurements in surface waters from the underway thermosalinograph (Amundsen Science Data Collection, 2021d) were used to determine correlations with atmospheric measurements. Daily sea ice concentration data with 10 km resolution (AMSR-2, identifier OSI-408) by the Norwegian and Danish Meteorological Institutes was extracted from the Ocean and Sea Ice Satellite Application Facility EUMETSAT catalogue (https://thredds.met.no/thredds/osisaf/osisaf_seaiceconc.html; accessed: 2022-11-13).

3.2.4 Sea-air methane flux

The instantaneous sea-air CH_4 flux (F) was determined with the bulk flux equation (Wanninkhof, 2014),

$$F = k\,(C_w - C_a),$$

combining measured dissolved CH_4 concentrations (C_w) and air-equilibrated seawater CH_4 concentrations (C_a) (Equation 7, Wiesenburg and Guinasso, 1979) calculated with our atmospheric CH_4 measurements averaged between five minutes before and after the time of sampling, as well as water temperature and salinity measurements from the CTD (Amundsen Science Data Collection, 2021c). The gas transfer velocity (k) was determined after Ho et al. (2006) with

$$k = 0.254\,\overline{u_{10}}^2\,(Sc/660)^{-0.5},$$

making use of the Schmidt number (Sc) with a correction for salinity (average 4.9 % diffusivity decrease for dihydrogen and helium in a seawater-like solution) based on Jähne et al. (1987), following the example of Manning et al. (2022) and the respective code (Manning and Nicholson, 2022) was used as a reference (see Appendix A.2). Wind speeds were corrected to 10 m height via wind profile power law (Hsu et al., 1994) and averaged between five minutes before and after the time of sampling ($\overline{u_{10}}$). Positive sea-air fluxes indicated CH_4 flux from the ocean to the atmosphere. No flux was calculated for the Makkovik station since these samples were taken before atmospheric measurements had started.

3.3 Results and discussion

Seawater samples showed wide ranges of dissolved CH_4 concentrations at the different sample locations and water depths from undersaturated (25 %, 0.9 nM) to highly oversaturated (11324 %, 445.3 nM, Figure 11). The by far highest water column concentrations were measured at the known cold seep at Scott Inlet (station Stn0, Figure 32) close to the bottom of the ocean (about 250 m depth), decreasing to 133 % (3.6 nM) at the surface. The high concentrations close to the seafloor were not surprising given documented ebullition in the area (Cramm et al., 2021). The second depth profile taken in proximity to the seep, about 8 km northeast of its location (station SI2, Figure 32) showed a maximum of 25.4 nM (639 %, Figure 11) at 200 m depth and just slightly oversaturated surface water (113 %, 3.9 nM). Measurements from the year 2012 revealed CH_4 maxima of 65.8 nM at 200 m depth decreasing to 3.7 nM at the surface roughly 40 km northwest from the seep location (Punshon et al., 2019). Large temporal fluctuations of dissolved CH_4 levels between 9 and 609 nM within 24 hours were found close to the seafloor (~250 m) at the seep in 2018 (Cramm et al., 2021). Similarly, other studies manifested the temporal variability of seafloor seep degassing (Boles et al., 2001; Cramm et al., 2021; Dølven et al., 2022; Leifer and Boles, 2005; Shakhova et al., 2014). Concentrations at the water surface of the seep were in the single digits previously (Cramm et al., 2021), which was confirmed in this study (from 3.9 nM at station SI2 to 5.3 nM at station SE−1K, Figure 12). Considering the findings from Punshon et al. (2019), Cramm et al. (2021), and the present study, depths of 200−250 m around the Scott Inlet seep location seemed most prominent for CH_4 maxima. Furthermore, water columns supersaturated with CH_4 in proximity to this location over several years show the persistence of the seep activity. Surface concentrations close to the atmospheric equilibrium in 2012, 2018 and 2021 in this area may indicate significant oxidation of CH_4 within the upper

water column. The Scott Inlet stations should not be considered as representative of the Baffin Bay as a whole, but rather specific to the seep location.

Seawater oversaturated with CH_4 (338 %, 12.9 nM) was also found at 250 m depth at Makkovik (Figure 11), the southernmost station in this study. The Makkovik station was characterized by a strong gradient of water masses, with warm (6.3 °C) surface water, cold (~0 °C) sub-surface water featuring its CH_4 maximum and again warmer (3.8 °C) water at the seafloor.

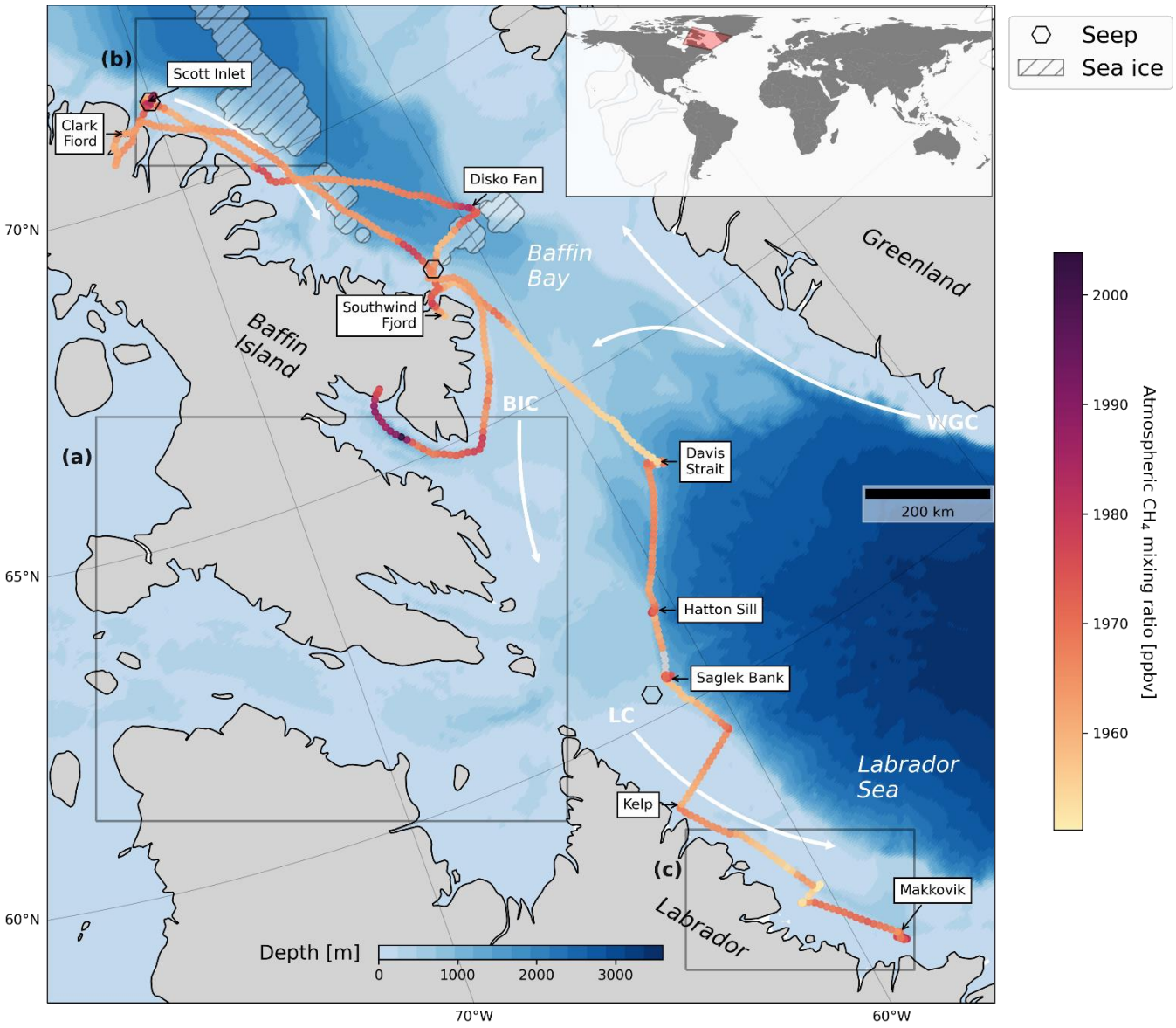

Figure 10: The ship's trajectory and atmospheric CH_4 levels as averages over consecutive 10 km sections. The black arrows point to the locations where water measurements were taken. The three black hexagons indicate confirmed or suspected locations of gas seepage (Cramm et al., 2021; Punshon et al., 2019, 2014). White arrows represent the West Greenland Current (WGC), Baffin Island Current (BIC) and Labrador Current (LC). Water depth was retrieved from the NOAA server (Amante and Eakins, 2009). Areas labelled a, b and c indicate the extents for each panel in Figure 33. Shaded areas represent sea ice cover above 10 % (copyright 2021, EUMETSAT).

Dissolved CH_4 levels of similar range were measured at Southwind Fjord with a maximum of 227 % oversaturation (8.8 nM) at about 30 m depth, 148 % (5.2 nM) at the surface, and 114 % (4.5 nM) at the bottom (100 m). Occurrences of highly supersaturated waters in Artic and sub-Arctic fjords have been documented previously: up to 33.5 nM and 974 % super-saturation in the Isfjorden, Svalbard, Norway (Damm et al., 2021), up to 72.3 nM and ~2000 % super-saturation in the Storfjorden, Svalbard, Norway (Mau et al., 2013) and up to 459.2 nM at the head of the Canadian sub-Arctic Saguenay fjord (Li et al., 2021). Most likely, the recent disturbance from iceberg groundings and subsequent landslides at Southwind Fjord (Normandeau et al., 2021) led to CH_4 release into the water column from a fresh supply of organic matter and lowered oxygen levels (Bonaglia et al., 2022). Other possible sources of enhanced dissolved CH_4 concentrations at this location could be terrestrial runoff (Castro-Morales et al., 2022), although Manning et al. (2022) found that rivers did not discharge significant amounts of CH_4 to the North American Arctic Ocean in the summers of 2017−2019. Advection of CH_4-rich water from other sources within the Baffin Bay could play an important role given the evidence of oil slicks off Cape Dyer for example (Budkewitsch et al., 2013). Otherwise, gas hydrates or CH_4-bearing pore water in the seafloor sediment disturbed by the turbulence of local landslides (Paull et al., 2002) could have resulted in CH_4 release into the water column. Overall, we recommend follow-up sampling to assess the persistence of the CH_4 oversaturation and its source at Southwind Fjord.

CH_4 saturations at the remaining stations ranged between 25−178 % (0.9−6.9 nM) at varying depths. Compared to measurements at nearby locations in 2012 and 2016 (Punshon et al., 2019, 2014), dissolved CH_4 concentrations in 2021 at the stations Hatton Sill, HiBio-C, and Disko Fan were very similar ranging between 0.9−5.6 nM (Figure 11). While concentrations at HiBio-A in all years showed similar ranges, a CH_4 peak of 6.8 nM (181 % saturation) in relatively shallow

water at 50 m depth was observed in 2021 suggesting advection of CH_4 within subsurface water masses from elsewhere. Similar, relatively shallow CH_4-rich water masses brought along by the Labrador Current may have provoked the CH_4 maxima at Kelp and Makkovik. Methane concentrations in the general Davis Strait area measured one decade before (Punshon et al., 2014) were in good agreement with our findings for the respective station (1.8−5.4 nM).

In 2021, surface water concentrations were above saturation at all stations including further locations around the Scott Inlet seep and at Clark Fiord where only surface samples were taken (3.6−5.3 nM, 115−153 %, Figure 12). Even though some sea ice was observed during the cruise, none of the water sample locations were in proximity to any significant sea ice cover (>10 %), so that local accumulation of CH_4-rich water below a surface ice layer as found previously (Damm et al., 2015) did not play a role here. A significant positive correlation of mixed layer mean dissolved CH_4 and oxygen levels at those stations where depth profiles were taken was found in this study (Spearman $R^2 = 0.63$, $p < 0.01$), which may suggest aerobic CH_4 production (Karl et al., 2008). Or else, sea ice melt may have discharged other precursors used by microbes to form CH_4 despite increasing oxygen levels towards the surface (Damm et al., 2015).

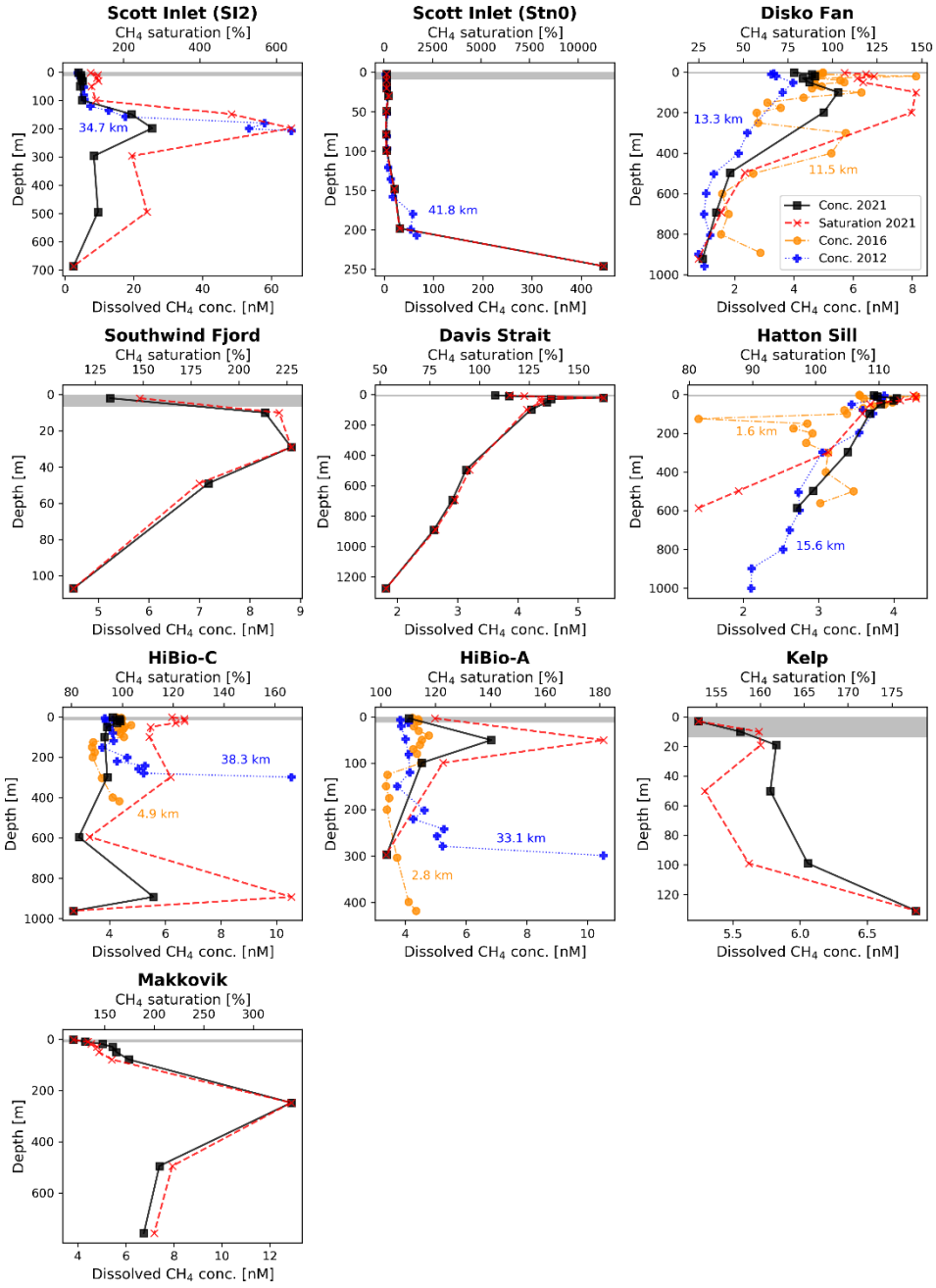

Figure 11: Depth profiles of dissolved CH_4 concentrations (black) and saturations (red, dashed line) throughout the water column. Station names are given and can be located in Figure 10 and Figure 32. Profiles from Punshon et al. (2014, 2019) conducted in 2012 and 2016 were included for each year's closest stations within 50 km of the ones from 2021 and are shown in blue (2012) and orange (2016). Distances between respective nearby stations are given in kilometres. The mixed layer depths are indicated by gray areas.

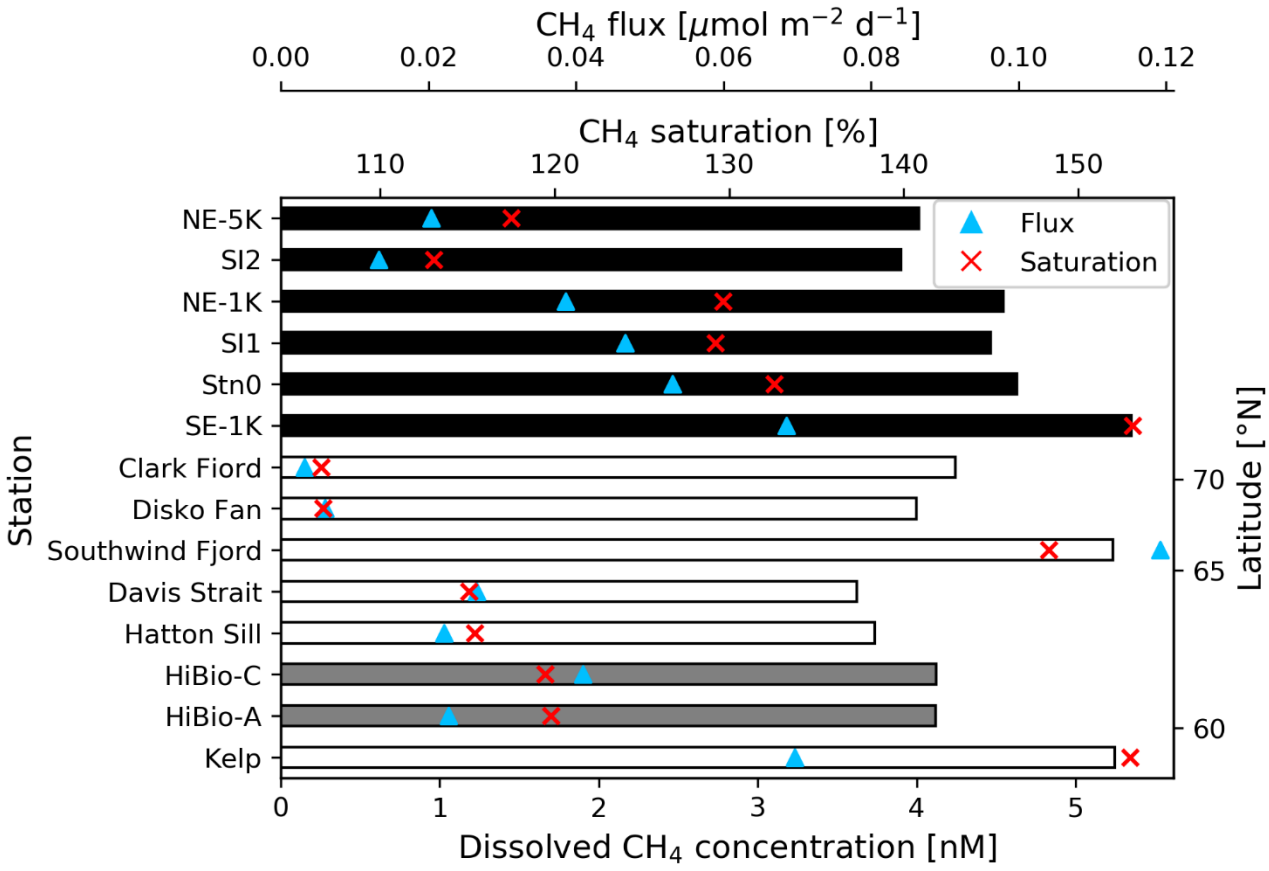

Figure 12: Dissolved CH_4 concentrations at the water surface (bars) for all stations where CTD-Rosette samples and atmospheric measurements were collected. Gray bars represent two sample locations in the Saglek Bank area, and black bars reflect samples in the Scott Inlet area, both close to seafloor seep locations (station names correspond to those in Figure 32). CH_4 saturations (red crosses) and estimated sea-air fluxes (blue triangles) are shown as well. Latitudes are not to scale.

The distribution of CH_4 with respect to water masses accounting for data from Punshon et al. (2014, 2019) and this study are visualized in a temperature-salinity diagram (Figure 13). Samples span the known upper and intermediate depth of water masses of the region, mainly Halocline Water (HW), followed by Irminger Water (IW), Labrador Shelf Water (LShW) and Baffin Bay Water (BBW). Highest concentrations were found in Arctic HW (mean: 10.3 nM, range: 2.4−445.3 nM), which was largely forced by the presence of the Scott Inlet seep (Figure 13). This

seep, and possibly others, could enrich the HW with CH_4 as HW travels southward in form of the Baffin Island Current. The overall shallowest water mass, the LShW, held the second highest CH_4 concentrations (mean: 4.3 nM, range: 1.1−21.1 nM) partially due to direct seep impacts, and possibly the influence of the Baffin Island Current transporting CH_4-rich water southward or of the West Greenland Current carrying elevated CH_4 levels westward, which may have provoked elevated CH_4 concentrations in LShW for example at Southwind Fjord, HiBio-A and possibly even at the Makkovik station. Warmer IW masses owned the third highest concentrations (mean: 3.2 nM, range: 1.0−10.5 nM). Increased oxygen availability was found in the Irminger Sea in 2015 (Fröb et al., 2016), but dissolved oxygen levels during our Rosette casts showed lower oxygen concentrations on average in the IW than in the shallower HW and LShW. The colder and deeper BBW mass showed lower CH_4 concentrations (mean: 1.7 nM, range: 0.2−17.0 nM) than the mostly oversaturated HW, LShW, and IW, whereas measurements in proximity to the Scott Inlet seep in 2021 and roughly 45 km north of the suggested seep at Cape Dyer in 2011 contributed to the high end (> 9 nM) of the concentration range for BBW. Most likely, both CH_4 production and consumption co-occurred in the BBW (Fenwick et al., 2017).

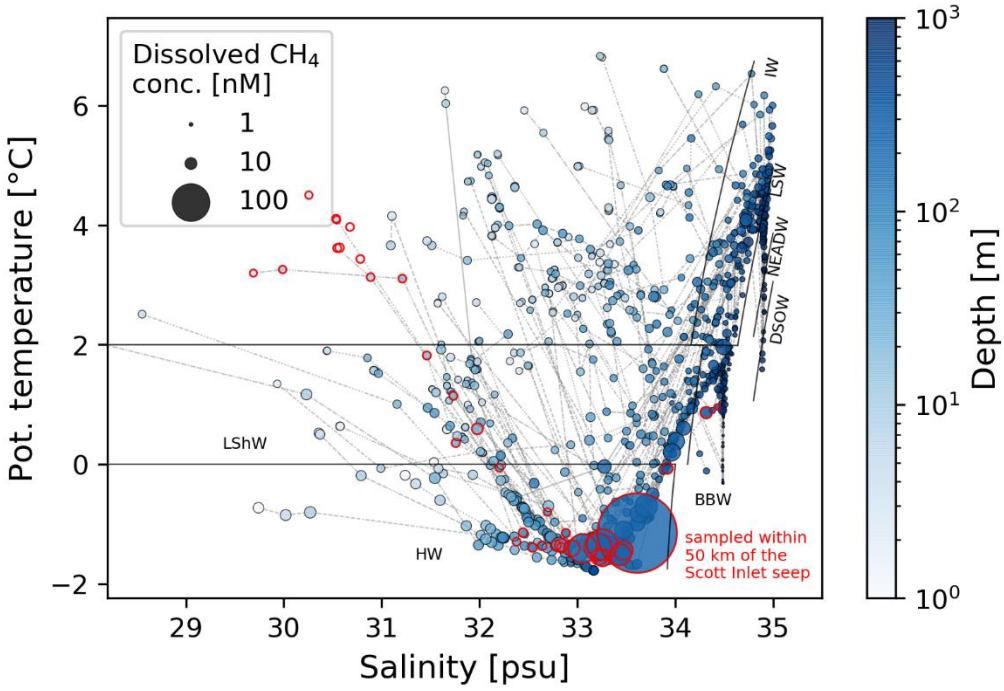

Figure 13: Temperature-salinity diagram of all measurements from 2021 and from the studies by Punshon et al. (2014, 2019) for the Baffin Bay and Davis Strait area. Dissolved CH_4 concentrations are shown with different marker sizes, colors indicate the water depth. Black lines distinguish between water masses: Halocline Water (HW), Labrador Shelf Water (LShW), Irminger Water (IW), Labrador Sea Water (LSW), Northeast Atlantic Deep Water (NEADW) and Denmark Strait Overflow Water (DSOW). Gray lines connect measurements from the same CTD-Rosette cast. For better visualization, salinities below 28 psu measured at the surface of the two fjords in 2021 are not shown. Red circles highlight the sample locations within 50 km of the seep in Scott Inlet.

Atmospheric CH_4 mixing ratios during the expedition ranged between 1944 ppbv off the coast of northern Labrador and 2012 ppbv in the Cumberland Sound in Nunavut (Figure 10), with an overall mean (± standard deviation) of 1966±8 ppbv. Wind speeds did not exceed 15 m s^{-1}. After applying the Savitzky-Golay filter to the measured data, baseline mixing ratios ranged between 1954 ppbv and 1981 ppbv (Figure 14). These concentrations were higher than global monthly

mean CH_4 mixing ratios in July (1886 ppbv) and August (1892 ppbv) of the sampling year 2021 (Dlugokencky, 2022), but were within range of values from surface flask-air measurements from the year 2020 from northern stations of the NOAA Global Greenhouse Gas Reference Network, e.g. Summit, Greenland (July: 1939 ppbv; August: 1947 ppbv) and Alert, Nunavut (July: 1933 ppbv; August: 1946 ppbv) (Dlugokencky et al., 2021). The mixing ratios measured in this study are higher than those determined from flask samples possibly due to the influence of a generally large number of CH_4 seeps in our study area. Our measured CH_4 values were consistent with the known latitudinal gradient and recent increase in atmospheric CH_4 (Lan et al., 2021). The baseline estimates suggest a local background CH_4 fluctuation of roughly 27 ppbv in the studied area. A recent study found a contribution of 42.5±25.2 ppbv to total CH_4 mixing ratios measured during a cruise in the eastern Arctic Ocean, suggesting that atmospheric CH_4 levels over the ocean can be affected by distant wetland CH_4 sources (Berchet et al., 2020).

Persistent enhancements of CH_4 mixing ratios above the baseline lasting over more than four hours were detected repeatedly over the length of the expedition (Figure 14). We investigated potential atmospheric origins of CH_4 maxima at three locations, Cumberland Sound, Scott Inlet, and the Labrador Trough, using ensemble back-trajectories (Figure 33). At Cumberland Sound, the maximum of 2012 ppbv coincided with prevailing westerly winds based on our measurements. Therefore, we assumed that those ensemble trajectories indicating air transport from or across the inland on the western side best reflected the observed meteorological conditions (Figure 33a). Since no water samples were taken in the Cumberland Sound, where the highest atmospheric CH_4 levels were observed, we could not rule out an ocean-related atmospheric input of CH_4 at this location. Instead, the back-trajectory analysis suggests that the elevated CH_4 mixing ratios could have originated from along the trajectories leading onshore,

where potential sources such as waterbodies or wetlands could be located (Berchet et al., 2020; Fisher et al., 2011; Thonat et al., 2017). The second highest CH_4 peak of 1994 ppbv was detected roughly 13 km northeast of the Scott Inlet seep with dominating easterly winds (Figure 33b). Given the distance of roughly 500 km from Greenland, the origin of this CH_4 enhancement could be ocean-based, with origins from further seeps along the continental shelf east of Scott Inlet (Gautier et al., 2011; Gregersen and Bidstrup, 2008; Nielsen et al., 2014). Trajectories for the third highest CH_4 levels of 1990 ppbv measured in the Labrador Trough coupled with west-south-west wind directions may suggest onshore sources from northern Labrador (Figure 33c).

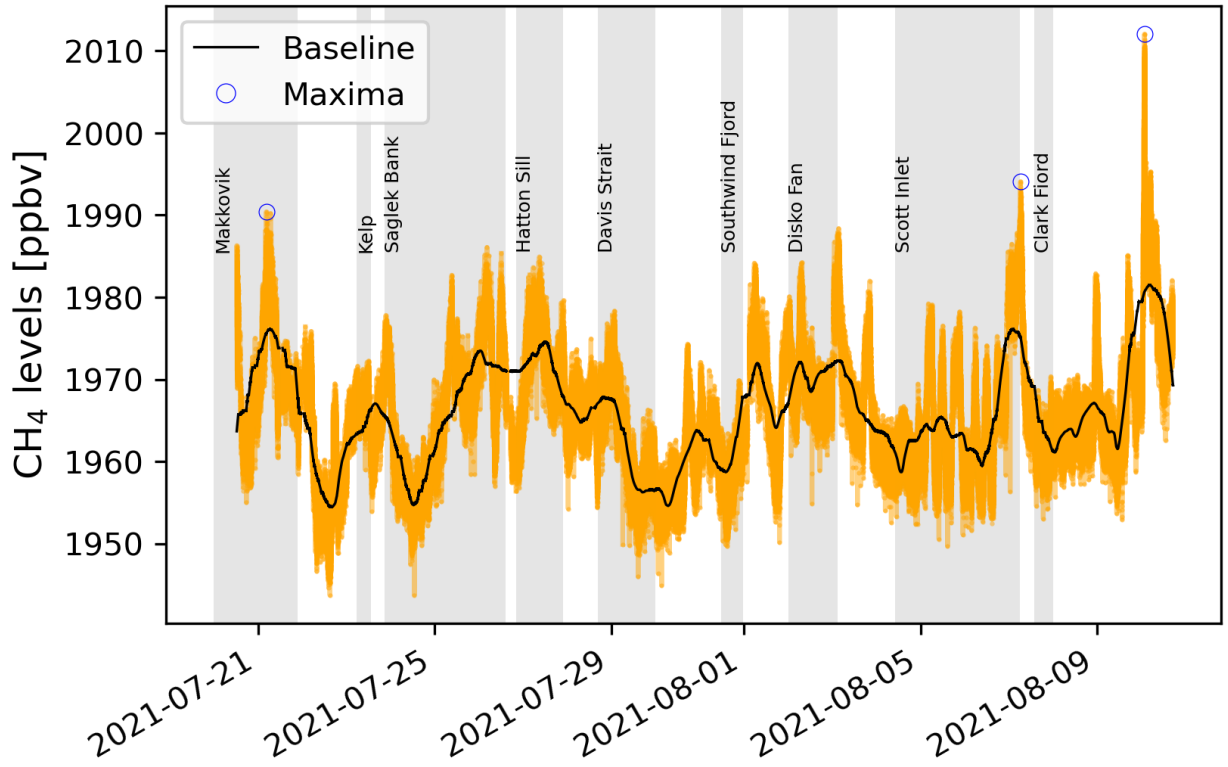

Figure 14: Timeseries of atmospheric CH_4 levels (orange points) and the derived baseline (black line) over the entire measurement period. Gray parts show the approximate duration at the stations (Amundsen Science Data Collection, 2021e), where seawater samples were collected. Blue circles reflect the three maxima of atmospheric CH_4.

Linear correlations between atmospheric and dissolved CH_4 levels based on our dataset were not found. Due to the atmosphere-sea surface barrier, and complexities added by wind conditions, ocean currents, bacterial activity within the water column and other processes, the atmosphere-ocean system essentially describes a decoupled system locally, so that increased CH_4 concentrations are not necessarily found alongside rising atmospheric CH_4 levels (Cramm et al., 2021; Law et al., 2010; Punshon et al., 2019; Zhao et al., 2022). Accordingly, simple linear correlations of CH_4 mixing ratios with available auxiliary data (latitude, longitude, speed, wind speed and direction, air temperature, humidity, dew point temperature, atmospheric pressure, water temperature, salinity, hour of day) were not found, suggesting more complex relationships. Instead, results of a Generalized Additive Model proposed spatial (latitude, longitude), temporal (hour of day) and meteorological (atmospheric pressure, dew point temperature) influences on hourly averaged atmospheric CH_4 mixing ratios with a good fit ($n = 171$, $R^2 = 0.84$, 88 % explained deviance) for the parts of the cruise when these data were available. Therefore, we suggest that atmospheric CH_4 levels were influenced by a number of processes including, but not limited to seafloor seeps, upwind distant land-based sources like wetlands and other waterbodies, weather conditions and ultimately temporal and spatial differences.

Based on our measurements, we determined a near-zero net flux of CH_4 from the ocean to the atmosphere, which amounted to a mean of 0.039 ± 0.031 µmol m^{-2} d^{-1} along Baffin Island and Labrador in 2021, compared to 1.6 µmol m^{-2} d^{-1} in Davis Strait in 2011 (Punshon et al., 2014). Overall, sea-air fluxes in this study peaked at 0.119 µmol m^{-2} d^{-1} in the Southwind Fjord, exceeding the flux rates at the Scott Inlet seep (Figure 12). As a result, fluxes in the northern Labrador Sea and Baffin Bay were negligible in summer 2021 in comparison to mean estimates of 8.7 µmol m^{-2} d^{-1} for the Chukchi Sea (Thornton et al., 2020), of 1.3 µmol m^{-2} d^{-1} for the Bering

Sea to Baffin Bay (Fenwick et al., 2017), or of 0.4 μmol m^{-2} d^{-1} for the Baffin Bay and Davis Strait from measurements between 2015−2019 (Manning et al., 2022).

3.4 Conclusion

Continuous measurements of atmospheric CH_4 levels in the northern Labrador Sea and Baffin Bay were above the global marine average with small instantaneous input from the ocean. Differences in dissolved CH_4 concentrations were mainly affected by ocean currents and seafloor sources, while atmospheric CH_4 levels showed interrelations with environmental conditions, location, and time with small temporal fluctuations. Both ocean-based CH_4 sources as well as onshore waterbodies and wetlands likely contributed to atmospheric CH_4 levels. Further investigation is necessary to confirm potential CH_4 sources, for example through analyses of carbon isotopic ratios and more extensive back-trajectory modelling. We suggested baseline CH_4 mixing ratios between 1954 ppbv and 1981 ppbv for the studied area which can be used to validate global-scale measurements and modelling. Depth profiles and their comparison with measurements from previous years in the studied area revealed little interannual variation and ongoing CH_4 to the hydrosphere from the Scott Inlet cold seep. More extensive investigation of the chemical composition of sediments, bacterial activity, and riverine input could help explain elevated CH_4 levels within the shallow water column at Southwind Fjord, where recent landslides triggered by an iceberg were observed. Even though the Arctic Ocean does currently not contribute significantly to the global CH_4 budget as found by other studies, monitoring and investigation of CH_4 levels in and over the sea remain relevant to assess potential impacts of climate change in regions susceptible to permafrost thaw, destabilization of CH_4 hydrates and reduced sea ice cover.

3.5 Acknowledgements

We would like to thank the teams from Amundsen Science and the Canadian Coast Guard for their incredible work in preparation of, and during leg 2 of the 2021 expedition. Some of the data presented herein were collected by the Canadian research icebreaker CCGS *Amundsen* and made available by the Amundsen Science program, which is supported through Université Laval by the Canada Foundation for Innovation. We also thank FluxLab members for their support during equipment preparation, especially Isaac Ketchum and Daniel Wesley. We thank Dr. Carrie-Ellen Gabriel and Darlene Childs for analyzing the seawater samples, and Dr. Simone Booker, Shaomin Chen and other cruise participants who assisted in the sample collection. Funding was provided by an NSERC ship time grant to Dr. Owen Sherwood and others (RGPST-544990-2020) and a NSERC Discovery Grant awarded to Dr. Owen Sherwood (RGPIN-2018-05590). Seawater analysis was funded through The Aquatic Climate Change Adaptation Services Program (ACCASP) of DFO.

Chapter 4: Active and inactive oil and gas sites contribute to methane emissions in western Saskatchewan, Canada

Preamble

This chapter was published in Elementa: Science of the Anthropocene. I helped conceptualize the study and led the field work. Furthermore, I gathered external data, analyzed all measurements, produced figures and tables, and wrote the manuscript. During the preparation of the field work for this study, the pandemic hit, and last-minute adjustments had to be made due to travel restrictions and shutdowns, which added complications to the execution of the project. In addition, health protocols had to be followed in the field, including an isolation period post-field. This study was conducted under supervision of my current supervisor, David Risk. The manuscript was co-authored with Justin Laforest, Mark Argento, Sarah Kennedy, Evelise Bourlon, Martin Lavoie, and David Risk. Justin Laforest, Mark Argento, and Sarah Kennedy assisted with field measurements. Evelise Bourlon processed the collected data, developed the method for the analysis of stationary measurements and assisted in the interpretation of the results. Martin Lavoie helped conceptualize the study, provided insights regarding the interpretation of measured and external data. David Risk supported the conceptualization of the study, supervised, gathered funding and provided insights regarding the interpretation of the data. All co-authors provided helpful comments for the preparation of the final manuscript.

4.0 Abstract

The oil and gas industry is Canada's largest contributor to national methane (CH_4) emissions. To quantify the input of active and inactive (suspended and abandoned) oil and gas infrastructure to regional CH_4 budgets, we conducted truck-based measurements (transect-based and OTM 33A)

with a greenhouse gas analyzer, complimented with optical gas imaging at oil-producing sites of Saskatchewan, including understudied regions. We found that inactive sites regionally accounted for roughly 43% of total measured CH_4 emissions in Lloydminster, 9% in Kindersley and 0% in Swift Current. Thus, CH_4 emissions from oil production in southwestern Saskatchewan are underestimated by almost 25% if emissions from inactive sites are ignored. Measured mean CH_4 emissions of actively producing oil and gas infrastructure in Lloydminster were at least 50% lower (36±7 m^3 day^{-1}) than found in previous studies potentially due to declines in production schemes, effective implementation of emission reduction approaches, or spatial differences between sampled sites. Unlike previous studies, measured emissions in Lloydminster were lower than reported values (147±10 m^3 day^{-1}). In contrast, measured emissions in Kindersley (64±17 m^3 day^{-1}) and Swift Current (23±16 m^3 day^{-1}) were close to reported emissions despite observed tank vents and unlit flares. Unlit flares emitted at least three times more CH_4 than other infrastructure types, and were the "super-emitters" in this study. Currently, provincial and federal regulations target only active infrastructure but regulators may consider extending regulations to inactive sites where data suggests significant emission reduction potential.

4.1 Introduction

The oil and gas industry is Canada's largest contributor to national methane (CH_4) emissions (Environment and Climate Change Canada, 2019). In the upstream oil and gas sector, the greenhouse gas CH_4 is mostly released to the atmosphere in the form of vented (intentional) or fugitive (unintentional, uncontrolled leaks) emissions. CH_4 is rated a toxic and flammable gas, which also has a high potential to warm the Earth (up to 83 times greater than that of the greenhouse gas carbon dioxide over a 20-year period (Forster et al., 2021). Therefore, CH_4 emissions from the oil and gas industry should be reduced to mitigate global warming.

Saskatchewan is the second largest oil producing province in Canada. In 2019, the Canadian province of Saskatchewan released Oil and Gas Emissions Management Regulations together with a Methane Action Plan (Ministry of Energy and Resources, Government of Saskatchewan, 2019a). With these initiatives, the Government of Saskatchewan plans to target CH_4 emission reductions from the upstream oil and gas sector by 4.5 million tonnes CO_2 equivalent annually by 2025, and will enforce a subsequent emissions cap until 2030. Some argue that the Saskatchewan measures fall short of the federal targets and measures introduced earlier (Gorski, J., 2019) but the federal government did accept the provincial measures as equivalent. Due to the impact of the COVID-19 pandemic on the oil and gas industry, the provincial government introduced temporary relief measures of CH_4 emission regulations, including exemptions regarding leak detection and repair surveys (Ministry of Energy and Resources, Government of Saskatchewan, 2020a).

Federal and provincial regulations were crafted with only partial understanding of present-day emission levels and sources. Various oversight studies using trucks and aircraft have pegged emissions at higher levels than inventory estimates (Atherton et al., 2017; Baillie et al., 2019; Chan et al., 2020; Johnson et al., 2017; Lan et al., 2015; Li et al., 2020; MacKay et al., 2021, 2019; O'Connell et al., 2019; Yacovitch et al., 2015; Zavala-Araiza et al., 2018). By now, most oil and gas regions in western Canada have been measured but oil-producing sites in western Saskatchewan have escaped oversight. Emission rates may vary significantly per region (MacKay et al., 2021), infrastructure type (Lavoie et al., 2022), and over time assuming adaptation to new CH_4 emission reduction regulations. Therefore, it is important to frequently conduct measurements covering a wide geographical region with different infrastructure types to obtain an accurate picture of overall CH_4 emissions.

In a global assessment of CH_4 emissions from the oil and gas sector, suspended and abandoned infrastructure was assumed to be non-emitting (Scarpelli et al., 2020). However, several studies identified that abandoned infrastructure also emits measurable amounts of CH_4 to the atmosphere (Boothroyd et al., 2016; Kang et al., 2016, 2014; Pekney et al., 2018; Riddick et al., 2019; Saint-Vincent et al., 2021; Townsend-Small et al., 2016; Williams et al., 2019). The Canadian federal inventory does account for emissions from suspended and abandoned infrastructure, but not in a clear way since emission factors are based on a single study restricted to a selection of abandoned wells, which may be plugged or unplugged in the US (Environment and Climate Change Canada, 2020; Townsend-Small and Hoschouer, 2021). However, in Canada jurisdictions differ among provinces, so that the plugging status of a well often remains unclear based on the information reported by operators when comparing nationwide. In addition, numbers of abandoned wells and their associated CH_4 emissions generally constitute large uncertainties in CH_4 emission inventories, particularly in Canada and the US (Environment and Climate Change Canada, 2020; Williams et al., 2021). The contribution of suspended and abandoned infrastructure to CH_4 emissions on a provincial and federal level remains unclear, as this infrastructure type is often ignored in measurement-based studies. If the overall contribution is significant, but remains overseen, Canada may fall short on achieving CH_4 emission reduction targets in the near future.

To quantify the contribution of suspended and abandoned oil and gas infrastructure compared to emissions from active infrastructure in western Saskatchewan, we conducted mobile and stationary truck-based measurements in three different regions.

4.2 Materials and Methods

4.2.1 Study area

For this study, three different oil and gas producing regions in Canada's western province Saskatchewan were selected: Swift Current, Kindersley and Lloydminster. In the surveyed areas, wells produce oil and gas from the Hogeland Basin in Swift Current, from the Bow Island Arch in Kindersley and from the Athabasca Oil Sand Zone (Alberta Basin) in Lloydminster. Its economic distinction as the 'Heavy Oil Capital of the World' correctly implies that Lloydminster produces mostly heavy oil. Production in Kindersley is dominated by gas and light oil, whereas Swift Current is characterized by gas and medium-dense oil production (Ministry of Energy and Resources, Government of Saskatchewan, 2021, 2020b).

4.2.2 Reported emissions

In Saskatchewan, solution gas emissions from the oil and gas industry are reported to the provincial government each month. Emissions are assessed by reporting facility connected with a certain number of wells via pipelines. The reports are made public each year, including the volume of solution gas emitted to the atmosphere through fuel processes, venting and flaring (Ministry of Energy and Resources, Government of Saskatchewan, 2020c). The CH_4 content of solution gas is roughly 80% in Swift Current, 85% in Kindersley and 90% in Lloydminster. We assumed that for fuel emissions CH_4 was fully combusted and did not contribute to CH_4 release to the atmosphere, whereas 5% of flared and 100% of vented emissions were associated with reported CH_4 emissions. In addition to the publicly available annual report, we obtained the monthly report for September 2020 from the Government of Saskatchewan upon request.

4.2.3 Field measurements

All field measurements were conducted in September 2020 with a mobile laboratory. This laboratory consisted of a truck equipped with an Off-Axis Integrated Cavity Output Spectrometer measuring CH_4, CO_2 and H_2O (Ultraportable Greenhouse Gas Analyzer, Los Gatos Research, USA), a heated 2D Ultrasonic anemometer (Model 86004, RM Young, USA), a high-sensitivity GPS sensor (GPS 18x 5 Hz, Garmin, USA), and an electronic compass (Model 32500, RM Young, USA) to collect atmospheric measurements at a 2 Hz frequency (further details in Appendix B, Figure 34). During times when the GPS sensor was not working properly, we used auxiliary truck positions obtained with a cellphone (GPS Tracker Application). Real-time data were monitored on a laptop and simultaneously recorded on a datalogger (CR1000X, Campbell Scientific, Canada). In addition, we used a hand-held optical gas imaging (OGI) camera (FLIR GF320, USA) to visually detect gas leaks and vents *in situ*.

4.2.4 Mobile surveys

To obtain CH_4 emission rates attributed to oil and gas infrastructure located within the three studied regions (Appendix B, Figure 35 and Figure 36), measured CH_4 and carbon dioxide (CO_2) concentrations, wind parameters, GPS locations and compass directions were analyzed based on an established algorithm modeled after Zavala-Araiza et al. (2018) and further described elsewhere (Atherton et al., 2017; Hurry et al., 2016). In brief, we first filtered out inconclusive values, corrected and smoothed wind parameters with GPS and compass data and linearly interpolated gaps. Subsequently, we identified excess levels of CH_4 and CO_2 (Appendix B, Figure 35 and Figure 36) subtracting background levels determined with a running minimum over a moving window varying between 1−30 minutes depending on the best fit. Where the ratio of excess (*e*) concentrations eCO_2:eCH_4 < 100 indicated significant CH_4 enhancement relative to

the regular atmospheric concentration, we conducted back trajectory analysis in an effort to attribute the enhancement to known infrastructure upwind and within 400 m. The eCO$_2$:eCH$_4$ ratio was used to distinguish biological and combustion sources from oil and gas-related emitters, which are subject to substantial CH$_4$ relative to CO$_2$ enhancement. Where attribution was possible, CH$_4$ emission rates were estimated for each detected anomaly with an inverse Gaussian plume model considering peaks of enhanced CH$_4$ concentrations, height of the attributed source, distance to the source as well as atmospheric stability determined using meteorological data from nearest weather stations.

Truck-based measurements occurred at a site-level, and cannot be used to discriminate between co-located infrastructure. For this study, we grouped co-located infrastructure at a radius of 45 m, where all infrastructure within the radius was associated with the same group. The groups consisted of 1-12 wells or facilities. The terms ‘group’ and ‘site’ are used interchangeably in this study.

Infrastructure groups were considered sampled when the truck passed by downwind within a distance of 400 m at least twice. If anomalous CH$_4$ concentrations were detected from sampled infrastructure on more than 50% of passes, the group was tagged as emitting. However, if several upwind groups fulfilled this criterion, only the closest group was tagged as emitting.

Infrastructure groups were classified according to production status. Active groups consisted of at least one piece of active infrastructure plus any number of inactive infrastructure. Inactive groups consisted solely of inactive infrastructure. Suspended and abandoned wells were defined as inactive. Following the provincial Directive PNG032 (Ministry of Energy and Resources, Government of Saskatchewan, 2018), suspended wells are those which are capable, but temporarily not producing and usually unplugged. We assume here that abandoned wells must be

plugged as per Saskatchewan's provincial Directive (Ministry of Energy and Resources, Government of Saskatchewan, 2019b), which differs from jurisdictions in other provinces in that well infrastructure may still be present albeit plugged. All other wells were assumed to be actively producing or injecting fluid. Inactive facilities were either decommissioned or suspended, although facility data did not distinguish between suspended and abandoned status. This classification relies on compliance of oil and gas operators who report and update well and facility status. Therefore, the distinction between active and inactive groups may be inaccurate in rare cases, but we assume that databases are correct. Emissions from active infrastructure might consist of both vented and fugitive emission sources, but since inactive sites should not be emitting, all emissions would be considered as fugitive in nature.

For in-depth analysis of emissions from inactive sites, we sub-categorized inactive infrastructure groups based on the well status (suspended or abandoned), disregarding facility status in case the group was assigned a facility. The sub-categories for inactive infrastructure groups were thus ‘suspended’, ‘abandoned’, ‘suspended and abandoned’ for mixed groups, or ‘unknown’ for groups only consisting of facilities where the distinction between suspended and abandoned status was unclear based on our dataset.

Sampled infrastructure was measured several times, and we report the mean estimates for each emitting group. In addition to standard statistics on a regional level, bootstrapped confidence intervals (CI) of the mean were also determined with 1000 bootstrap samples generated with replacement using the bootstrap percentile method (Efron and Tibshirani, 1986). The emission estimation approach used in this study entails a standard error (SE) of roughly 63% for point-sources and tends to underestimate the emission rate as described in O’Connell et al. (2019). The same approach was used in numerous studies investigating emissions from oil and gas sites from

mobile surveys (Atherton et al., 2017; Baillie et al., 2019; Hurry et al., 2016; Lavoie et al., 2022; MacKay et al., 2021, 2019; O'Connell et al., 2019).

Where emission rates resulted from a one-time emission only despite several passes with the truck, we verified if the respective infrastructure group was misattributed through visual inspection. As a note, active sites were prioritized over inactive sites for emission attribution during this process. Emission rates for misattributed sites (23 total) were reset to zero.

The emission frequency for each region was assessed by dividing the number of emitting infrastructure groups by the number of sampled infrastructure groups (emitting and non-emitting). Regional per-site emission rates were determined as the mean of all emission rate estimates including zeros, which corresponds to the product of the emission frequency and the mean emission rate of all emitting infrastructure groups per surveyed area.

During mobile CH_4 measurements, we followed pre-determined routes within the three regions stretching over nearly 2000 km in total (Appendix B, Figure 35 and Figure 36). These routes were subdivided into transects, with each transect surveyed consecutively in triplicate. Whenever we identified potentially high oil and gas-related CH_4 sources during mobile surveys, we conducted stationary CH_4 measurements.

4.2.5 Stationary measurements

To complement our understanding of high emitters, we also applied a method similar to the stationary Other Test Method 33A (Edie et al., 2020) (hereafter: OTM) developed by the U.S. Environmental Protection Agency. The most recent study suggests a 2σ error of ±70% for a single OTM 33A measurement and a low bias of roughly 5% for an ensemble of measurements (Edie et al., 2020). In addition, several studies agreed upon the fact that OTM-based emission

rates tend to be underestimated (Bell et al., 2017; Brantley et al., 2014; Edie et al., 2020; Robertson et al., 2017).

In this study, we conducted mobile surveys and stationary measurements consecutively. When a high-emitting source was identified during mobile surveys, we subsequently returned to the source location and confirmed the emitting source with the OGI camera if possible (Appendix B, Figure 38). Then, the truck was parked downwind of the emitter and free of major obstructions, while the gas analyzer and other instruments were recording measurements and were powered by the truck battery. For emission rate estimation purposes, the distance from the truck to the source was measured using a laser range finder and the source height was estimated visually. Stationary CH_4 measurements lasted between 20 to 45 minutes at each site, at distances between 27 to 209 m from the source.

As for mobile surveys, the inverse Gaussian plume approach was applied to obtain emission rate estimates for OTMs. The stationary field measurements were conducted under the U.S. Environmental Protection Agency framework with slightly different data processing procedures. For rate estimation purposes, data obtained during OTMs was split into 20-minute long overlapping intervals shifted by one minute from each other. Therefore, at least one emission estimate was calculated per source (for a 20-minute long OTM) and up to 25 emission estimates (for a 45-minute long OTM). We assumed that the local ambient background concentration of CH_4 was measured during these 20-minute windows. The lowest 10% quantile of the measured CH_4 values was subtracted to obtain eCH_4. The initial azimuth of the source relative to the truck location was derived from the wind direction from which we observed highest eCH_4 concentrations. The wind speed was assumed constant over the 20-minute intervals and equal to the median wind speed. Both the final source azimuth and atmospheric stability class were

chosen based on the best fit of the model. The vertical and horizontal spread of the emission plume was calculated using the Turner model (Turner, 1970). The emission rate was estimated for each 20-minute window based on wind direction versus *e*CH_4 profiles, and the median of these emission rate estimates for each location was used for further analysis. To adequately meet the Gaussian dispersion assumption, truck-to-source distances had to exceed a minimum of three times the source height. In this study, all stationary measurements satisfied this criterion.

In the field, we visually assigned each OTM to the emitting infrastructure, and using field notes, photos and infrastructure databases (further details in Appendix B) we determined whether the infrastructure was active or inactive (suspended or abandoned).

4.3 Results and Discussion

During mobile surveys, we sampled 1220 infrastructure groups consisting of 1 to 12 single pieces of infrastructure each. This corresponded to 2226 pieces of infrastructure, primarily wells and batteries, injection plants and meter stations. In total, we attributed CH_4 emission rates to 317 infrastructure groups, which resulted in an overall emission frequency of 26%. 57% of total sampled infrastructure groups were categorized active and the remaining 43% inactive. Among the groups tagged as emitting, 69% were active and 31% inactive.

For stationary measurements, we estimated CH_4 emission rates at 19 different locations. Eighteen of them were conducted downwind of active sites, and one at an inactive site. The OTM sources of interest were mostly tanks, but also flare stacks, wellheads and pneumatic or engine sheds.

4.3.1 CH_4 emissions from active infrastructure groups

CH_4 emission rate estimates of active infrastructure in this study varied widely among surveyed areas (Figure 15), showing the characteristic heavy-tailed emission rate distributions as

documented in other studies (Brandt et al., 2016; Zavala-Araiza et al., 2018). Only 7 emitting (out of 120 sampled) active groups were identified in the Swift Current region during mobile surveys, however the emitters were individually large which meant that the estimated mean CH_4 emissions in Swift Current exceeded those found in Kindersley and Lloydminster (Table 3). The highest number (142 out of 405) of emitting active groups were found in Kindersley, followed by Lloydminster with 71 (out of 167) emitting active groups but lower mean emissions than in the other two regions (Table 3).

Emission frequencies were 6% for Swift Current, 36% for Kindersley and 44% for Lloydminster (Table 3). Mean per-site emission rates (±SE) for active infrastructure including non-emitting sites in Swift Current were 23±16 m^3 day^{-1} (95% CI: 1−59 m^3 day^{-1}), 64±17 m^3 day^{-1} Kindersley (36−101 m^3 day^{-1}), and 36±7 m^3 day^{-1} in Lloydminster (24−52 m^3 day^{-1}) based on our mobile surveys (Figure 16).

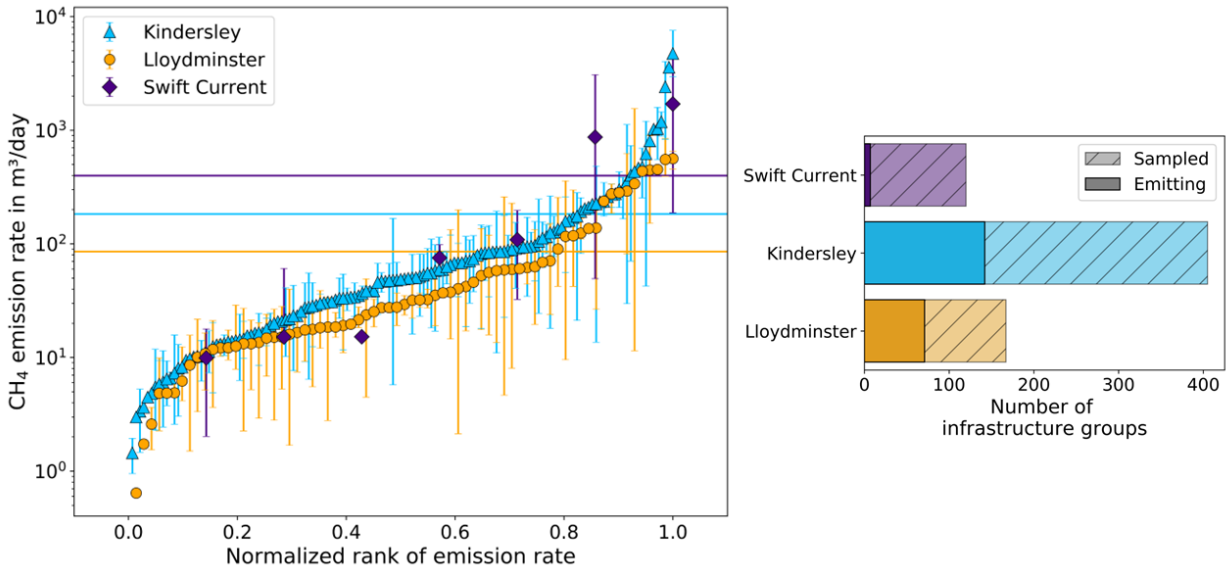

Figure 15: Ranked emission rates for active infrastructure. Left: The individual points indicate mean CH_4 emission rate estimates for each active infrastructure group that was tagged as emitting during mobile surveys. The bottom of the whiskers represents the minimum emission rate estimate per emitting group and the top represents the maximum. Mean CH_4 emission rates of emitting sites in each development are shown as continuous horizontal lines. According to their normalized rank, emission rates are listed from small (0 on x-axis) to large (1). Note that the y-axis is logarithmic and that non-emitting sites are not shown in this panel. Right: Number of active infrastructure groups sampled and emitting in the three regions.

Table 3: Emission frequencies and rates for active infrastructure. Emission frequencies are given in percent, emission rates in $m^3\ day^{-1}$ per area for all emitting, active groups: Mean, median, minimum, maximum, 25th and 75th percentile, standard deviation (SD) and error (SE) and bootstrapped 95% confidence interval (CI) of the mean for 1000 bootstrap resamples with replacement. Minimum and maximum were associated with group emission estimates per anomaly, the remainder with group-mean emission rates. Values were rounded.

Stats.	**Unit**	**Area**		
		Swift Current	**Kindersley**	**Lloydminster**
Freq.	%	6	36	44
Mean	$m^3\ day^{-1}$	399	183	86
Med.	$m^3\ day^{-1}$	75	49	29
Min.	$m^3\ day^{-1}$	2	1	1
Max.	$m^3\ day^{-1}$	4497	7550	1548
25%	$m^3\ day^{-1}$	15	18	15
75%	$m^3\ day^{-1}$	488	103	66
SD	$m^3\ day^{-1}$	652	551	134
SE	$m^3\ day^{-1}$	246	46	16
95% CI	$m^3\ day^{-1}$	36−872	107−280	58−121

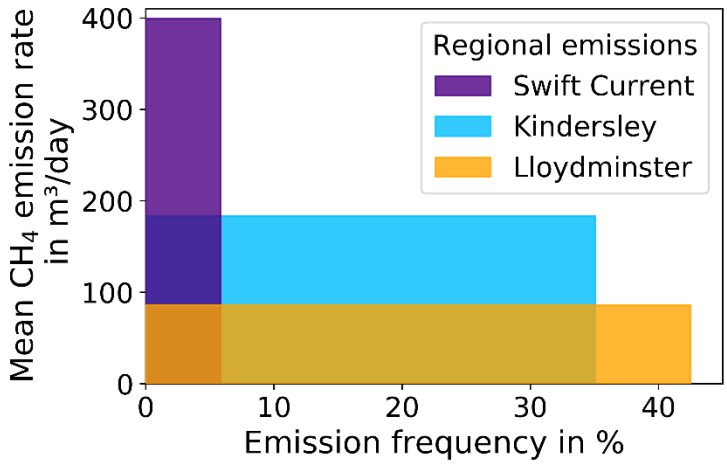

Figure 16: Site-level emission rates. The rectangles show the regional emission rates for active infrastructure groups in $m^3\ day^{-1}$ per area as a product of emission frequency (x-axis) and mean CH_4 emission rate (y-axis). Thus, the larger the area of the rectangle, the higher the regional emissions.

OTM-based emission rate estimates for active infrastructure ranged from 45−4155 $m^3\ day^{-1}$ with highest emissions from unlit flares (Figure 17). Top-emitter rate estimates from active infrastructure during mobile surveys were in the same order of magnitude as the top OTM-based estimates. In the Kindersley area, highest group estimates from mobile surveys (mean±SE; 4719±1303 $m^3\ day^{-1}$) slightly exceeded hotspot OTM-based estimates, whereas top estimates in Swift Current (1700±1400 $m^3\ day^{-1}$) and Lloydminster (562±54 $m^3\ day^{-1}$) were lower during mobile surveys. OTM-based emission estimates for active infrastructure were generally higher than in-motion estimates due to the fact that the truck was stationary for up to 45 minutes allowing for local concentration increases within the emission plume to be captured as opposed to quick passes with the moving truck. Although we observed differences between the two approaches, the differences were not systematic. Both types of measurements are shown in Figure 18.

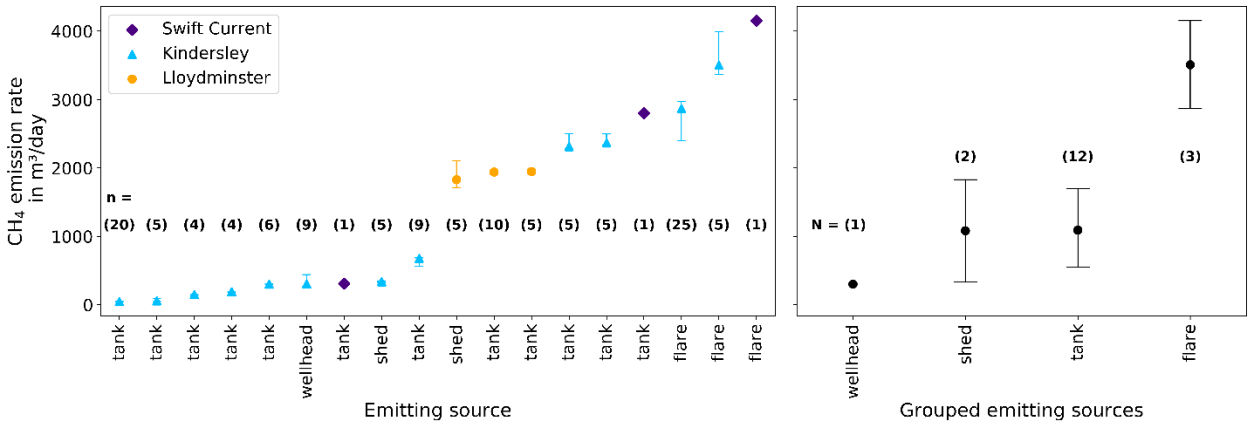

Figure 17: OTM-based emission rate estimates. CH_4 emission rate estimates for active infrastructure from OTM measurements in Swift Current, Kindersley and Lloydminster. Emission estimates as the median of all observations are shown per individual location on the left. The mean of those emission rate estimates grouped by emitting sources are shown on the right. The errorbars indicate the bootstrapped 95% CI of emission rates using 1000 bootstrap iterations. The numbers in brackets represent the numbers of observations per source (n), and the number of surveyed sources per grouped source (N).

Figure 18: Comparison of emission estimates from mobile and stationary measurements. CH_4 emission rate estimates for active and inactive infrastructure based on mobile surveys and OTMs for the three regions. The bigger the bubbles the higher the emission rate. Locations correspond to the centroid of emitting infrastructure groups for mobile surveys, and to truck locations for OTMs.

According to our field observations during OTMs, which we carried out at large-emitting sites, we noticed a dominance of venting tanks in Kindersley, but unlit flares generally tended to emit highest amounts of CH_4 (Figure 17). Overall, unlit flares emitted (mean±SE) 3508±371 m^3 day^{-1}, venting tanks 1091±311 m^3 day^{-1}, venting pneumatic or engine sheds 1082±747 m^3 day^{-1} and

leaks from wellheads 301 m^3 day^{-1}. Therefore, unlit flares emitted on average at least three times more CH_4 to the atmosphere than any of the other active oil and gas infrastructure. Based on our OTM measurements, 40% of total estimated CH_4 emissions were attributed to emissions caused by (three) unlit flares and 50% to (twelve) venting tanks, while the remaining 10% were emissions from sheds and wellheads. While CH_4 emissions from unlit flares can *per se* be easily avoided, tank vents are a known issue contributing to large CH_4 emissions (Tyner and Johnson, 2021). However, regulations currently do not explicitly target the mitigation of tank vents (Environment and Climate Change Canada, 2019) and preventative measures are needed.

CH_4 emission rates from the upstream oil and gas sector in western Canada have been determined in previous OGI, stationary, truck-based, and airborne studies (Anhalt, J., 2016; Atherton et al., 2017; Baillie et al., 2019; Chan et al., 2020; Johnson et al., 2017; MacKay et al., 2021, 2019; Roscioli et al., 2018; Zavala-Araiza et al., 2018). Mean site-level CH_4 emissions varied widely from < 1 m^3 day^{-1} in the Weyburn CO_2-Enhanced Oil Recovery field (MacKay et al., 2019) to 324±79 m^3 day^{-1} (reported as 24.1±5.9 t h^{-1}) in Lloydminster, Alberta (Johnson et al., 2017). Compared to other studies, mean per-site CH_4 emission rates estimated for Swift Current were on the same order as Drayton Valley (26 m^3 day^{-1}, reported as 6 t yr^{-1} (Anhalt, J., 2016)) and Red Deer (27 m^3 day^{-1}, reported as 7 t yr^{-1} (Anhalt, J., 2016); 29 m^3 day^{-1} (MacKay et al., 2021)) in Alberta, and Midale in southeastern Saskatchewan (20 m^3 day^{-1} (Baillie et al., 2019)). Mean per-site emission rates in Kindersley were comparatively high, similar to emission estimates previously measured in Lloydminster (72 m^3 day^{-1} in 2016 and 74 m^3 day^{-1} in 2017 (MacKay et al., 2021)).

Most emission quantification studies in western Canada assessed that measured emissions exceed the amount reported to provincial regulatory bodies and in national CH_4 emission inventories

(Atherton et al., 2017; Baillie et al., 2019; Chan et al., 2020; Johnson et al., 2017; MacKay et al., 2021; Roscioli et al., 2018; Zavala-Araiza et al., 2018). We compared measured emission rates in each region with emission values reported to the Government of Saskatchewan. These reported emissions comprise both vented and flared emission estimates, which are typically intentional, whereas emission estimates obtained from our mobile surveys also include uncontrolled fugitive emissions where present. We compared measured to reported emissions in Figure 19, assuming that our momentary emission estimates were representative for emissions during the course of 2020. Facility-level emissions based on measurements in September 2020 were not significantly different from annual or monthly reported emissions in Swift Current (95% CI: 38−58 m^3 day^{-1} in 2020, 49−76 m^3 day^{-1} in September 2020) and Kindersley (65−79 m^3 day^{-1} in 2020, 77−97 m^3 day^{-1} in September 2020). However, measured emissions in Lloydminster (24−52 m^3 day^{-1}) were significantly lower than emissions reported for the whole year of 2020 (86−106 m^3 day^{-1}), and even lower than those reported for September 2020 only (128−166 m^3 day^{-1}) as shown in Figure 19. The discrepancy between Lloydminster's emissions in the annual and monthly reports can be explained by the fact that production peaked in September 2020 after recuperating from pandemic-driven draw-backs.

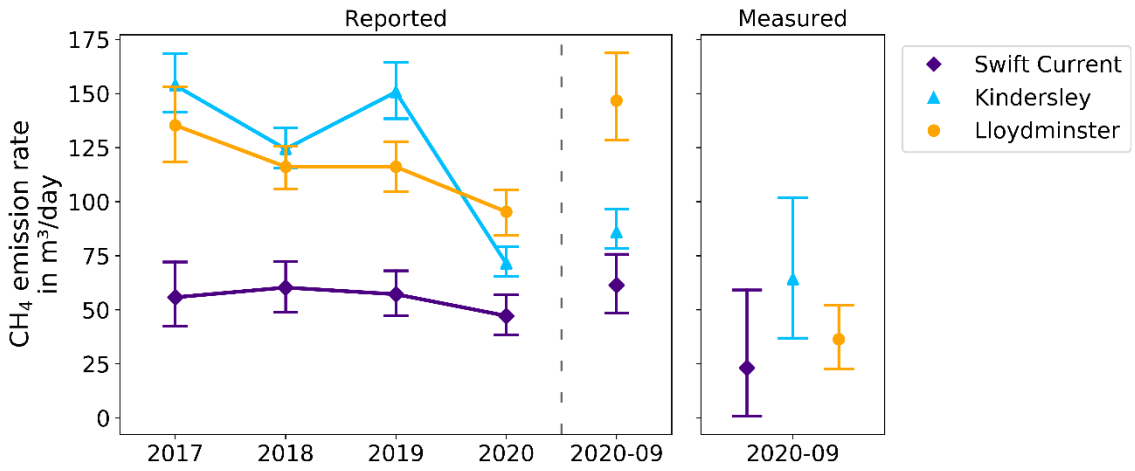

Figure 19: Measured versus reported emissions. Mean annual reported emission rates from 2017 until 2020, mean monthly reported emission rates for September 2020, and mean emission rates from active infrastructure in this study in September 2020 for Swift Current, Kindersley and Lloydminster. Reported emissions were given per reporting facility linked to other infrastructure. Measured emission rates were determined on a site-level. Error bars show bootstrapped 95% CIs using 1000 bootstrap iterations. Numbers of reporting facilities (n) in the annual report for 2020 were 516 in Swift Current, 4463 in Kindersley, and 2325 in Lloydminster. In September 2020 only, numbers of reporting facilities were 380 in Swift Current, 3284 in Kindersley, and 1388 in Lloydminster.

Among all Canadian oil and gas CH_4 emission quantification studies, the Lloydminster region has always shown the highest mean site-level emissions, varying slightly between years and measurement methods: around 70 m^3 day^{-1} in 2016 and 2017 were found by MacKay et al. (2021), roughly 100 m^3 day^{-1} in 2016 according to O'Connell et al. (2019) and Zavala-Araiza et al. (2018), 170 m^3 day^{-1} in 2018 (MacKay et al., 2021), all from truck-based measurements, and 324 m^3 day^{-1} in 2016 for airborne measurements (Johnson et al., 2017). In this study, we measured only 36 m^3 day^{-1} on average in Lloydminster, which is a fraction of previously established rates for this development.

Why were measured values in Lloydminster so much lower in this study than past measurement estimates? There are a few possibilities. Differences in sample population could be the first explanation. Although we identified that most sampled and emitting wells produced oil (Appendix B, Figure 39), and that facilities were mainly the same heavy crude oil single-well batteries (Appendix B, Figure 40) deemed responsible for high CH_4 emissions in previous studies (Johnson et al., 2017; Roscioli et al., 2018; Sentio Engineering, 2015; Tyner and Johnson, 2018), spatial differences in sampled infrastructure could have explained some of the departure from results shown in previous studies (further detailed in Appendix B, Figure 41). We also sampled fewer sites involving cold heavy oil production with sand (Petroleum Technology Research Centre, 2020) which was previously found to contribute largely to vented emissions (Johnson et al., 2017; Roscioli et al., 2018; Sentio Engineering, 2015; Tyner and Johnson, 2018). Declines in production could have explained the drop in observed emissions. Although Lloydminster's oil and gas production significantly dropped at the beginning of the COVID-19 pandemic, pre-pandemic production levels were reattained by September 2020 when this study was carried out (Appendix B, Figure 38). But while production levels had recovered, fewer high-yield wells were contributing to production as the number of producing wells in Lloydminster has decreased by roughly half in past years (Appendix B, Figure 38). This decrease of active wells was verified and we found that numbers of suspended well counts increased by 3% between 2017 and 2020 in the studied area of Lloydminster. Therefore, some of the inactive sites in Lloydminster may have undergone recent suspension or abandonment, and possibly shut-in work and respective status reports may not have been transmitted into databases. The change in the character of production may have driven down CH_4 emissions if marginal low production−high emission intensity wells were preferentially removed from service. Lastly, new regulation could have resulted in reduced emissions as compared with prior years. Overall, this study was carried out at an interesting

moment in time, in a pandemic and during an oil price surge, in an oil and gas development in transition, where a slightly different population of oil and gas infrastructure was sampled than in past studies. We conclude that spatial and temporal variability are important determinants of methane emissions, and that neither can be considered as constants.

4.3.2 CH_4 emissions from inactive infrastructure

In this study, 35% of all sampled sites were inactive in Swift Current, 31% in Kindersley and 63% in Lloydminster (Figure 18). The inactive site emission frequencies in Swift Current, Kindersley, and Lloydminster were 0%, 19%, and 22% respectively (Table 4), which was lower than for active sites (Table 3). Roughly 9% of total (active plus inactive) site emissions in Kindersley were attributable to inactive groups of infrastructure, given that we sampled only about half as many inactive groups as active. In Lloydminster, 43% of total emissions came from inactive sites but we sampled about 50% more inactive sites than active. We did not detect any inactive site emissions in the Swift Current region despite having sampled almost 70 groups composed entirely of inactive infrastructure. Per-site mean emission estimates for inactive infrastructure (Table 4, Figure 20) were 16±5 m^3 day^{-1} in Lloydminster, 15±4 m^3 day^{-1} in Kindersley, and 0 m^3 day^{-1} in Swift Current. For this study, we only conducted one OTM at an inactive site, which was located in Swift Current. The respective infrastructure was a leaking suspended water injection well according to our infrastructure database. The corresponding emission rate estimate was 12 m^3 day^{-1}, which was the lowest emission estimate among all OTMs.

Table 4: Emission frequencies and rates for inactive infrastructure. CH_4 emission frequency in percent, and rates in $m^3\ day^{-1}$ per area for all emitting, inactive groups: mean, median, minimum, maximum, 25th and 75th percentile, standard deviation (SD) and error (SE), and bootstrapped 95% confidence interval (CI) of the mean for 1000 bootstrap resamples with replacement. Minimum and maximum were associated with group emission estimates per anomaly, the remainder with group-mean emission rates. No emissions from inactive sites were detected in Swift Current.

Stats.	**Unit**	**Area**		
		Swift Current	**Kindersley**	**Lloydminster**
Freq.	%	0	19	22
Mean	$m^3\ day^{-1}$	NaN	15	16
Med.	$m^3\ day^{-1}$	NaN	0	0
Min.	$m^3\ day^{-1}$	NaN	2	1
Max.	$m^3\ day^{-1}$	NaN	837	1874
25%	$m^3\ day^{-1}$	NaN	0	0
75%	$m^3\ day^{-1}$	NaN	0	0
SD	$m^3\ day^{-1}$	NaN	57	91
SE	$m^3\ day^{-1}$	NaN	4	5
95% CI	$m^3\ day^{-1}$	NaN	48−118	39−127

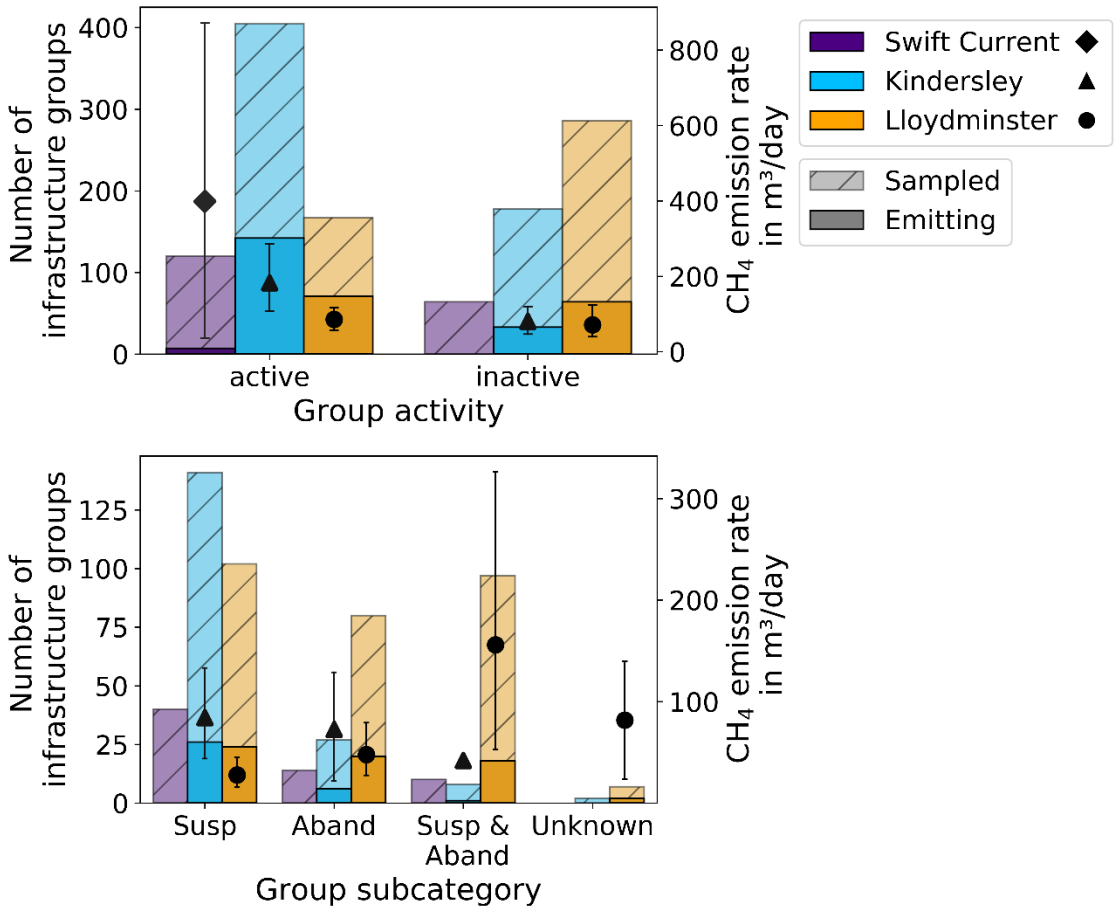

Figure 20: Active and inactive infrastructure groups and emission rates. Comparisons between number of sampled and emitting infrastructure groups (left y-axis, colored bars) as well as CH_4 emission rates (right y-axis, black markers) from active and inactive infrastructure (top), and a sub-categorized analysis for inactive infrastructure are shown (bottom).

Compared to CH_4 emissions from active infrastructure, inactive infrastructure tended to emit less CH_4 in the surveyed areas (Figure 20) on a per-site basis. Respective proportions of emissions from active and inactive infrastructure to emitting sites are shown in Figure 21. The further the lines are from the baseline, the higher the percentage of sites that emit most CH_4. Accordingly, Kindersley showed the highest percentage of sites emitting most CH_4 for active infrastructure groups, while Lloydminster outweighed Kindersley for inactive infrastructure groups (Table 5).

Additionally, the emission distribution in Lloydminster was slightly more heavy-tailed for inactive than for active infrastructure groups. A more heavy-tailed distribution implies that a small number of heavier emitting sites skewed the distribution and the mean emission rates.

Therefore, this study shows that CH_4 emissions from inactive infrastructure can be substantial and should be included in CH_4 emission inventories. In addition, this study emphasizes the importance of limiting the period of well suspension, or to extend CH_4 regulation to these sites. Age, reservoir potential to emit, gas migration, and many other factors could drive CH_4 emissions from suspended sites. The fact that inactive site emissions are very different across geographies suggests that reservoir or subsurface properties or age could be important. Work is needed to determine what causes fugitive emissions at inactive sites so that the issues can be addressed with sensible regulation.

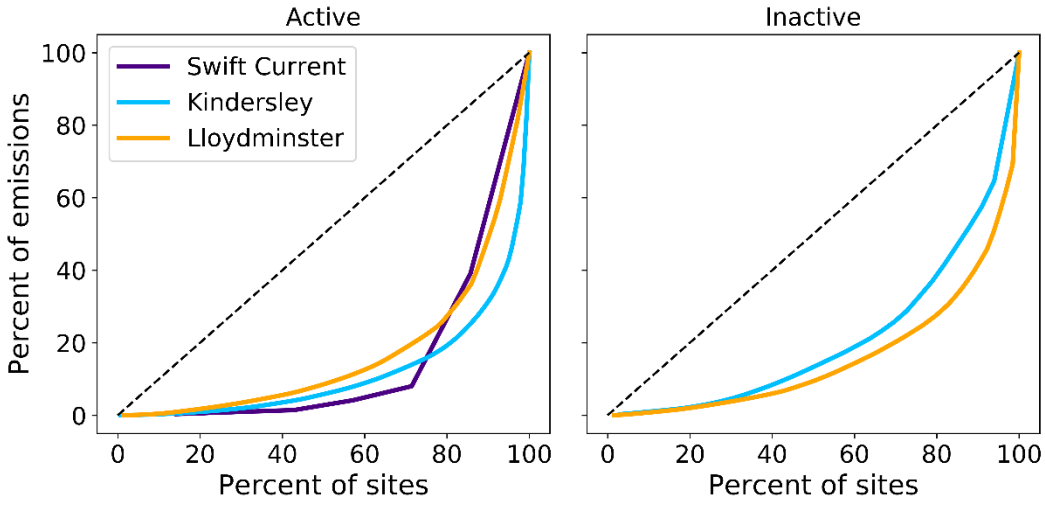

Figure 21: Lorenz curves. The curves show the proportion of overall CH_4 emission rates per percentage of active (left) and inactive (right) infrastructure groups. The dashed black line represents the baseline of a perfect distribution with all infrastructure groups emitting the same amount of CH_4. Corresponding Gini coefficients are shown in Table 5.

Table 5: Gini coefficients. Gini coefficients in percent for active and inactive infrastructure groups in the surveyed areas. The Gini coefficient represents a measure of the distribution of emissions across emitting sites, derived by the Lorenz curve in Figure 21.

Area	**Status**	**Gini coeff. [%]**
Swift Current	active	70.3
	inactive	NaN
Kindersley	active	76.6
	inactive	57.4
Lloydminster	active	65.8
	inactive	67.7

A breakdown of emissions from inactive sites into suspended and abandoned is shown in Figure 20. A reasonable distinction of suspended and abandoned groups was possible for Kindersley where only 10 (out of 178) groups consisted of either both suspended and abandoned infrastructure or of facilities with unknown inactivity status. However, for Lloydminster a large fraction of inactive groups (104 out of 286) could not be categorized as either suspended or abandoned, so that conclusions on emission rate quantification from these sites could not confidently be drawn for this region. In Kindersley, we found that site-level mean emission rates amounted to 16 m^3 day^{-1} for both only suspended and only abandoned groups, whereas emissions did not exceed 6 m^3 day^{-1} for other inactive sites. However, we emphasize that for reliable component-level emission quantification, particularly at inactive oil and gas sites, methods other than transect-based mobile measurements are more adequate.

Previous studies focusing on CH_4 fluxes from abandoned wells in the US (Kang et al., 2016, 2014; Pekney et al., 2018; Riddick et al., 2019; Saint-Vincent et al., 2021; Townsend-Small et al.,

2016; Townsend-Small and Hoschouer, 2021) showed a wide range of emissions from below detection limit up to roughly 2 m^3 day^{-1} per well (reported as $6.0 \cdot 10^4$ mg h^{-1} per well) (Kang et al., 2016), with an average estimate of 0.21 m^3 day^{-1} per well for the US and Canada (reported as 6.0 g h^{-1} per well) (Williams et al., 2021). The values in this study were appreciably higher in some regions which suggest that either inactive well-related emissions are higher than expected, or that associated aboveground infrastructure is also a root cause. Overall, it is hard to draw precise parallels between inactive infrastructure in Canada and the US because definitions and jurisdictional expectations differ. In Canada, a suspended well or facility (or site) is temporarily out of production (without a time limit) but theoretically capable of production, and where production infrastructure may be largely intact, CH_4 leakage is possible. Generally, a well that has been plugged can be considered abandoned. Some US studies focus specifically on abandoned wells, which would have less potential to emit than suspended sites comprised of wells and associated intact infrastructure including flow lines and tanks. In contrast to Canada, many US states do not allow for long-term suspension of sites, and Canadian regulators also differ in their guidance. As a result of these variations, and the regional differences we observed, it is difficult to estimate the potential inventory of CH_4 attributable to inactive sources nationally. More work is needed to understand inactive site emissions and their root cause.

4.4 Implications

Our study showed that emissions in the much-studied Lloydminster area were lower than expected, and lower than in previous years, which might be attributable to changes in well count or other spatio-temporal factors. This finding also shows the need to repeatedly conduct emission assessments. We hypothesize that marginal wells have been taken offline in favour of fewer higher-yield wells from which emissions are more tightly controlled because these larger sites

would have greater potential to emit and therefore would be equipped with emissions control equipment. If true, this would be a positive change because previous studies seem to show it is a standout region for emissions whereas other highly productive heavy oil regions in Canada like Peace River have been much less emissions-intensive owing to hydrogen sulphide levels and the need for emissions control (Lavoie et al., 2022). More analysis is needed to understand the observed changes. Other oil producing regions we measured here emitted moderate amounts of CH_4 on a per-site basis, and values were generally in line with regulatory reports. But in these areas, tank venting and unlit flares were major contributors to emissions and to a heavy tail distribution, and could be readily avoided. CH_4 emission reductions by preventing unlit flares should be targeted, for example by igniting unlit flares to guarantee combustion of CH_4 or by incorporating flare-gas-to-power projects. For future emission reduction efforts, we also suggest applying existing and developing new capture and commercialization opportunities.

Inactive infrastructure emitted less often and with less severity than active infrastructure, but emission levels were in some cases significant. In developments with high counts of suspended wells, and predisposing factors (which are unknown at this time but seem geography-specific), inactive sites could have a significant impact on overall CH_4 emissions. Inactive site emissions may help reconcile some top-down mass balance studies, which sample bulk emissions from all sources, against other studies and regulatory reports that focus solely on emissions from active infrastructure. If CH_4 control regulations are not extended soon to inactive sites, we would propose that such sites at least be measured occasionally, to help define the scope of the issue. In the three western provinces, there are roughly 200,000 suspended wells and facilities, and more than 300,000 abandoned wells (numbers from AccuMap®, 31.03a Currency Update, by IHS Markit). If we scale up our mean per-site CH_4 emission rate estimates with numbers of active (n_a)

and inactive (n_i) infrastructure groups in the broader regions of Swift Current (n_a =883, n_i = 521), Kindersley (n_a = 3664, n_i = 2120) and Lloydminster (n_a = 1176, n_i = 2108), almost 300,000 m^3 day^{-1} are emitted by active and 66,000 m^3 day^{-1} by inactive infrastructure in southwestern Saskatchewan. This means around 22% of overall emissions were attributed to inactive sites. Consequently, current provincial and federal CH_4 emission estimates may be underestimated significantly if suspended and abandoned infrastructure is not included. As emissions from regulated active sources fall over the coming years, emissions from inactive legacy assets may become important in the inventory. We encourage further emission quantification studies of inactive infrastructure in different areas to manifest their importance and potential with regards to achieving Canada's emission reduction target.

4.5 Acknowledgements

We thank Environment and Climate Change Canada, Mitacs, and Geoverra for their support of this work. We also appreciate the Ministry of Energy and Resources at the Government of Saskatchewan for facilitating access to various datasets.

Chapter 5: Cross-sector comparison of methane emissions from anthropogenic sources: A case study in Canada

Preamble

This chapter is under preparation for submission. I conceptualized the study and prepared, organized, and led the field work. Furthermore, I conducted most data processing steps myself, analyzed all measurements, gathered external data, produced figures and tables, and wrote the manuscript. Due to pandemic-related reasons, this study was affected by supply-chain problems, ultimately delaying the field work, and reducing the dimension and width of the study. This study was conducted under supervision of my current supervisor, David Risk. Gilles Perrine assisted with field measurements. Evelise Bourlon assisted with data processing and the interpretation of the results. Martin Lavoie provided insights regarding the interpretation of measured and external data. David Risk supported the conceptualization of the study, supervised, gathered funding, and provided insights regarding the interpretation of the data. All co-authors provided helpful comments for the preparation of the final version of this chapter.

5.0 Abstract

Anthropogenic methane (CH_4) emissions to the atmosphere have driven climatic changes in recent decades. Emission reduction strategies are necessary to avoid the continued increase of global temperatures. To inform mitigation, policymakers need a good understanding of release patterns across different economic sectors, which can be achieved by acquiring broad-scale measurements. As cross-sector emission quantification studies are scarce, we conducted a case study in Grande Prairie, a small city in Canada's west dominated by oil and gas production and agriculture. Measurements were obtained using a high-precision gas analyzer mounted in a truck,

and emission rates for multiple co-located sectors were estimated with an inverse Gaussian plume model. Average CH_4 emissions from oil and gas production sites were low on a site-level (3.6 m^3 day^{-1}) compared to others we have measured in Canada (6.9−168.5 m^3 day^{-1}). We also detected CH_4 emissions from cattle farms (1.0−33.5 m^3 day^{-1}), and especially from a landfill (268.2 m^3 day^{-1}). Methane emitted from oil and gas production contributed most to total regional emissions (71%) given the abundance of assets (n = 256), followed by a 20% contribution by the single landfill. Therefore, further emission mitigation in the oil and gas, and waste sectors are possible and crucial to achieve emission reduction targets of the Global Methane Pledge. In addition, long-term stationary measurements gave insight into temporal concentration patterns and landscape-driven impacts on CH_4 levels. Studies like this one show a wide range of anthropogenic CH_4 emission sources and quantify emission rates from the upstream oil and gas industry, agriculture, and waste management. These cross-sector comparisons are needed to advance CH_4 emission reduction targets and to establish a multi-disciplinary understanding of regional emission patterns.

5.1 Introduction

Anthropogenic methane (CH_4) emissions are generated in several economic sectors, including agriculture, waste management, oil and gas production, and others. Canada ranks within the top five oil producers globally (International Energy Statistics, 2021), produces more than a million tonnes of beef per year (Food and Agriculture Organization of the United Nations, 2022), and shares the world's largest waste production per capita with the United States (Nanda and Berruti, 2021). As a result, the CH_4 emission potential is high in parts of Canada where all these activities co-occur.

During oil and gas production, CH_4 is commonly vented or escapes to the atmosphere as fugitive emission resulting from leaks. Regarding emissions from livestock, CH_4 is generated through enteric fermentation in the digestive system of ruminants, where ingested carbohydrates undergo microbial decomposition producing CH_4 as a by-product, which is then released by the animal. Moreover, the storage of livestock manure can provoke CH_4 production resulting from anaerobic degradation of organic matter leading to emissions depending on the management system (Dalby et al., 2021). In landfills, waste is buried, covered, and CH_4 is generated as a by-product of microbial decomposition of organic waste underneath the soil cover. From there, the gas either vents to the atmosphere, is captured and collected in a processing facility for repurposing or is oxidized to CO_2 in the cover soil.

Methods to quantify anthropogenic CH_4 emissions range from handheld techniques prominent in the oil and gas sector, to spaceborne measurements especially effective in pin-pointing super-emitters (Fox et al., 2019), whereas temporal and spatial constraints or high costs may limit their implementation. Mobile ground-based measurements have proven effective to survey large areas in a screening fashion in the oil and gas sector (Atherton et al., 2017; von Fischer et al., 2017; Yacovitch et al., 2015). The tracer gas method is not only popular in the oil and gas sector (Mitchell et al., 2015; Roscioli et al., 2015), but also widely used to quantify emissions from ruminants (McCaughey et al., 1997; McGinn et al., 2009; Storm et al., 2012) and waste facilities (Fredenslund et al., 2010; Scheutz and Kjeldsen, 2019). Nonetheless, this method comes with various restrictions as it is time-consuming, usually requires immediate site access, is invasive and costly. Therefore, we chose the mobile technique over the gas tracer method to determine CH_4 emissions from various source types (oil and gas, agriculture, waste) due to its effectiveness and practicality to repeatedly survey large areas restricted to travelling on public roads within a

limited (two-week) timeframe. To add insights of the temporal variation of CH_4 levels which is not captured by the mobile technique and to contextualize concentration ranges, we additionally considered long-term stationary data recorded by established regional networks.

Measurements of CH_4 emissions from the oil and gas sector in Canada are motivated by the fact that numerous studies suggest a significant underestimation of emissions in the federal inventory (Chan et al., 2020; Johnson et al., 2017; Lu et al., 2022; MacKay et al., 2021; Scarpelli et al., 2021). Emission reductions are expected over time given that national regulations for the oil and gas industry came into effect in 2020, but measurements are necessary to verify compliance and to identify areas of improvement to further curb emissions toward a net-zero future. In the national inventory the total CH_4 emission rate composed of vented, flared and fugitive emissions for the Canadian oil and gas industry was estimated at approximately $6.2 \cdot 10^6$ m^3 day^{-1}, whereas CH_4 emissions from livestock (including enteric fermentation and manure management) amounted to $4.5 \cdot 10^6$ m^3 day^{-1}, and to $2.6 \cdot 10^6$ m^3 day^{-1} for solid waste in 2018 (Scarpelli et al., 2021). The western provinces of Alberta and Saskatchewan showed the highest emissions from the oil and gas industry and from enteric fermentation (Ominski et al., 2007; Scarpelli et al., 2021). Differences in livestock breed, feed intake and quality, age and region in addition to contrasting methodologies cause large discrepancies in CH_4 emission estimates in the agricultural sector (Basarab et al., 2005; Goopy et al., 2020; Kebreab et al., 2006; Lassey, 2007). Whereas emission mitigation strategies for livestock involving for example diet manipulation exist (Ugbogu et al., 2019), their widespread implementation remains largely unsuccessful despite their proposed effectiveness (Reisinger et al., 2021). Therefore, there is potential to curb emissions in the agricultural sector and measurements are needed to identify mitigation opportunities. Similarly, a transition in CH_4 emission mitigation from the waste sector is

desirable, and diversion and recovery of the produced gas are necessary to curb emissions, which are currently not projected to decrease in Canada until 2030 if policies for more effective practices are not advanced (Environment and Climate Change Canada, 2022b). Landfill emission estimates are traditionally based on simple models that entail large uncertainties, and broad-scale measurement-based verification of these models is needed.

So far, few studies determine anthropogenic emissions across different source types (e.g. Ars et al., 2020), but these studies are valuable for the development of effective emission reduction strategies in compliance with the Global Methane Pledge, which aims to limit global warming to 1.5°C with 121 participating nations. To quantify emissions from oil and gas, livestock, and the waste sector and their respective contributions to regional emissions, we conducted a cross-sector study in Grande Prairie, a small city in Canada's west dominated by oil and gas production and agriculture. We measured atmospheric mixing ratios of CH_4 on transects using a high-precision gas analyzer mounted in a truck, and estimated emission rates using an inverse Gaussian plume model. This type of study is applicable on a global level and results inform policymakers to further emission reduction targets.

5.2 Methods

5.2.1 Study area

In this study, we focused on the region of Grande Prairie in Canada's most important oil and gas-producing province Alberta. Since Grande Prairie is not only a hub for oil and gas production within the Montney formation, but also plays a prominent role in livestock farming, the area was well suited for our emission surveys targeting mainly CH_4 sources. The driven routes were chosen based on road accessibility and recently reported emissions from oil and gas

infrastructure. We passed by active, suspended, and abandoned oil and gas infrastructure, cattle and bison farms, a greenhouse farm, power-generating plants, and an active landfill (Figure 22). The public and open landfill treats household and yard waste, uncontaminated fill material and furniture, but also manages the recycling of plastics, metals, electronics, cardboard, wood, hazardous waste, etc. A gas collection or flaring system was not present, so that most of the gas generated at the landfill was emitted to the atmosphere, minus the fraction that underwent microbial oxidation under aerobic conditions within the top layer of the landfill cover.

5.2.2 Mobile surveys

We used a truck equipped with a greenhouse gas analyzer (G2210-i, Picarro Inc., USA) in concentration mode to conduct mobile measurements of atmospheric CH_4, ethane (C_2H_6), and carbon dioxide (CO_2) levels. An air inlet connected with the gas analyzer was mounted at a height of 2.01 m on a mast at the front of the truck, together with a 2D heated Ultrasonic anemometer (Model 86004, RM Young, USA) and a GPS (18x 5 Hz, Garmin, USA). The routes were surveyed in triplicate between November 5-15, 2021. The collected data was monitored in real-time on a laptop and recorded on a datalogger (CR1000X, Campbell Scientific, Canada) at a 2-Hz frequency.

The pre-processing of the data included the correction of the measured wind vector to account for the truck's motion and the linear interpolation of missing datapoints. In addition, the background levels of CH_4 and CO_2 were derived from a running minimum over a moving window (1−30 minutes) and subtracted from measured values to obtain excess concentrations. Excess CH_4 detections above the threshold CH_4:CO_2 ratio of 1:100 were considered for emission attribution, as these detections represent CH_4 that is significantly higher than normal including in areas like river valleys where ground- and water-emitted CH_4 and CO_2 can pool under low wind conditions

(Hurry et al., 2016). The CH_4 maxima from over-ratio detections were attributed to potential CH_4 sources within 400 m (empirically chosen as an adequate distance between available roads and sources) downwind from the point of detection, whereas distances up to roughly 1000 m were considered for the landfill due to its large size (roughly 600 m by 700 m). The algorithm described here was previously applied for emission estimation in the oil and gas industry (Atherton et al., 2017; Baillie et al., 2019; Hurry et al., 2016; Lavoie et al., 2022; MacKay et al., 2019, 2021; O'Connell et al., 2019; Vogt et al., 2022). For oil and gas sources, we retrieved information about the location, type, and status of individual pieces of infrastructure from a GIS database by IHS Markit based on monthly reports by operators to regulators. Subsequently, we grouped infrastructure co-located within 45 m which we empirically consider a common size of oil and gas pads. Oil and gas groups were sub-categorized as 'active' when at least one piece of infrastructure was producing oil or gas. If all group components were suspended, the group was tagged as 'suspended'. Likewise, groups were sub-categorized as 'abandoned'. When a group was comprised of both suspended and abandoned and no component of another status, it was tagged as 'suspended and abandoned'. All remaining groups had at least one component of either cancelled or unknown status and were tagged as 'unknown'. Locations of non-oil and gas infrastructure were manually added to the database wherever grazing livestock herds or other obvious indicators (e.g., signs) were observed in the field. Once elevated atmospheric CH_4 concentrations were attributed to a source, the emission rates were estimated based on an inverse Gaussian plume model accounting for wind speed, distance to and height of the source, inlet height and atmospheric stability. Whenever we passed an infrastructure group downwind but did not detect enhanced CH_4 concentrations, the group was tagged as sampled. As a means of quality control, we verified proper attribution of oil and gas groups, when emissions were only detected on one pass with the truck and excluded emission rates for misattributed groups. The method

used here does not capture differences between fugitive and vented CH_4 emissions and does not distinguish between enteric fermentation and manure.

5.2.3 Uncertainties

The emission rate estimation method applied here entails an uncertainty of roughly 63% for three passes with the truck – compared to a >10,000% range of typically heavy-tailed oil and gas emissions (Frankenberg et al., 2016) – following the uncertainty analysis outlined in Zavala-Araiza et al. (2018) and is further detailed elsewhere (O'Connell et al., 2019). This method was broadly applied in oil and gas emission detection and quantification studies (Atherton et al., 2017; Baillie et al., 2019; Hurry et al., 2016; Lavoie et al., 2022; MacKay et al., 2019, 2021; O'Connell et al., 2019; Vogt et al., 2022). While CH_4 sources from oil and gas infrastructure can be considered as individual point-sources, for example from venting tanks, agricultural or landfill sources are different and usually characterized by multiple point-sources, for example from individual cows on a pasture. Nonetheless, we treated all source types as point-sources, which is a reasonable assumption when measuring at greater distances because plumes will coalesce. However, at closer distances, this approach will generally lead to an underestimation of CH_4 emissions. In the field, upon passing a pasture with grazing livestock at speeds of around 60 km h^{-1}, we often detected CH_4 concentrations that reflected overlapping plumes depending on the dispersion of the cattle herd on the pasture, their movement between repeated passes and their distance to the truck. Similarly, landfills are often not limited to a single point-source. In this study, the terrain of the landfill extended over roughly 600 m by 700 m. Since the exact release point at the landfill was unknown, we split the terrain into a 0.001° x 0.001° grid (equivalent to approximately 100 m in this area) with 36 grid points, each representing a potential release point. We subsequently determined the emission rate for each potential release point individually in an

iterative manner. The distance to the truck was used as a proxy of release point uncertainty, to obtain a range of possible emission rates for the landfill assuming that only a single point was emitting on all passes.

For agricultural sources and the landfill, we applied an additive error propagation (in percent) to yield the overall uncertainty (U, Equation 1). The baseline uncertainty for mobile emission estimation of 63% (U_1) determined previously (O'Connell et al., 2019) was combined in Equation 1 with the uncertainty (U_2) for each source type determined from available data.

$$U = \sqrt{{U_1}^2 + {U_2}^2} \quad (1)$$

In a sensitivity analysis, we assumed that livestock could have been located at any distance between 10 to 400 m from the truck on each pass. Based on that, the standard deviation of all yielded emission rate estimates for individual passes as a percentage of the mean emission rate was used to account for the herd location uncertainty. Since this uncertainty was derived from single-pass estimates, we implicitly considered different locations of the herd during different passes. Therefore, emission rate estimates for livestock entailed an uncertainty of 144% (U_2), so the overall uncertainty (U) for livestock emissions in this study amounted to 157%. Although the uncertainty for this source type was very high, we still use the emission rate estimates in this study for reference.

Under consideration of different potential release points on the landfill, we determined that the standard deviation of emission rate estimates among all points as a percentage of the overall mean emission rate best represented the release point uncertainty amounting to 58% (U_2) and resulting in an overall uncertainty (U) of 86% for landfill emission estimates in this study.

For clarification, we assumed that the source location uncertainty did not apply to oil and gas-related sources, so that U_2 in Equation 1 drops, and the overall uncertainty (U) for oil and gas sites was 63% as determined previously (O'Connell et al., 2019).

Furthermore, to interpret the results, we determined bootstrapped 95% confidence intervals (CI) for mean emission rate estimates for each anthropogenic sector with random sampling and replacement of 1,000 samples.

In the study, emission rates varied by >10,000% from the largest to smallest source, so in relative terms quantification errors of 60−200% are modest and preserve a good signal-to-noise ratio allowing for a good understanding of sectoral emission patterns.

5.2.4 Long-term stationary measurements

Regional networks within the province of Alberta, called Airsheds, performed the continuous monitoring of the local air quality involving the measurement of environmental parameters, greenhouse gases and particulate matter, whereas CO_2 measurements are not included in the framework. We used CH_4 and wind measurements from 30-second resolution datasets from two stations in the Grande Prairie area to compare with our mobile measurements and draw further conclusions about the temporal variation of atmospheric CH_4 levels in the area. The station "Henry Pirker" was located within the city of Grande Prairie at the border between a recreational park and a residential area (Latitude: 55.176667, Longitude: −118.8075), and air quality parameters were recorded since 2018. The station "Wembley" was positioned about 22 km southwest of the Henry Pirker station, adjacent to an area of active oil and gas production in 2018 (Latitude: 55.082835, Longitude: −119.12579) but was relocated to a different industrial area roughly 27 km northwest of the Henry Pirker station in October 2021 (Latitude: 55.30431, Longitude: −119.1852) and subsequently re-named to "Poplar" (Figure 22). CH_4 data was

available from October 2018−October 2021 for Henry Pirker, from October 2018−September 2021 for Wembley and from October 2021−January 2022 for Poplar.

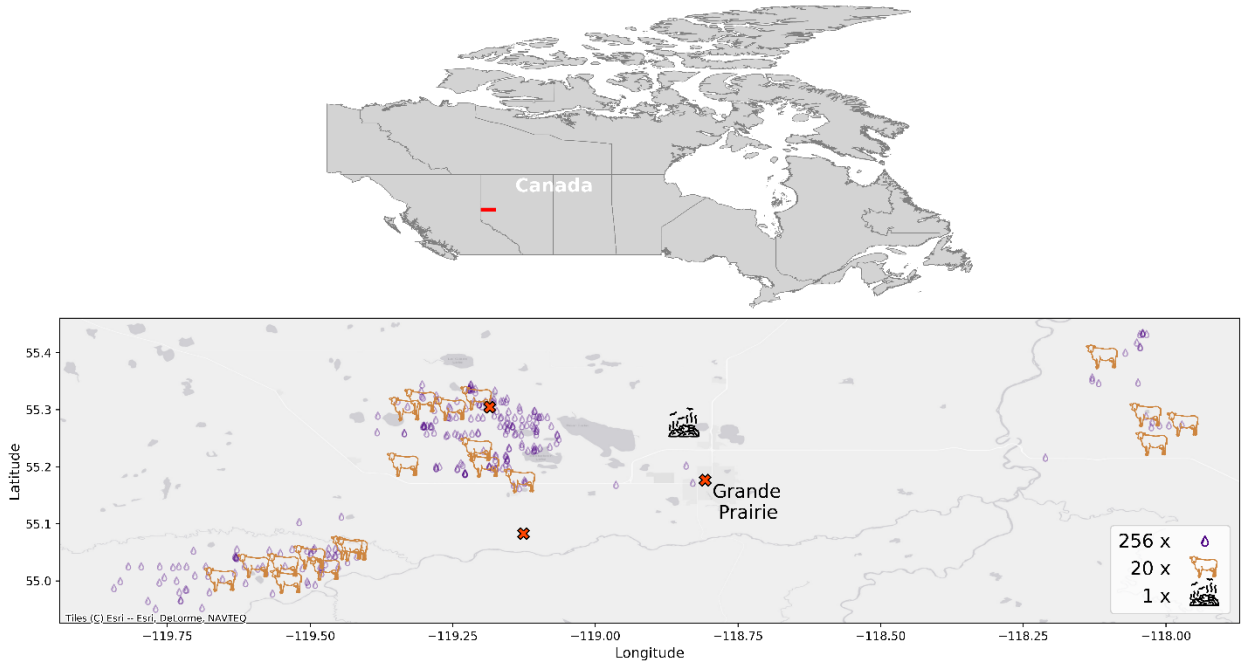

Figure 22: Map of the study area around the city of Grande Prairie in western Canada. The lower map is a close-up of the red rectangle shown on the upper map. Locations and numbers of sampled oil and gas infrastructure, agricultural sites and a landfill are shown. The three red crosses indicate the locations of Airshed stations.

5.2.5 Miscellaneous data

We retrieved reported emissions from Petrinex, Canada's Petroleum Information Network where oil and gas companies are required to submit monthly emission estimates on a component level. Vented gas emissions were selected, which describe solution gas commonly containing between 70−90% of CH_4 as well as other gases, CO_2 or H_2O for example. In addition, we obtained oil and gas production data for sampled wells from an IHS Markit product for November 2021, the time

we conducted measurements. The latter was used to determine emission intensities on a regional level (as described in MacKay et al., 2021).

5.3 Results and Discussion

5.3.1 Oil and gas

Among the 256 oil and gas infrastructure groups that were sampled during mobile surveys in Grande Prairie, 61 groups (24%) were emitting up to 147.0 m^3 day^{-1} (Figure 23). Mean oil and gas-related emission rates were 15.2 m^3 day^{-1} among all emitting sites. Site-level emissions including zeros regionally amounted to 3.6 m^3 day^{-1} (bootstrapped 95% CI: 2.0−5.6 m^3 day^{-1}). CH_4 emissions were substantially lower than for several other regional oil and gas-based estimates in western Canada determined in previous studies (Johnson et al., 2017; MacKay et al., 2021; Roscioli et al., 2018), but magnitudes compared to emission rate estimates from south-eastern Saskatchewan (6.9 m^3 day^{-1}, 2015) and the nearby Peace River (11.1 m^3 day^{-1}, 2018) (MacKay et al., 2021). The low emissions could be a result of predominant gas production in Grande Prairie, where venting is minimized to preserve the saleable product. The recent provincial and federal government incentive programs to reduce gas leaks may have also had an effect. The neighbouring development in Peace River faced stringent regulations in 2017 because of odour complaints due to the composition of emitted gases, which may have resulted in similar attempts to reduce adverse effects on air quality in the Grande Prairie region.

Measured C_2H_6:CH_4 ratios for oil and gas sites in the studied area did not exceed 5% C_2H_6, whereas two wells in British Columbia, roughly 200 km northwest of Grande Prairie within the same oil and gas formation showed a substantially higher C_2H_6:CH_4 ratio of 15% and 21% (Wood et al., 2021).

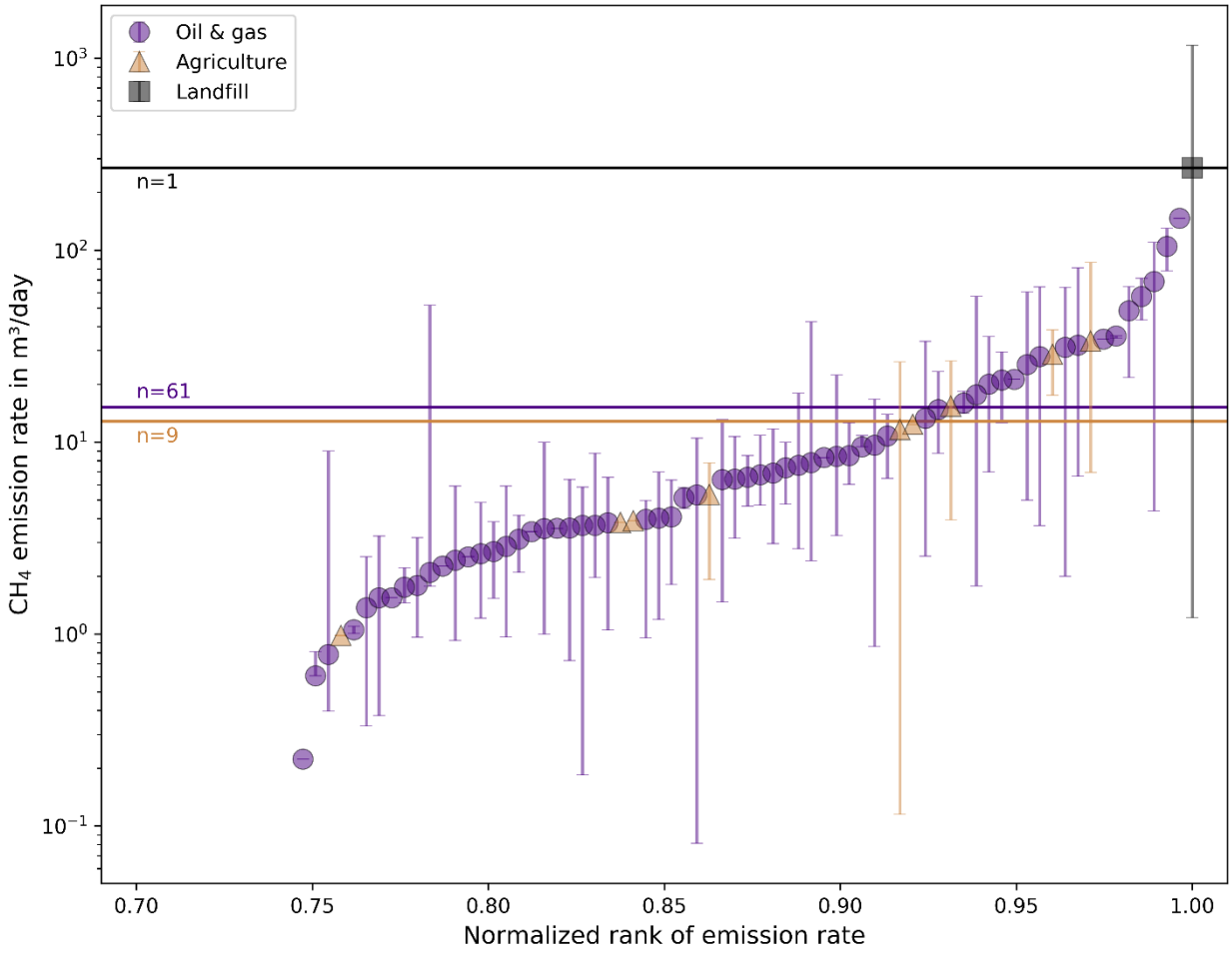

Figure 23: Ranked CH4 emission rates for oil and gas-related, agricultural and landfill sources. Points show mean group-level estimates, error bars show minimum and maximum estimates per group. Horizontal lines represent the overall mean of emitting groups of each source type with respective numbers of estimates.

Considering the sub-categories of oil and gas sites, mostly active sites were sampled and found emitting (Figure 24). However, mean site-level emissions were higher for groups with unknown status. Nonetheless, active groups contributed 70% to total emissions from oil and gas in the area, followed by groups with unknown status (24%), abandoned groups (5%), and suspended, or suspended and abandoned groups contributed the least (1%). The substantial contribution of total emissions from groups with unknown status expresses not only the need to clarify infrastructure

status in data products, but also shows that attribution of emissions to specific oil and gas groups has limitations in this study. According to emission reports by operators, between 2.3 m^3 day^{-1} and 285.0 m^3 day^{-1} were emitted in the area investigated in this study in November 2021 with an average of 14.8 m^3 day^{-1} (assuming 70% CH_4 content of vented solution gas) to 19.1 m^3 day^{-1} (90% CH_4 content), which is also substantially higher than our measurement-based estimates. However, it should be noted that the choice of the study area was constrained by road access and terrain, whereas a significant amount of oil and gas infrastructure with higher reported emissions was located south and west of Grande Prairie in a rather complex topography with poor road access. Possibly, aircraft or Unmanned Aerial Vehicle (UAV)-based methods could verify emission levels in these areas more effectively. A national CH_4 emission hotspot at an oil and gas production facility roughly 90 km south of Grande Prairie was identified in a recent study with respective emission rates equivalent to 69000 m^3 day^{-1} over a roughly 10 km x 10 km grid cell (Scarpelli et al., 2021). Therefore, regional emission estimates for the studied area may show larger discrepancies if other subregions were chosen.

Considering oil and gas production levels, we determined an emission intensity of 0.07±0.05 gCO_2e MJ^{-1}, which represents one of the lowest known emission intensities in Canada so far (MacKay et al., 2021). This finding reflects that Grande Prairie was a high-production/low-emission oil and gas development in November 2021, which raises hope that the oil and gas industry in parts of Canada is on the right path to achieving the ambitious goal to reduce CH_4 emissions by 75% of 2012 levels by 2030 (Environment and Climate Change Canada, 2022a).

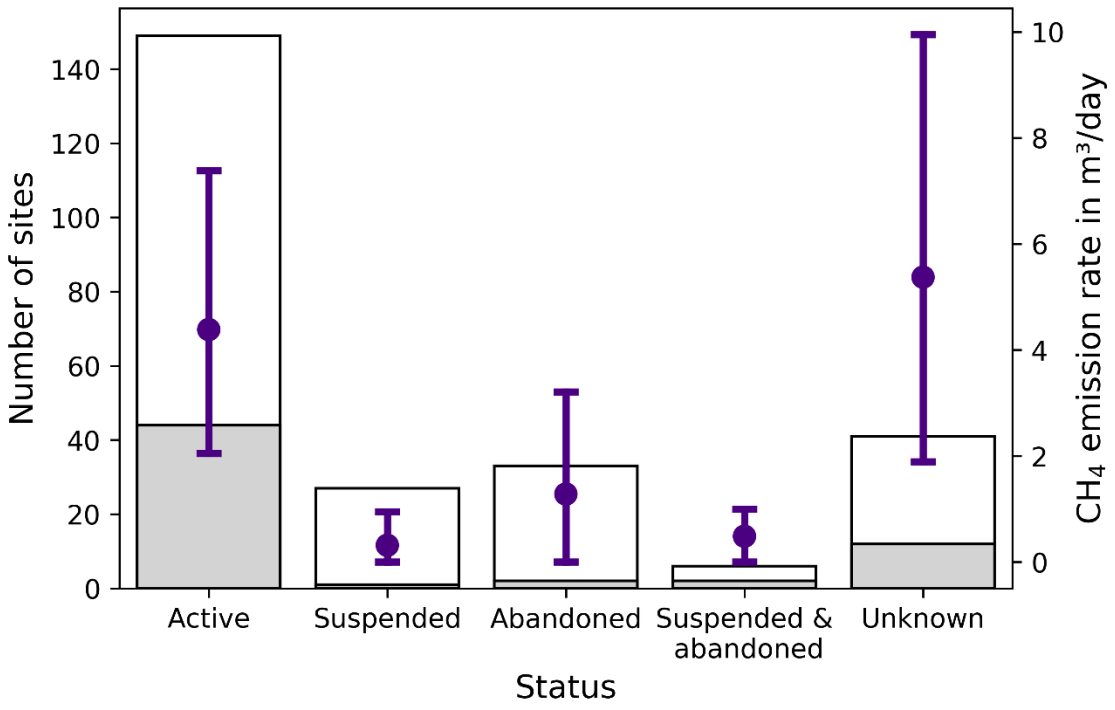

Figure 24: Sub-categories of oil and gas groups with respective counts of sampled (white bar) and emitting (gray bar) groups, and site-level emission rates including zeros (points) with bootstrapped 95% confidence interval (error bar) are shown.

5.3.2 Agriculture

Out of the 20 agricultural sites that we passed downwind, 14 were cattle farms, four were bison farms, one supported both cattle and bison, and one was a greenhouse farm (Figure 25). In total, nine farms were emitting CH_4 between 1.0−33.5 m^3 day^{-1} (Figure 25). Although the sample size of farms in this study was small, cattle farms contributed 99% to total emissions from agricultural farming. Due to limited information about the greenhouse farm, we were unable to draw conclusions about the possible source of the small CH_4 emission on site (1.0 m^3 day^{-1}). We could not rule out livestock emissions, but soil preparation such as composting could also have led to emissions at the greenhouse farm (Peigné and Girardin, 2004). The mean of all sampled cattle farms resulted in a per-farm emission estimate of 8.2 m^3 day^{-1} (95% CI: 3.4−14.8 m^3 day^{-1}). As

numbers vary, we assumed a cattle herd size of 69 (Canadian average according to Canada's Beef Industry, 2021) and suggest an emission rate of 0.1 m^3 day^{-1} per head, which compares well with other studies (Johnson and Johnson, 1995; Ominski et al., 2007; Sejian et al., 2011), although large uncertainties were identified caused by differences not limited to species, breed and diet. The Canadian greenhouse gas inventory uses CH_4 emission factors between 0.2−0.6 m^3 day^{-1} per head for dairy and beef cattle in Canada in 2019 (Environment and Climate Change Canada, 2021b). A study determining CH_4 emissions on a municipality level in Alberta, Canada, based on data from 2011 found total emissions from enteric fermentation and manure management of roughly 19000 m^3 day^{-1} attributed to 4269 dairy and 60786 beef cattle for the Grande Prairie County No. 1, representing roughly 1% of total CH_4 emissions from cattle in the province (Shen et al., 2019). In that study, emissions from enteric fermentation amounted to 90% and from manure management to 10% in the county based on simple emission factor calculations.

Generally, some degree of underestimation (relative to emission factors) was expected because of methodological limitations and uncertainties (of ~157%). Despite the high uncertainty of emission rate estimates, we are confident about the detection of non-zero CH_4 plumes from cattle farms in this study given the lack of other potential sources in proximity to the farms. In future work, the high uncertainty of emission rates could be reduced by using different approaches including joint-inversion of all detected peaks (instead of the maximum only) and/or incorporating a Monte Carlo analysis with random cluster distribution of cattle in the field.

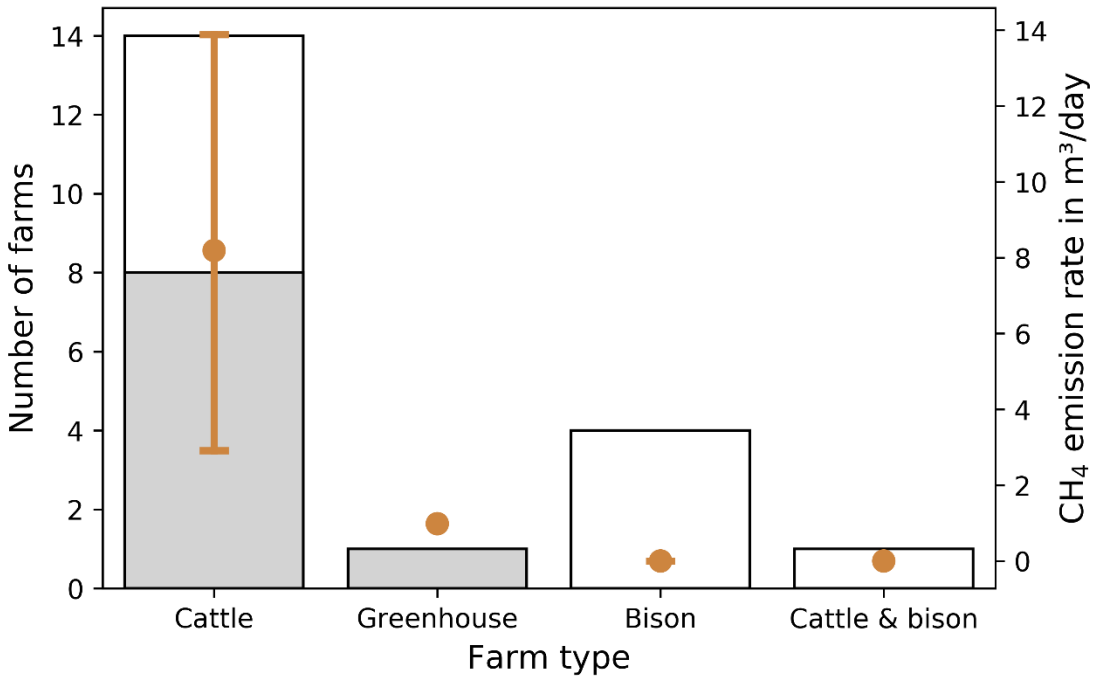

Figure 25: Numbers of sampled (white bar) and emitting (gray bar) farms are shown with respective mean emission rate estimates on a per-farm level including farms that were not emitting (points) and bootstrapped 95% confidence interval (error bar). The uncertainty for agricultural sources amounted to 157%.

5.3.3 Landfill

The elevation of measured CH_4 concentrations on three downwind passes along the landfill was clearly distinguishable from ambient concentrations (Figure 26). Emission rates from the 36 possible source points within the landfill terrain ranged widely from 19.1−626.8 m³ day^{-1} for truck-to-source distances between 76−1014 m (Figure 27). The mean for this landfill amounted to 268.2 m³ day^{-1} (bootstrapped 95% CI: 217.9−316.8 m³ day^{-1}).

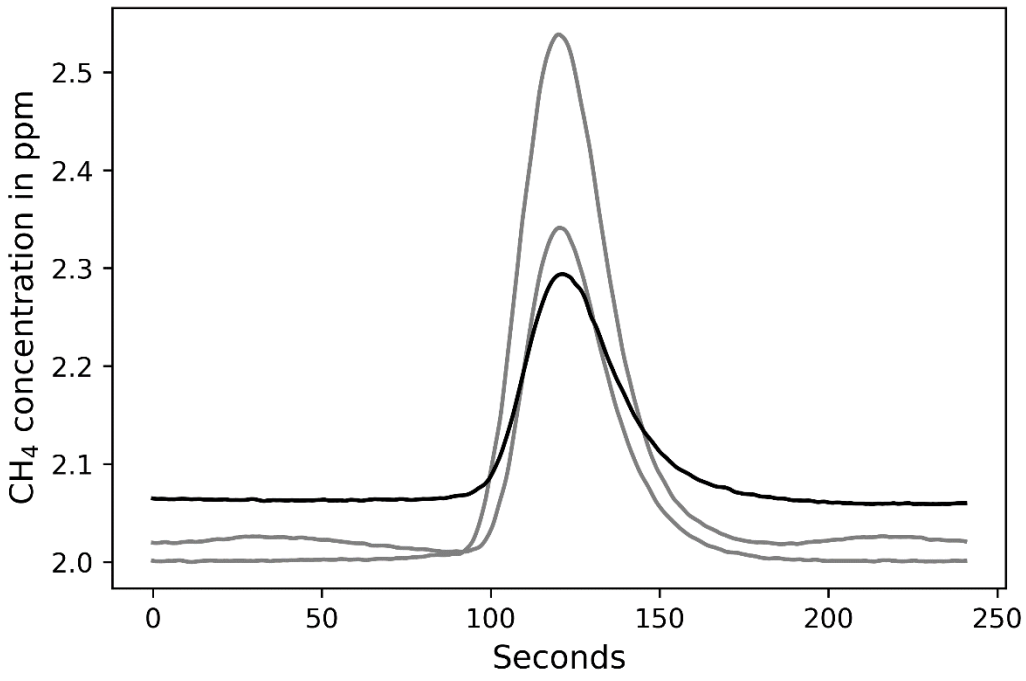

Figure 26: CH4 concentrations measured while passing the landfill downwind. Peaks are centred with a buffer of 120 seconds before and after the maximum. Gray lines represent subsequent passes, while measurements indicated with the black line were taken on a different day.

Nine landfills in the US showed emissions ranging from 778−43344 m^3 day^{-1} (Mosher et al., 1999). For a landfill in Switzerland, emissions varied depending on the measurement method, and daily fluctuations from CH_4 uptake to emissions of 181 m^3 day^{-1} according to flux chamber measurements, and from 57−1865 m^3 day^{-1} based on eddy covariance measurements were detected (Schroth et al., 2012). Further studies show large temporal differences in landfill emissions depending on weather conditions (Delkash et al., 2022; Jain et al., 2021; Xu et al., 2014), as well as variation between landfill type and operation (Zeiss, 2006), abatement measures in place (Cai et al., 2018) and region (Du et al., 2017). Although we were able to successfully detect CH_4 emissions from the landfill, the inverse Gaussian plume model applied here assuming a single point-source as opposed to an areal source, provided large ranges of emission rate

estimates. Therefore, we encourage the use of other techniques to quantify CH_4 emissions from the waste sector including airborne remote sensing (Cusworth et al., 2020) or UAV-based methods as well as long-term measurements with stationary instrumentation setups (Mønster et al., 2019). CH_4 emissions from landfills in Canada are currently poorly understood and federal regulations will be implemented soon to curb CH_4 release into the atmosphere.

Figure 27: Point-level emission rates within the landfill terrain in Grande Prairie. The black circles on the road represent the points during the truck survey when CH4 peaks were detected downwind of the landfill on three different passes on two days. Blue arrows indicate the direction the wind is blowing to at the time of detection.

5.3.4 Contributions to total anthropogenic emissions

Overall, oil and gas-related emissions contributed 71% to total determined emissions in Grande Prairie, whereas 29% could be attributed to sources unrelated to oil and gas production (Figure 28). This finding does not consider that more oil and gas-producing sites were targeted in this study than agricultural farms. Nevertheless, active oil and gas sites accounted for 50% of emissions in Grande Prairie, the landfill alone for 20%, the unknown oil and gas sub-category for 17%, cattle farms for 9%, abandoned oil and gas sites for 3% and all other sub-categories together for less than 1%. For comparison with the federal inventory, CH_4 emissions from the oil and gas sector amounted to 45%, 31% from livestock, 17% from waste, and 7% from other sources including residential combustion and coal on a national level in 2018 (Scarpelli et al., 2021).

5.3.5 Airshed stations

Long-term stationary CH_4 measurements in and around Grande Prairie peaked at 6.5 ppm for Poplar, 20.1 ppm for Henry Pirker and 6.8 ppm for Wembley at different times, which could indicate that CH_4 was released from several sources in proximity to the stations. As long-term measurements allow for the analysis of temporal differences, we found a slight depression of CH_4 concentrations at all three stations in the afternoon when wind speeds were highest, and typically strongest vertical mixing occurs (Shipham et al., 1998). In contrast, higher concentrations were measured during the night when atmospheric mixing is slowed down (Appendix C, Figure 42).

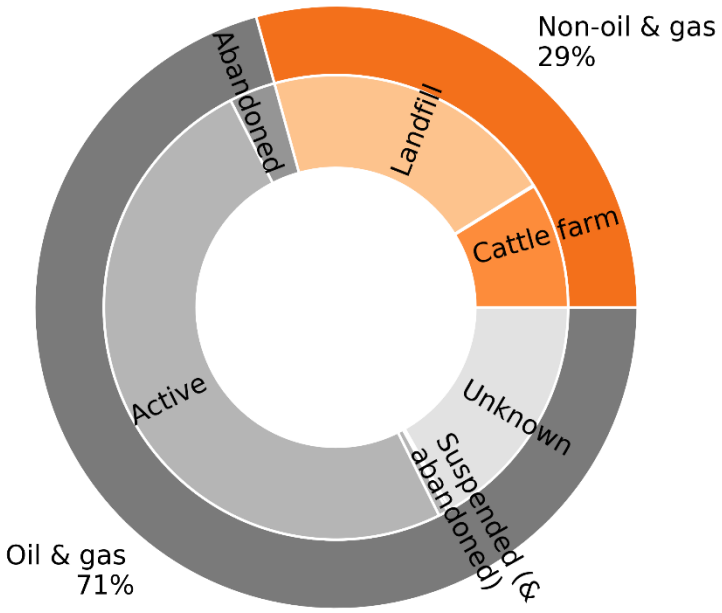

Figure 28: Contributions of source types to total anthropogenic emissions determined in Grande Prairie, Alberta, Canada in November 2021. Main categories represent oil and gas-related sources (gray) and those unrelated to oil and gas production (orange). Contributions of sub-categories are shown in the inner circle. 'Suspended' and 'suspended & abandoned' oil and gas sites are shown as one sub-category due to their small contributions. For the same reason, the visualization of the greenhouse farm was omitted.

Methane concentration measurements further indicated variation within a year, and concentrations tended to be higher in the winter months and lowest in the summer (Appendix C, Figure 43). This is related to the fact that tropospheric hydroxyl radicals, which act as CH_4 oxidants, face reduced production in winter due to a decrease in sunlight. As a result, the atmospheric CH_4 sink is reduced and CH_4 concentrations tend to peak in winter. Shorter days and overall less vertical atmospheric mixing in the winter may also have favoured increased CH_4 concentrations. This trend was especially pronounced at the urban Henry Pirker station. Possibly, concentrations were particularly elevated during the winter at this station as a result of emissions

from residential heating (Merrin and Francisco, 2019), traffic or other urban sources (Ars et al., 2020). According to the federal inventory, residential combustion contributed 4% to total anthropogenic CH_4 emissions in Canada in 2018 (Scarpelli et al., 2021). At the Poplar station, north-western wind directions prevailed, and thus elevated CH_4 concentrations (> 2 ppm) were mostly measured 1500 m downwind of a wastewater disposal plant (Figure 29). The Wembley station was situated in an area with high vegetation cover and generally showed lower concentrations. Possibly, slightly elevated CH_4 concentrations at this station could have originated from the approximately 1 km distant creek (Bastviken et al., 2011).

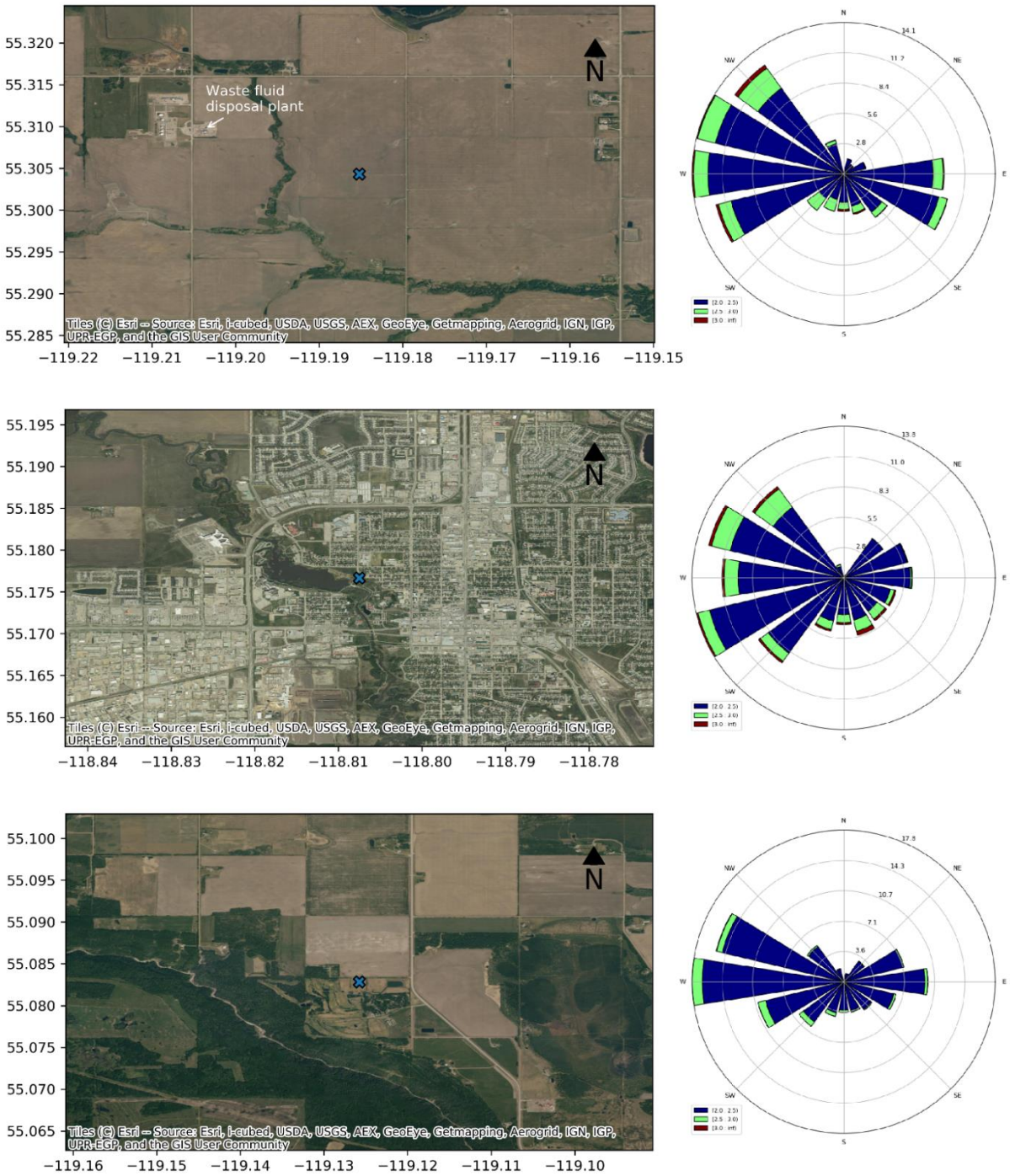

Figure 29: Maps of airshed locations (blue cross; from top to bottom: Poplar, Henry Pirker, Wembley) and their surroundings (roughly 2 km in each direction) together with respective concentration roses. Binned CH_4 concentration frequencies with concentrations above 2 ppm were coupled with wind direction.

5.4 Conclusion

This study shows a wide range of possible anthropogenic CH_4 emission sources for the city of Grande Prairie and its surroundings, with the intention to quantify emission rates from the upstream oil and gas industry, agriculture, and waste management. Despite large uncertainties for agriculture and waste management, mean observed emission rates were similar for individual oil and gas sites and agricultural sources – although oil and gas sites significantly outnumbered farms. In this area, oil and gas-related emissions were lower than found for other regions in past studies, possibly due to operator culture or the effect of recently introduced regulation. Although further emission reduction potential exists for the oil and gas industry in Grande Prairie, this area performs well relative to other sites in Canada. The low emissions of sites in Grande Prairie show that emission mitigation in the oil and gas sector is possible, which will be needed to achieve emission reduction targets, including those embedded in the Global Methane Pledge. Emissions from a landfill showcased the need for emission regulations in the waste sector. Moreover, we presume further emission sources from urban and residential areas, for example from heating.

Insights from long-term stationary measurements were valuable to better understand patterns of temporal differences and the effect of varying landscapes on CH_4 concentrations. However, we propose an integration of CO_2 measurements into the framework as an indicator of emissions from combustion and traffic, and to facilitate the attribution of potential CH_4 sources. Future studies in different regions in Alberta will provide a better picture of regional CH_4 emissions and complement this study to establish a measurement-based CH_4 inventory against which top-down approaches will be compared.

5.5 Acknowledgements

We thank Environment and Climate Change Canada (Award number: GCXE21S043) and the Alberta Energy Regulator for their support of this work. We also thank the Peace Airshed Zone Association for sharing their data from long-term stationary measurements.

Chapter 6: Summary and discussion

Greenhouse gas emissions to the atmosphere provoke positive climate feedbacks, for example leading to changes in plant productivity, disturbance through fires or permafrost thaw, and we must curb the release of anthropogenic greenhouse gases to decelerate global warming. Fast and effective emission mitigation requires measurements and a good understanding of source magnitude. An ideal strategy to emission mitigation includes measurements repeated regularly over time since emission patterns are not static but may change and evolve with ongoing warming. As such, pristine natural ecosystems such as boreal peatlands have mainly acted as carbon sinks over centuries or millennia, but those that have faced severe degradation because of human disturbance may have shifted to net carbon sources. In addition, new technologies allow for capture of greenhouse gases and may have the potential to counteract increasing atmospheric greenhouse gas mixing ratios. Hence, a comprehensive and temporally explicit assessment of greenhouse gas emissions is essential to adapt mitigation practices on the road to net-zero. The four parts of this thesis comprise measurement-based studies that investigate natural ecosystems (peatlands) and regions (Arctic) that are among the most vulnerable to human-induced disturbance, as well as the main CH_4-emitting anthropogenic sectors (energy, agriculture, waste) which are currently underregulated in Canada.

The second chapter focused on the impacts of anthropogenic degradation of a boreal peatland on N_2O fluxes in comparison to an adjacent undisturbed bog. Measurement techniques were based on flux chamber sampling and subsequent gas chromatography to determine N_2O concentration changes over time. Although human-induced disturbance led to differences of several environmental conditions including moisture content, nutrient availability, and vegetation composition between the compared peatland sites, N_2O fluxes were not substantially different.

This study supports the understanding of peatland responses to a chain of anthropogenic disturbances and even though effects on N_2O fluxes were negligible, an increased carbon sink capacity of the disturbed peatland was shown previously due to higher aboveground biomass (Wang et al., 2019, 2018).

The third chapter investigated CH_4 levels in and over the ocean in sub-Arctic and Arctic regions that are most severely affected by climate change. These climate-driven impacts may cause permafrost thaw or reduction of sea ice cover, possibly enhancing CH_4 production pathways within the ocean water column, and thus increasing the potential for emissions to the atmosphere. Continuous measurements of atmospheric CH_4 levels were conducted on a ship complemented with repeated seawater sampling. This study showed sustained high concentrations of CH_4 within the water column in proximity to seeps, while atmospheric CH_4 levels were likely influenced both by on- and offshore sources. Due to ongoing global warming and expected climate feedbacks in the Arctic, the relevance of continued monitoring of greenhouse gases in high-latitude northern regions becomes apparent. Given the geographic disparity of global warming that has Arctic regions experience highest temperature increases, collective climate action is required (Van Houtan et al., 2021). The path towards net-zero can only be followed with a holistic understanding of greenhouse gas emissions, and as the lowest-hanging fruit anthropogenic emissions are to be reduced.

Subsequent chapters focused on anthropogenic CH_4 emissions. The fourth chapter examined emissions from the oil and gas industry and showed that a few certain types of infrastructure were responsible for a large fraction of regional CH_4 emissions. The analysis included the quantification of emissions from oil and gas sites that were not producing at the time of measurement, which yielded a substantial contribution to overall emissions compared to active

infrastructure. Nonetheless, the comparison to studies in previous years showed a decreasing trend of oil and gas emissions in a hotspot region. These reductions are crucially needed to stay on track to net-zero but can only be achieved by compliance to regulations and assessed through regular measurements. This study revealed significant gaps in current regulations in the oil and gas sector.

In the fifth chapter, the contribution of the main anthropogenic emission sectors to regional CH_4 emissions was quantified. Results showed regionally low emissions, and on average similar CH_4 emissions from oil and gas and livestock. However, the contribution of the oil and gas industry to total regional emissions was highest due to the large number of sites compared to the number of farms. In addition, we detected significant CH_4 emissions from a single landfill. Large uncertainties of emission estimates confirmed existing challenges to uniformly detect and quantify CH_4 emissions across sources, which effectively reflects difficulties to abate cross-sector emissions on a regulatory level. This study reinforced the potential to reduce emissions in the underregulated agricultural and waste sectors on a regional level, and the continued importance of mitigation in the oil and gas industry.

The studies presented in this thesis show cases of overall mild N_2O and CH_4 input to the atmosphere compared to other studies in the respective fields. However, it should not be forgotten that Canada remains within the top-10 global players that contribute to climate change (Jones et al., 2023). The oil and gas industry constitutes the lowest-hanging fruit for CH_4 emission mitigation among anthropogenic sources in Canada, and several studies have shown that inventories derivate from actually measured emissions (Johnson et al., 2017; MacKay et al., 2021; Scarpelli et al., 2021). Although regulations to curb anthropogenic CH_4 emissions are partially in place, this thesis identified gaps in regulations, so that more stringent mitigation and

compliance are required to achieve the ambitious emission reduction targets on a national level. The underestimation of emissions in the national inventory is problematic in that it increases set target emission levels, misallocates attention of policymakers and stakeholders, and decreases incentives for emission abatement. The establishment of broad-scale monitoring observatories could help improve inventories, bring forward more effective regulations, manifest compliance, and ultimately approach net-zero targets. Such observatories could entail techniques and approaches as shown in this thesis, plus could be fostered by the development of more accessible instrumentation. A variety of measurement techniques already exist, ranging from ground-based to space-borne methods. Even though these measurements were proven effective in the detection of large emissions (e.g. Irakulis-Loitxate et al., 2022; Maasakkers et al., 2022), common limitations are labor-intensive data acquisition generally leading to data scarcity, high costs, as well as coarse temporal and spatial resolutions (Erland et al., 2022). Therefore, future efforts should focus on the advancement of technologies to overcome these limitations, for example by merchandising precise low-cost greenhouse gas analyzers to establish a broader network of observational systems (Bastviken et al., 2022). These broad-scale observational systems could include "vessels of opportunity" carrying plug-and-play measurement devices, therefore serving a double-purpose by continuously recording atmospheric greenhouse gas levels on commercial trains, ships, planes, or public transportation vehicles. A larger, more continuous data coverage would also benefit data-driven decision support (Niloofar et al., 2021) and machine learning approaches (Hsu et al., 2022), possibly advancing the establishment of more effective mitigation practices in a sustainable future. Such developments could support measurement networks across sectors and tackle the lack of available observational data to reduce uncertainties of local to regional emission estimates.

Even though the energy sector plays a major role in emission mitigation in Canada, uncertainties in the global CH_4 budget are highest for wetlands and inland waters (Saunois et al., 2020). Therefore, future research should focus on the emission quantification in these ecosystems. In addition, further investigation of future trends of hydroxyl radicals that oxidize CH_4 would shed light on the CH_4 sink capacity, which was found to be reduced as a result of lockdowns during the pandemic (Peng et al., 2022). While natural climate solutions are an opportunity to foster carbon sequestration, for example through afforestation, that alone will not be enough to limit global warming to below 2°C (Griscom et al., 2019).

As we move towards net-zero, emission mitigation should focus on the main anthropogenic sectors: energy, agriculture, and waste. As shown in this thesis, more aggressive CH_4 emission mitigation closing gaps in regulations, for example by including inactive sites, is needed beyond already existing regulatory frameworks in the Canadian oil and gas sector. In the agricultural and waste sectors, there is currently little to no regulation of CH_4 emissions, while efforts to reduce landfill gas emissions are underway. While the oil and gas sector plays a major role in CH_4 emission mitigation, there is clearly a need to quantify CH_4 emissions from agriculture and waste and to include these sectors in policy action plans if Canada is to reach its net-zero goals.

References

Aerts, R., Logtestijn, R., van Staalduinen, M., Toet, S., 1995. Nitrogen supply effects on productivity and potential leaf litter decay of *Carex* species from peatlands differing in nutrient limitation. Oecologia 104, 447–453. https://doi.org/10.1007/BF00341342

Aerts, R., Ludwig, F., 1997. Water-table changes and nutritional status affect trace gas emissions from laboratory columns of peatland soils. Soil Biology and Biochemistry 29, 1691–1698. https://doi.org/10.1016/S0038-0717(97)00074-6

Alm, J., Saarnio, S., Nykänen, H., Silvola, J., Martikainen, P.J., 1999. Winter CO_2, CH_4 and N_2O fluxes on some natural and drained boreal peatlands. Biogeochemistry 44, 163–186. https://doi.org/10.1023/A:1006074606204

Amante, C., Eakins, B.W., 2009. ETOPO1 1 Arc-Minute Global Relief Model: Procedures, Data Sources and Analysis. NOAA Technical Memorandum NESDIS NGDC 24, 19.

Amundsen Science Data Collection, 2021a. CCGS Amundsen Navigation (NAV) data recorded during the annual science expeditions in the Canadian Arctic. Canadian Cryospheric Information Network (CCIN), Waterloo, Canada, ArcticNet Inc., Québec, Canada Complete data Version 1. https://doi.org/10.5884/12447

Amundsen Science Data Collection, 2021b. AVOS Meteorological Data collected by the CCGS Amundsen in the Canadian Arctic. Canadian Cryospheric Information Network (CCIN), Waterloo, Canada, ArcticNet Inc., Québec, Canada Processed data. https://doi.org/10.5884/12518

Amundsen Science Data Collection, 2021c. CTD-Rosette data collected by the CCGS Amundsen in the Canadian Arctic. Canadian Cryospheric Information Network (CCIN), Waterloo, Canada, ArcticNet Inc., Québec, Canada Processed data Version 1. https://doi.org/10.5884/12713

Amundsen Science Data Collection, 2021d. TSG data collected by the CCGS Amundsen in the Canadian Arctic. Canadian Cryospheric Information Network (CCIN), Waterloo, Canada Processed data Version 3. https://doi.org/10.5884/12715

Amundsen Science Data Collection, 2021e. Amundsen Science field station lists. Canadian Cryospheric Information Network (CCIN), Waterloo, Canada.

Anhalt, J., 2016. Greenpath 2016 Alberta Fugitive and Vented Emissions Inventory Study.

Ars, S., Vogel, F., Arrowsmith, C., Heerah, S., Knuckey, E., Lavoie, J., Lee, C., Pak, N.M., Phillips, J.L., Wunch, D., 2020. Investigation of the Spatial Distribution of Methane Sources in the Greater Toronto Area Using Mobile Gas Monitoring Systems. Environ. Sci. Technol. 54, 15671–15679. https://doi.org/10.1021/acs.est.0c05386

Atherton, E., Risk, D., Fougère, C., Lavoie, M., Marshall, A., Werring, J., Williams, J.P., Minions, C., 2017. Mobile measurement of methane emissions from natural gas developments in northeastern British Columbia, Canada. Atmospheric Chemistry and Physics 17, 12405–12420. https://doi.org/10.5194/acp-17-12405-2017

Azetsu-Scott, K., Petrie, B., Yeats, P., Lee, C., 2012. Composition and fluxes of freshwater through Davis Strait using multiple chemical tracers. Journal of Geophysical Research: Oceans 117. https://doi.org/10.1029/2012JC008172

Baillie, J., Risk, D., Atherton, E., O'Connell, E., Fougère, C., Bourlon, E., MacKay, K., 2019. Methane emissions from conventional and unconventional oil and gas production sites in southeastern Saskatchewan, Canada. Environmental Research Communications 1, 011003. https://doi.org/10.1088/2515-7620/ab01f2

Banaś, K., Gos, K., 2004. Effect of peat-bog reclamation on the physico-chemical characteristics of the ground water in peat. Polish Journal of Ecology 52, 69–74.

Barnes, R.O., Goldberg, E.D., 1976. Methane production and consumption in anoxic marine sediments. Geology 4, 297–300. https://doi.org/10.1130/0091-7613(1976)4<297:MPACIA>2.0.CO;2

Basarab, J.A., Okine, E.K., Baron, V.S., Marx, T., Ramsey, P., Ziegler, K., Lyle, K., 2005. Methane emissions from enteric fermentation in Alberta's beef cattle population. Canadian Journal of Animal Science 85, 501–512. https://doi.org/10.4141/A04-069

Bastviken, D., Tranvik, L.J., Downing, J.A., Crill, P.M., Enrich-Prast, A., 2011. Freshwater Methane Emissions Offset the Continental Carbon Sink. Science 331, 50–50. https://doi.org/10.1126/science.1196808

Bastviken, D., Wilk, J., Duc, N.T., Gålfalk, M., Karlson, M., Neset, T.-S., Opach, T., Enrich-Prast, A., Sundgren, I., 2022. Critical method needs in measuring greenhouse gas fluxes. Environ. Res. Lett. 17, 104009. https://doi.org/10.1088/1748-9326/ac8fa9

Bell, C.S., Vaughn, T.L., Zimmerle, D., Herndon, S.C., Yacovitch, T.I., Heath, G.A., Pétron, G., Edie, R., Field, R.A., Murphy, S.M., Robertson, A.M., Soltis, J., 2017. Comparison of methane emission estimates from multiple

measurement techniques at natural gas production pads. Elementa: Science of the Anthropocene 5. https://doi.org/10.1525/elementa.266
Berchet, A., Pison, I., Crill, P.M., Thornton, B., Bousquet, P., Thonat, T., Hocking, T., Thanwerdas, J., Paris, J.-D., Saunois, M., 2020. Using ship-borne observations of methane isotopic ratio in the Arctic Ocean to understand methane sources in the Arctic. Atmospheric Chemistry and Physics 20, 3987–3998. https://doi.org/10.5194/acp-20-3987-2020
Bhatti, J., Tarnocai, C., 2009. Influence of Climate and Land Use Change on Carbon in Agriculture, Forest, and Peatland Ecosystems across Canada, in: Lal, R. and Follett, R. (Ed.), Soil Carbon Sequestration and the Greenhouse Effect, SSSA Special Publication 57. Soil Science Society of America, pp. 47–70.
Bjelm, L., 1980. Geological interpretation with subsurface interface radar (SIR) in peat lands, in: 6th International Peat Congress, Duluth, Minnesota. pp. 7–8.
Blodau, C., 2002. Carbon cycling in peatlands: a review of processes and controls. Environmental Reviews 10, 111–134. https://doi.org/10.1139/A02-004
Boles, J.R., Clark, J.F., Leifer, I., Washburn, L., 2001. Temporal variation in natural methane seep rate due to tides, Coal Oil Point area, California. Journal of Geophysical Research: Oceans 106, 27077–27086. https://doi.org/10.1029/2000JC000774
Bonaglia, S., Rütting, T., Kononets, M., Stigebrandt, A., Santos, I.R., Hall, P.O.J., 2022. High methane emissions from an anoxic fjord driven by mixing and oxygenation. Limnology and Oceanography Letters 7, 392–400. https://doi.org/10.1002/lol2.10259
Boothroyd, I.M., Almond, S., Qassim, S.M., Worrall, F., Davies, R.J., 2016. Fugitive emissions of methane from abandoned, decommissioned oil and gas wells. Science of The Total Environment 547, 461–469. https://doi.org/10.1016/j.scitotenv.2015.12.096
Brandt, A.R., Heath, G.A., Cooley, D., 2016. Methane Leaks from Natural Gas Systems Follow Extreme Distributions. Environmental Science & Technology 50, 12512–12520. https://doi.org/10.1021/acs.est.6b04303
Brantley, H.L., Thoma, E.D., Squier, W.C., Guven, B.B., Lyon, D., 2014. Assessment of Methane Emissions from Oil and Gas Production Pads using Mobile Measurements. Environmental Science & Technology 48, 14508–14515. https://doi.org/10.1021/es503070q
Bryden, H.L., 1973. New polynomials for thermal expansion, adiabatic temperature gradient and potential temperature of sea water. Deep Sea Research and Oceanographic Abstracts 20, 401–408. https://doi.org/10.1016/0011-7471(73)90063-6
Budkewitsch, P., Pavlic, G., Oakey, G., Jauer, C., Decker, V., 2013. Reconnaissance mapping of suspect oil seep occurrences in Baffin Bay and Davis Strait using satellite radar: preliminary results. Geological Survey Canada 7068. https://doi.org/10.4095/292280
Cai, B., Lou, Z., Wang, J., Geng, Y., Sarkis, J., Liu, J., Gao, Q., 2018. CH_4 mitigation potentials from China landfills and related environmental co-benefits. Science Advances 4. https://doi.org/10.1126/sciadv.aar8400
Canada's Beef Industry, 2021. Canada's Beef Industry Fast Facts. Canadian Beef.
Castro-Morales, K., Canning, A., Arzberger, S., Overholt, W.A., Küsel, K., Kolle, O., Göckede, M., Zimov, N., Körtzinger, A., 2022. Highest methane concentrations in an Arctic river linked to local terrestrial inputs. Biogeosciences 19, 5059–5077. https://doi.org/10.5194/bg-19-5059-2022
Chan, E., Worthy, D.E.J., Chan, D., Ishizawa, M., Moran, M.D., Delcloo, A., Vogel, F., 2020. Eight-Year Estimates of Methane Emissions from Oil and Gas Operations in Western Canada Are Nearly Twice Those Reported in Inventories. Environmental Science & Technology 54, 14899–14909. https://doi.org/10.1021/acs.est.0c04117
Chapin, F.S., Woodwell, G.M., Randerson, J.T., Rastetter, E.B., Lovett, G.M., Baldocchi, D.D., Clark, D.A., Harmon, M.E., Schimel, D.S., Valentini, R., Wirth, C., Aber, J.D., Cole, J.J., Goulden, M.L., Harden, J.W., Heimann, M., Howarth, R.W., Matson, P.A., McGuire, A.D., Melillo, J.M., Mooney, H.A., Neff, J.C., Houghton, R.A., Pace, M.L., Ryan, M.G., Running, S.W., Sala, O.E., Schlesinger, W.H., Schulze, E.-D., 2006. Reconciling Carbon-cycle Concepts, Terminology, and Methods. Ecosystems 9, 1041–1050. https://doi.org/10.1007/s10021-005-0105-7
Chapuis-Lardy, L., Wrage, N., Metay, A., Chotte, J.-L., Bernoux, M., 2007. Soils, a sink for N_2O - A review. Global Change Biology 13, 1–17. https://doi.org/10.1111/j.1365-2486.2006.01280.x
Chuvilin, E., Ekimova, V., Davletshina, D., Sokolova, N., Bukhanov, B., 2020. Evidence of Gas Emissions from Permafrost in the Russian Arctic. Geosciences 10, 383. https://doi.org/10.3390/geosciences10100383
Cramm, M.A., Neves, B. de M., Manning, C.C.M., Oldenburg, T.B.P., Archambault, P., Chakraborty, A., Cyr-Parent, A., Edinger, E.N., Jaggi, A., Mort, A., Tortell, P., Hubert, C.R.J., 2021. Characterization of marine microbial

communities around an Arctic seabed hydrocarbon seep at Scott Inlet, Baffin Bay. Science of The Total Environment 762, 143961. https://doi.org/10.1016/j.scitotenv.2020.143961
Cui, Q., Song, C., Wang, X., Shi, F., Wang, L., Guo, Y., 2016. Rapid N_2O fluxes at high level of nitrate nitrogen addition during freeze-thaw events in boreal peatlands of Northeast China. Atmospheric Environment 135, 1–8. https://doi.org/10.1016/j.atmosenv.2016.03.053
Cusworth, D.H., Duren, R.M., Thorpe, A.K., Tseng, E., Thompson, D., Guha, A., Newman, S., Foster, K.T., Miller, C.E., 2020. Using remote sensing to detect, validate, and quantify methane emissions from California solid waste operations. Environmental Research Letters 15, 054012. https://doi.org/10.1088/1748-9326/ab7b99
Dalby, F.R., Hafner, S.D., Petersen, S.O., VanderZaag, A.C., Habtewold, J., Dunfield, K., Chantigny, M.H., Sommer, S.G., 2021. Understanding methane emission from stored animal manure: A review to guide model development. Journal of Environmental Quality 50, 817–835. https://doi.org/10.1002/jeq2.20252
Damm, E., Ericson, Y., Falck, E., 2021. Waterside convection and stratification control methane spreading in supersaturated Arctic fjords (Spitsbergen). Continental Shelf Research 224, 104473. https://doi.org/10.1016/j.csr.2021.104473
Damm, E., Kiene, R.P., Schwarz, J., Falck, E., Dieckmann, G., 2008. Methane cycling in Arctic shelf water and its relationship with phytoplankton biomass and DMSP. Marine Chemistry 109, 45–59. https://doi.org/10.1016/j.marchem.2007.12.003
Damm, E., Rudels, B., Schauer, U., Mau, S., Dieckmann, G., 2015. Methane excess in Arctic surface water- triggered by sea ice formation and melting. Sci Rep 5, 16179. https://doi.org/10.1038/srep16179
DeGrandpre, M., Evans, W., Timmermans, M.-L., Krishfield, R., Williams, B., Steele, M., 2020. Changes in the Arctic Ocean Carbon Cycle With Diminishing Ice Cover. Geophysical Research Letters 47, e2020GL088051. https://doi.org/10.1029/2020GL088051
Delkash, M., Chow, F.K., Imhoff, P.T., 2022. Diurnal landfill methane flux patterns across different seasons at a landfill in Southeastern US. Waste Management 144, 76–86. https://doi.org/10.1016/j.wasman.2022.03.004
Denmead, O.T., 2008. Approaches to measuring fluxes of methane and nitrous oxide between landscapes and the atmosphere. Plant Soil 309, 5–24. https://doi.org/10.1007/s11104-008-9599-z
Dinsmore, K.J., Skiba, U.M., Billett, M.F., Rees, R.M., 2008. Effect of water table on greenhouse gas emissions from peatland mesocosms. Plant and Soil 318, 229. https://doi.org/10.1007/s11104-008-9832-9
Dlugokencky, E., Tans, P., 2022. NOAA /GML [WWW Document]. URL https://gml.noaa.gov/ccgg/trends/ (accessed 4.4.22).
Dlugokencky, E.J., 2022. Trends in Atmospheric Methane. NOAA/GML gml.noaa.gov/ccgg/trends_ch4/.
Dlugokencky, E.J., 2016. Atmospheric Methane Dry Air Mole Fractions (1983-2015) and Atmospheric Carbon Dioxide Dry Air Mole Fractions (1968-2015) from the NOAA ESRL Carbon Cycle Cooperative Global Air Sampling Network, original data files. NOAA, Bremerhaven. https://doi.org/10/2/co2_mm_mlo_201508_2016-08-30.zip
Dlugokencky, E.J., Crotwell, A.M., Mund, J.W., Crotwell, M.J., Thoning, K.W., 2021. Atmospheric Methane Dry Air Mole Fractions from the NOAA GML Carbon Cycle Cooperative Global Air Sampling Network, 1983-2020 Version 2021-07-30. https://doi.org/10.15138/VNCZ-M766
Dølven, K.O., Ferré, B., Silyakova, A., Jansson, P., Linke, P., Moser, M., 2022. Autonomous methane seep site monitoring offshore western Svalbard: hourly to seasonal variability and associated oceanographic parameters. Ocean Science 18, 233–254. https://doi.org/10.5194/os-18-233-2022
Du, M., Peng, C., Wang, X., Chen, H., Wang, M., Zhu, Q., 2017. Quantification of methane emissions from municipal solid waste landfills in China during the past decade. Renewable and Sustainable Energy Reviews 78, 272–279. https://doi.org/10.1016/j.rser.2017.04.082
Duan, Z., Kjeldsen, P., Scheutz, C., 2022. Efficiency of gas collection systems at Danish landfills and implications for regulations. Waste Management 139, 269–278. https://doi.org/10.1016/j.wasman.2021.12.023
Edie, R., Robertson, A.M., Field, R.A., Soltis, J., Snare, D.A., Zimmerle, D., Bell, C.S., Vaughn, T.L., Murphy, S.M., 2020. Constraining the accuracy of flux estimates using OTM 33A. Atmospheric Measurement Techniques 13, 341–353. https://doi.org/10.5194/amt-13-341-2020
Efron, B., Tibshirani, R., 1986. Bootstrap Methods for Standard Errors, Confidence Intervals, and Other Measures of Statistical Accuracy. Statistical Science 1, 54–75. https://doi.org/10.1214/ss/1177013815
Environment and Climate Change Canada, 2022a. Reducing methane emissions from Canada's oil and gas sector: Discussion paper. Government of Canada.
Environment and Climate Change Canada, 2022b. Reducing methane emissions from Canada's municipal solid waste landfills: Discussion paper. Government of Canada.

Environment and Climate Change Canada, 2021a. Canada confirms its support for the Global Methane Pledge and announces ambitious domestic actions to slash methane emissions.
Environment and Climate Change Canada, 2021b. National Inventory Report 1990-2019: Greenhouse gas sources and sinks in Canada. United Nations Framework Convention on Climate Change Part 2.
Environment and Climate Change Canada, 2020. National Inventory Report 1990–2018: Greenhouse Gas Sources and Sinks in Canada: Executive Summary.
Environment and Climate Change Canada, 2019. Regulations Respecting Reduction in the Release of Methane and Certain Volatile Organic Compounds (Upstream Oil and Gas Sector).
Erland, B.M., Thorpe, A.K., Gamon, J.A., 2022. Recent Advances Toward Transparent Methane Emissions Monitoring: A Review. Environ. Sci. Technol. 56, 16567–16581. https://doi.org/10.1021/acs.est.2c02136
Etiope, G., Sherwood Lollar, B., 2013. Abiotic Methane on Earth. Reviews of Geophysics 51, 276–299. https://doi.org/10.1002/rog.20011
European Commission, 2021. Launch by United States, the European Union, and Partners of the Global Methane Pledge to Keep 1.5C Within Reach (Text).
Ewing, J.M., Vepraskas, M.J., 2006. Estimating primary and secondary subsidence in an organic soil 15, 20, and 30 years after drainage. Wetlands 26, 119–130. https://doi.org/10.1672/0277-5212(2006)26[119:EPASSI]2.0.CO;2
Fang, Y., Naik, V., Horowitz, L.W., Mauzerall, D.L., 2013. Air pollution and associated human mortality: the role of air pollutant emissions, climate change and methane concentration increases from the preindustrial period to present. Atmospheric Chemistry and Physics 13, 1377–1394. https://doi.org/10.5194/acp-13-1377-2013
Fankhauser, S., Smith, S.M., Allen, M., Axelsson, K., Hale, T., Hepburn, C., Kendall, J.M., Khosla, R., Lezaun, J., Mitchell-Larson, E., Obersteiner, M., Rajamani, L., Rickaby, R., Seddon, N., Wetzer, T., 2022. The meaning of net zero and how to get it right. Nat. Clim. Chang. 12, 15–21. https://doi.org/10.1038/s41558-021-01245-w
Fenwick, L., Capelle, D., Damm, E., Zimmermann, S., Williams, W.J., Vagle, S., Tortell, P.D., 2017. Methane and nitrous oxide distributions across the North American Arctic Ocean during summer, 2015. Journal of Geophysical Research: Oceans 122, 390–412. https://doi.org/10.1002/2016JC012493
Fisher, R.E., Sriskantharajah, S., Lowry, D., Lanoisellé, M., Fowler, C.M.R., James, R.H., Hermansen, O., Lund Myhre, C., Stohl, A., Greinert, J., Nisbet-Jones, P.B.R., Mienert, J., Nisbet, E.G., 2011. Arctic methane sources: Isotopic evidence for atmospheric inputs. Geophysical Research Letters 38. https://doi.org/10.1029/2011GL049319
Fofonoff, P., Millard, R.C.Jr., 1983. Algorithms for computation of fundamental properties of seawater - UNESCO Digital Library. UNESCO Technical Papers in Marine Science 44.
Food and Agriculture Organization of the United Nations, 2022. Crops and livestock products [WWW Document]. URL https://www.fao.org/faostat/en/#data/ (accessed 4.27.22).
Forster, P., Storelvmo, T., Armour, K., Collins, W., Dufresne, J.-L., Frame, D., Lunt, Daniel.J., Mauritsen, T., Palmer, M.D., Watanabe, M., Wild, Zhang, H., 2021. Chapter 7: The Earth's Energy Budget, Climate Feedbacks, and Climate Sensitivity, in: Climate Change 2021: The Physical Science Basis. Contribution of Working Group I to the Sixth Assessment Report of the Intergovernmental Panel on Climate Change. Cambridge University Press, Cambridge, UK.
Fox, T.A., Barchyn, T.E., Risk, D., Ravikumar, A.P., Hugenholtz, C.H., 2019. A review of close-range and screening technologies for mitigating fugitive methane emissions in upstream oil and gas. Environmental Research Letters 14, 053002. https://doi.org/10.1088/1748-9326/ab0cc3
Fox-Kemper, B., Hewitt, H.T., Xiao, C., Aðalgeirsdóttir, G., Drijfhout, S.S., Edwards, T.L., Golledge, N.R., Hemer, M., Kopp, R.E., Krinner, G., Mix, A., Notz, D., Nowicki, S., Nurhati, I.S., Ruiz, L., Sallée, J.-B., Slangen, A.B.A., Yu, Y., 2021. Ocean, Cryosphere and Sea Level Change, in: Climate Change 2021: The Physical Science Basis. Contribution of Working Group I to the Sixth Assessment Report of the Intergovernmental Panel on Climate Change. Cambridge University Press, Cambridge, UK.
Frankenberg, C., Thorpe, A.K., Thompson, D.R., Hulley, G., Kort, E.A., Vance, N., Borchardt, J., Krings, T., Gerilowski, K., Sweeney, C., Conley, S., Bue, B.D., Aubrey, A.D., Hook, S., Green, R.O., 2016. Airborne methane remote measurements reveal heavy-tail flux distribution in Four Corners region. Proceedings of the National Academy of Sciences 113, 9734–9739. https://doi.org/10.1073/pnas.1605617113
Fratantoni, P.S., Pickart, R.S., 2007. The Western North Atlantic Shelfbreak Current System in Summer. Journal of Physical Oceanography 37, 2509–2533. https://doi.org/10.1175/JPO3123.1

Fredenslund, A.M., Scheutz, C., Kjeldsen, P., 2010. Tracer method to measure landfill gas emissions from leachate collection systems. Waste Management, Special Thematic Section: Sanitary Landfilling 30, 2146–2152. https://doi.org/10.1016/j.wasman.2010.03.013

Freeman, C., Lock, M.A., Reynolds, B., 1992. Fluxes of CO_2, CH_4, and N_2O from a Welsh peatland following simulation of water table draw-down: Potential feedback to climatic change. Biogeochemistry 19, 51–60. https://doi.org/10.1007/BF00000574

Friedlingstein, P., O'Sullivan, M., Jones, M.W., Andrew, R.M., Gregor, L., Hauck, J., Le Quéré, C., Luijkx, I.T., Olsen, A., Peters, G.P., Peters, W., Pongratz, J., Schwingshackl, C., Sitch, S., Canadell, J.G., Ciais, P., Jackson, R.B., Alin, S.R., Alkama, R., Arneth, A., Arora, V.K., Bates, N.R., Becker, M., Bellouin, N., Bittig, H.C., Bopp, L., Chevallier, F., Chini, L.P., Cronin, M., Evans, W., Falk, S., Feely, R.A., Gasser, T., Gehlen, M., Gkritzalis, T., Gloege, L., Grassi, G., Gruber, N., Gürses, Ö., Harris, I., Hefner, M., Houghton, R.A., Hurtt, G.C., Iida, Y., Ilyina, T., Jain, A.K., Jersild, A., Kadono, K., Kato, E., Kennedy, D., Klein Goldewijk, K., Knauer, J., Korsbakken, J.I., Landschützer, P., Lefèvre, N., Lindsay, K., Liu, J., Liu, Z., Marland, G., Mayot, N., McGrath, M.J., Metzl, N., Monacci, N.M., Munro, D.R., Nakaoka, S.-I., Niwa, Y., O'Brien, K., Ono, T., Palmer, P.I., Pan, N., Pierrot, D., Pocock, K., Poulter, B., Resplandy, L., Robertson, E., Rödenbeck, C., Rodriguez, C., Rosan, T.M., Schwinger, J., Séférian, R., Shutler, J.D., Skjelvan, I., Steinhoff, T., Sun, Q., Sutton, A.J., Sweeney, C., Takao, S., Tanhua, T., Tans, P.P., Tian, X., Tian, H., Tilbrook, B., Tsujino, H., Tubiello, F., van der Werf, G.R., Walker, A.P., Wanninkhof, R., Whitehead, C., Willstrand Wranne, A., Wright, R., Yuan, W., Yue, C., Yue, X., Zaehle, S., Zeng, J., Zheng, B., 2022. Global Carbon Budget 2022. Earth System Science Data 14, 4811–4900. https://doi.org/10.5194/essd-14-4811-2022

Fröb, F., Olsen, A., Våge, K., Moore, G.W.K., Yashayaev, I., Jeansson, E., Rajasakaren, B., 2016. Irminger Sea deep convection injects oxygen and anthropogenic carbon to the ocean interior. Nat Commun 7, 13244. https://doi.org/10.1038/ncomms13244

Frolking, S., Talbot, J., Jones, M.C., Treat, C.C., Kauffman, J.B., Tuittila, E.-S., Roulet, N., 2011. Peatlands in the Earth's 21st century climate system. Environ. Rev. 19, 371–396. https://doi.org/10.1139/a11-014

Gautier, D.L., Bird, K.J., Charpentier, R.R., Grantz, A., Houseknecht, D.W., Klett, T.R., Moore, T.E., Pitman, J.K., Schenk, C.J., Schuenemeyer, J.H., Sørensen, K., Tennyson, M.E., Valin, Z.C., Wandrey, C.J., 2011. Oil and gas resource potential north of the Arctic Circle. Arctic Petroleum Geology 35. https://doi.org/10.1144/M35.9

Geisseler, D., Scow, K.M., 2014. Long-term effects of mineral fertilizers on soil microorganisms – A review. Soil Biology and Biochemistry 75, 54–63. https://doi.org/10.1016/j.soilbio.2014.03.023

Glatzel, S., Kalbitz, K., Dalva, M., Moore, T., 2003. Dissolved organic matter properties and their relationship to carbon dioxide efflux from restored peat bogs. Geoderma 113, 397–411. https://doi.org/10.1016/S0016-7061(02)00372-5

Goopy, J.P., Korir, D., Pelster, D., Ali, A.I.M., Wassie, S.E., Schlecht, E., Dickhoefer, U., Merbold, L., Butterbach-Bahl, K., 2020. Severe below-maintenance feed intake increases methane yield from enteric fermentation in cattle. British Journal of Nutrition 123, 1239–1246. https://doi.org/10.1017/S0007114519003350

Gorski, J., 2019. Comparing Provincial and Federal Oil and Gas Methane Emissions Regulations – Factsheets for Policy Makers.

Gregersen, U., Bidstrup, T., 2008. Structures and hydrocarbon prospectivity in the northern Davis Strait area, offshore West Greenland. Petroleum Geoscience 14, 151–166. https://doi.org/10.1144/1354-079308-752

Griscom, B.W., Lomax, G., Kroeger, T., Fargione, J.E., Adams, J., Almond, L., Bossio, D., Cook-Patton, S.C., Ellis, P.W., Kennedy, C.M., Kiesecker, J., 2019. We need both natural and energy solutions to stabilize our climate. Global Change Biology 25, 1889–1890. https://doi.org/10.1111/gcb.14612

Hättenschwiler, S., Vitousek, P.M., 2000. The role of polyphenols in terrestrial ecosystem nutrient cycling. Trends in Ecology & Evolution 15, 238–243. https://doi.org/10.1016/S0169-5347(00)01861-9

He, X., Sun, L., Xie, Z., Huang, W., Long, N., Li, Z., Xing, G., 2013. Sea ice in the Arctic Ocean: Role of shielding and consumption of methane. Atmospheric Environment 67, 8–13. https://doi.org/10.1016/j.atmosenv.2012.10.029

Heiskanen, J., Brümmer, C., Buchmann, N., Calfapietra, C., Chen, H., Gielen, B., Gkritzalis, T., Hammer, S., Hartman, S., Herbst, M., Janssens, I.A., Jordan, A., Juurola, E., Karstens, U., Kasurinen, V., Kruijt, B., Lankreijer, H., Levin, I., Linderson, M.-L., Loustau, D., Merbold, L., Myhre, C.L., Papale, D., Pavelka, M., Pilegaard, K., Ramonet, M., Rebmann, C., Rinne, J., Rivier, L., Saltikoff, E., Sanders, R., Steinbacher, M., Steinhoff, T., Watson, A., Vermeulen, A.T., Vesala, T., Vítková, G., Kutsch, W., 2022. The Integrated Carbon Observation System in Europe. Bulletin of the American Meteorological Society 103, E855–E872. https://doi.org/10.1175/BAMS-D-19-0364.1

Hemond, H.F., 1983. The Nitrogen Budget of Thoreau's Bog. Ecology 64, 99–109. https://doi.org/10.2307/1937333

Ho, D.T., Law, C.S., Smith, M.J., Schlosser, P., Harvey, M., Hill, P., 2006. Measurements of air-sea gas exchange at high wind speeds in the Southern Ocean: Implications for global parameterizations. Geophysical Research Letters 33. https://doi.org/10.1029/2006GL026817

Holland, E.A., Robertson, G.P., Greenberg, J., Groffmann, P.M., Boone, R.D., Gosz, J.R., 1999. Soil CO_2, N_2O, and CH_4 exchange, in: Robertson, G.P., Coleman, D.C., Bledsoe, C.S., Sollins, P. (Eds.), Standard Soil Methods for Long-Term Ecological Research. Oxford University Press, pp. 185–201.

Holtan-Hartwig, L., Dörsch, P., Bakken, L.R., 2002. Low temperature control of soil denitrifying communities: kinetics of N_2O production and reduction. Soil Biology and Biochemistry 34, 1797–1806. https://doi.org/10.1016/S0038-0717(02)00169-4

Hou, K., Xu, X., 2022. Evaluation of the Influence between Local Meteorology and Air Quality in Beijing Using Generalized Additive Models. Atmosphere 13, 24. https://doi.org/10.3390/atmos13010024

Hsu, A., Wang, X., Tan, J., Toh, W., Goyal, N., 2022. Predicting European cities' climate mitigation performance using machine learning. Nat Commun 13, 7487. https://doi.org/10.1038/s41467-022-35108-5

Hsu, S.A., Meindl, E.A., Gilhousen, D.B., 1994. Determining the Power-Law Wind-Profile Exponent under Near-Neutral Stability Conditions at Sea. Journal of Applied Meteorology and Climatology 33, 757–765. https://doi.org/10.1175/1520-0450(1994)033<0757:DTPLWP>2.0.CO;2

Hugelius, G., Loisel, J., Chadburn, S., Jackson, R.B., Jones, M., MacDonald, G., Marushchak, M., Olefeldt, D., Packalen, M., Siewert, M.B., Treat, C., Turetsky, M., Voigt, C., Yu, Z., 2021. Maps of northern peatland extent, depth, carbon storage and nitrogen storage. Bolin Centre Database Dataset version 2. https://doi.org/10.17043/hugelius-2020-peatland-2

Hugelius, G., Loisel, J., Chadburn, S., Jackson, R.B., Jones, M., MacDonald, G., Marushchak, M., Olefeldt, D., Packalen, M., Siewert, M.B., Treat, C., Turetsky, M., Voigt, C., Yu, Z., 2020. Large stocks of peatland carbon and nitrogen are vulnerable to permafrost thaw. Proc Natl Acad Sci USA 117, 20438–20446. https://doi.org/10.1073/pnas.1916387117

Hurry, J., Risk, D., Lavoie, M., Brooks, B.-G., Phillips, C.L., Göckede, M., 2016. Atmospheric monitoring and detection of fugitive emissions for Enhanced Oil Recovery. International Journal of Greenhouse Gas Control 45, 1–8. https://doi.org/10.1016/j.ijggc.2015.11.031

Ingram, H. a. P., 1978. Soil Layers in Mires: Function and Terminology. Journal of Soil Science 29, 224–227. https://doi.org/10.1111/j.1365-2389.1978.tb02053.x

International Energy Statistics, 2021. Total oil (and other petroleum liquids) production [WWW Document]. URL https://www.eia.gov/international/data/world/petroleum-and-other-liquids/annual-refined-petroleum-products-production (accessed 4.27.22).

IPCC, 2021. Summary for Policymakers, in: Climate Change 2021: The Physical Science Basis. Contribution of Working Group I to the Sixth Assessment Report of the Intergovernmental Panel on Climate Change. In Press.

Irakulis-Loitxate, I., Guanter, L., Maasakkers, J.D., Zavala-Araiza, D., Aben, I., 2022. Satellites Detect Abatable Super-Emissions in One of the World's Largest Methane Hotspot Regions. Environ. Sci. Technol. 56, 2143–2152. https://doi.org/10.1021/acs.est.1c04873

Jackson, R.B., Saunois, M., Bousquet, P., Canadell, J.G., Poulter, B., Stavert, A.R., Bergamaschi, P., Niwa, Y., Segers, A., Tsuruta, A., 2020. Increasing anthropogenic methane emissions arise equally from agricultural and fossil fuel sources. Environ. Res. Lett. 15, 071002. https://doi.org/10.1088/1748-9326/ab9ed2

Jacob, D.J., Turner, A.J., Maasakkers, J.D., Sheng, J., Sun, K., Liu, X., Chance, K., Aben, I., McKeever, J., Frankenberg, C., 2016. Satellite observations of atmospheric methane and their value for quantifying methane emissions. Atmospheric Chemistry and Physics 16, 14371–14396. https://doi.org/10.5194/acp-16-14371-2016

Jähne, B., Heinz, G., Dietrich, W., 1987. Measurement of the diffusion coefficients of sparingly soluble gases in water. Journal of Geophysical Research: Oceans 92, 10767–10776. https://doi.org/10.1029/JC092iC10p10767

Jain, P., Wally, J., Townsend, T.G., Krause, M., Tolaymat, T., 2021. Greenhouse gas reporting data improves understanding of regional climate impact on landfill methane production and collection. PLOS ONE 16, e0246334. https://doi.org/10.1371/journal.pone.0246334

Jakober, C.A., Mara, S.L., Hsu, Y.-K., Herner, J.D., 2015. Mobile measurements of climate forcing agents: Application to methane emissions from landfill and natural gas compression. Journal of the Air & Waste Management Association 65, 404–412. https://doi.org/10.1080/10962247.2014.996269

James, R.H., Bousquet, P., Bussmann, I., Haeckel, M., Kipfer, R., Leifer, I., Niemann, H., Ostrovsky, I., Piskozub, J., Rehder, G., Treude, T., Vielstädte, L., Greinert, J., 2016. Effects of climate change on methane emissions from seafloor sediments in the Arctic Ocean: A review. Limnology and Oceanography 61, S283–S299. https://doi.org/10.1002/lno.10307

Jauer, C.D., Budkewitsch, P., 2010. Old marine seismic and new satellite radar data: Petroleum exploration of north west Labrador Sea, Canada. Marine and Petroleum Geology 27, 1379–1394. https://doi.org/10.1016/j.marpetgeo.2010.03.003

Jingguo, W., Bakken, L.R., 1997. Competition for nitrogen during decomposition of plant residues in soil: Effect of spatial placement of N-rich and N-poor plant residues. Soil Biology and Biochemistry 29, 153–162. https://doi.org/10.1016/S0038-0717(96)00291-X

Johnson, K.A., Johnson, D.E., 1995. Methane emissions from cattle. Journal of Animal Science 73, 2483–2492. https://doi.org/10.2527/1995.7382483x

Johnson, M.R., Tyner, D.R., Conley, S., Schwietzke, S., Zavala-Araiza, D., 2017. Comparisons of Airborne Measurements and Inventory Estimates of Methane Emissions in the Alberta Upstream Oil and Gas Sector. Environmental Science & Technology 51, 13008–13017. https://doi.org/10.1021/acs.est.7b03525

Jones, M.W., Peters, G.P., Gasser, T., Andrew, R.M., Schwingshackl, C., Gütschow, J., Houghton, R.A., Friedlingstein, P., Pongratz, J., Le Quéré, C., 2023. National contributions to climate change due to historical emissions of carbon dioxide, methane, and nitrous oxide since 1850. Sci Data 10, 155. https://doi.org/10.1038/s41597-023-02041-1

Joosten, H., 2009. The Global Peatland CO_2 Picture – Peatland status and drainage related emissions in all countries of the world. Wetlands International 20–30.

Jukaine, J.L., Vasander, H., Laiho, R., 1995. Long-Term Effects of Water Level Drawdown on the Vegetation of Drained Pine Mires in Southern Finland. Journal of Applied Ecology 32, 785–802. https://doi.org/10.2307/2404818

Kandel, T.P., Lærke, P.E., Elsgaard, L., 2018. Annual emissions of CO_2, CH_4 and N_2O from a temperate peat bog: Comparison of an undrained and four drained sites under permanent grass and arable crop rotations with cereals and potato. Agricultural and Forest Meteorology 256–257, 470–481. https://doi.org/10.1016/j.agrformet.2018.03.021

Kang, M., Christian, S., Celia, M.A., Mauzerall, D.L., Bill, M., Miller, A.R., Chen, Y., Conrad, M.E., Darrah, T.H., Jackson, R.B., 2016. Identification and characterization of high methane-emitting abandoned oil and gas wells. Proceedings of the National Academy of Sciences of the United States of America 113, 13636–13641. https://doi.org/10.1073/pnas.1605913113

Kang, M., Kanno, C.M., Reid, M.C., Zhang, X., Mauzerall, D.L., Celia, M.A., Chen, Y., Onstott, T.C., 2014. Direct measurements of methane emissions from abandoned oil and gas wells in Pennsylvania. Proceedings of the National Academy of Sciences of the United States of America 111, 18173–18177. https://doi.org/10.1073/pnas.1408315111

Karl, D.M., Beversdorf, L., Björkman, K.M., Church, M.J., Martinez, A., Delong, E.F., 2008. Aerobic production of methane in the sea. Nature Geosci 1, 473–478. https://doi.org/10.1038/ngeo234

Kasimir-Klemedtsson, Å., Klemedtsson, L., Berglund, K., Martikainen, P., Silvola, J., Oenema, O., 1997. Greenhouse gas emissions from farmed organic soils: a review. Soil Use and Management 13, 245–250. https://doi.org/10.1111/j.1475-2743.1997.tb00595.x

Kebreab, E., Clark, K., Wagner-Riddle, C., France, J., 2006. Methane and nitrous oxide emissions from Canadian animal agriculture: A review. Canadian Journal of Animal Science 86, 135–157. https://doi.org/10.4141/A05-010

Kitidis, V., Upstill-Goddard, R.C., Anderson, L.G., 2010. Methane and nitrous oxide in surface water along the North-West Passage, Arctic Ocean. Marine Chemistry 121, 80–86. https://doi.org/10.1016/j.marchem.2010.03.006

Klemedtsson, L., Von Arnold, K., Weslien, P., Gundersen, P., 2005. Soil CN ratio as a scalar parameter to predict nitrous oxide emissions. Global Change Biology 11, 1142–1147. https://doi.org/10.1111/j.1365-2486.2005.00973.x

Kokkonen, N., Laine, J., Vasander, H., Kurki, K., Gong, J., Tuittila, E.-S., 2018. Peatland plant community succession as forced by water table changes – a long-term field study in southern Finland. 20th EGU General Assembly.

Korsaeth, A., Molstad, L., Bakken, L.R., 2001. Modelling the competition for nitrogen between plants and microflora as a function of soil heterogeneity. Soil Biology and Biochemistry 33, 215–226. https://doi.org/10.1016/S0038-0717(00)00132-2

Kroeze, C., Mosier, A., Bouwman, L., 1999. Closing the global N_2O budget: A retrospective analysis 1500–1994. Global Biogeochemical Cycles 13, 1–8. https://doi.org/10.1029/1998GB900020

Kvenvolden, K.A., 1988. Methane hydrate — A major reservoir of carbon in the shallow geosphere? Chemical Geology, Origins of Methane in the Earth 71, 41–51. https://doi.org/10.1016/0009-2541(88)90104-0

Lai, D.Y.F., 2009. Methane Dynamics in Northern Peatlands: A Review. Pedosphere 19, 409–421. https://doi.org/10.1016/S1002-0160(09)00003-4

Laiho, R., Vasander, H., Penttilä, T., Laine, J., 2003. Dynamics of plant-mediated organic matter and nutrient cycling following water-level drawdown in boreal peatlands. Global Biogeochemical Cycles 17. https://doi.org/10.1029/2002GB002015

Laine, J., Silvola, J., Tolonen, K., Alm, J., Nykänen, H., Vasander, H., Sallantaus, T., Savolainen, I., Sinisalo, J., Martikainen, P.J., 1996. Effect of Water-Level Drawdown on Global Climatic Warming: Northern Peatlands. Ambio 25, 179–184. https://doi.org/10.2307/4314450

Lan, X., Basu, S., Schwietzke, S., Bruhwiler, L.M.P., Dlugokencky, E.J., Michel, S.E., Sherwood, O.A., Tans, P.P., Thoning, K., Etiope, G., Zhuang, Q., Liu, L., Oh, Y., Miller, J.B., Pétron, G., Vaughn, B.H., Crippa, M., 2021. Improved Constraints on Global Methane Emissions and Sinks Using δ13C-CH4. Global Biogeochemical Cycles 35, e2021GB007000. https://doi.org/10.1029/2021GB007000

Lan, X., Talbot, R., Laine, P., Torres, A., 2015. Characterizing Fugitive Methane Emissions in the Barnett Shale Area Using a Mobile Laboratory. Environmental Science & Technology 49, 8139–8146. https://doi.org/10.1021/es5063055

Lassey, K.R., 2007. Livestock methane emission: From the individual grazing animal through national inventories to the global methane cycle. Agricultural and Forest Meteorology, The Contribution of Agriculture to the State of Climate 142, 120–132. https://doi.org/10.1016/j.agrformet.2006.03.028

Lavoie, M., Baillie, J., Bourlon, E., O'Connell, E., MacKay, K., Boelens, I., Risk, D., 2022. Sweet and sour: A quantitative analysis of methane emissions in contrasting Alberta, Canada, heavy oil developments. Science of The Total Environment 807, 150836. https://doi.org/10.1016/j.scitotenv.2021.150836

Law, C.S., Nodder, S.D., Mountjoy, J.J., Marriner, A., Orpin, A., Pilditch, C.A., Franz, P., Thompson, K., 2010. Geological, hydrodynamic and biogeochemical variability of a New Zealand deep-water methane cold seep during an integrated three-year time-series study. Marine Geology, Methane seeps at the Hikurangi Margin, New Zealand 272, 189–208. https://doi.org/10.1016/j.margeo.2009.06.018

Leifer, I., Boles, J., 2005. Measurement of marine hydrocarbon seep flow through fractured rock and unconsolidated sediment. Marine and Petroleum Geology, Near-Surface Hydrocarbon Migration: Mechanisms and Seepage Rates 22, 551–568. https://doi.org/10.1016/j.marpetgeo.2004.10.026

Leonte, M., Kessler, J.D., Kellermann, M.Y., Arrington, E.C., Valentine, D.L., Sylva, S.P., 2017. Rapid rates of aerobic methane oxidation at the feather edge of gas hydrate stability in the waters of Hudson Canyon, US Atlantic Margin. Geochimica et Cosmochimica Acta 204, 375–387. https://doi.org/10.1016/j.gca.2017.01.009

Leppelt, T., Dechow, R., Gebbert, S., Freibauer, A., Lohila, A., Augustin, J., Drösler, M., Fiedler, S., Glatzel, S., Höper, H., Järveoja, J., Lærke, P.E., Maljanen, M., Mander, Ü., Mäkiranta, P., Minkkinen, K., Ojanen, P., Regina, K., Strömgren, M., 2014. Nitrous oxide emission budgets and land-use-driven hotspots for organic soils in Europe. Biogeosciences 11, 6595–6612. https://doi.org/10.5194/bg-11-6595-2014

Levy, E.M., MacIean, B., 1981. Natural Hydrocarbon Seepage At Scott Inlet and Buchan Gulf, Baffin Island Shelf: 1980 Update. Geological Survey of Canada, Current Research Part A 81–1A, 401–403. https://doi.org/10.4095/109550

Li, H.Z., Mundia-Howe, M., Reeder, M.D., Pekney, N.J., 2020. Constraining natural gas pipeline emissions in San Juan Basin using mobile sampling. Science of The Total Environment 748, 142490. https://doi.org/10.1016/j.scitotenv.2020.142490

Li, Y., Xie, H., Scarratt, M., Damm, E., Bourgault, D., Galbraith, P.S., Wallace, D.W.R., 2021. Dissolved methane in the water column of the Saguenay Fjord. Marine Chemistry 230, 103926. https://doi.org/10.1016/j.marchem.2021.103926

Liimatainen, M., Voigt, C., Martikainen, P.J., Hytönen, J., Regina, K., Óskarsson, H., Maljanen, M., 2018. Factors controlling nitrous oxide emissions from managed northern peat soils with low carbon to nitrogen ratio. Soil Biology and Biochemistry 122, 186–195. https://doi.org/10.1016/j.soilbio.2018.04.006

Limpens, J., Berendse, F., Blodau, C., Canadell, J., Freeman, C., Holden, J., Roulet, N., Rydin, H., Schaepman-Strub, G., 2008. Peatlands and the carbon cycle: from local processes to global implications – a synthesis. Biogeosciences 5, 1475–1491. https://doi.org/10.5194/bg-5-1475-2008

Liu, H., Zak, D., Rezanezhad, F., Lennartz, B., 2019. Soil degradation determines release of nitrous oxide and dissolved organic carbon from peatlands. Environmental Research Letters 14, 094009. https://doi.org/10.1088/1748-9326/ab3947

Lohila, A., Aurela, M., Hatakka, J., Pihlatie, M., Minkkinen, K., Penttilä, T., Laurila, T., 2010. Responses of N_2O fluxes to temperature, water table and N deposition in a northern boreal fen. European Journal of Soil Science 61, 651–661. https://doi.org/10.1111/j.1365-2389.2010.01265.x

Loncarevic, B.D., Falconer, R.K.H., 1977. An oil slick occurrence off Baffin Island. Report of Activities, Part A, Geological Survey of Canada, Paper 523–524.

Lozanovska, I., Kuzyakov, Y., Krohn, J., Parvin, S., Dorodnikov, M., 2016. Effects of nitrate and sulfate on greenhouse gas emission potentials from microform-derived peats of a boreal peatland: A ^{13}C tracer study. Soil Biology and Biochemistry 100, 182–191. https://doi.org/10.1016/j.soilbio.2016.06.018

Lu, X., Jacob, D.J., Wang, H., Maasakkers, J.D., Zhang, Y., Scarpelli, T.R., Shen, L., Qu, Z., Sulprizio, M.P., Nesser, H., Bloom, A.A., Ma, S., Worden, J.R., Fan, S., Parker, R.J., Boesch, H., Gautam, R., Gordon, D., Moran, M.D., Reuland, F., Villasana, C.A.O., Andrews, A., 2022. Methane emissions in the United States, Canada, and Mexico: evaluation of national methane emission inventories and 2010–2017 sectoral trends by inverse analysis of in situ (GLOBALVIEWplus CH_4 ObsPack) and satellite (GOSAT) atmospheric observations. Atmospheric Chemistry and Physics 22, 395–418. https://doi.org/10.5194/acp-22-395-2022

Luan, J., Wu, J., 2015. Long-term agricultural drainage stimulates CH4 emissions from ditches through increased substrate availability in a boreal peatland. Agriculture, Ecosystems & Environment 214, 68–77. https://doi.org/10.1016/j.agee.2015.08.020

Luan, J., Wu, J., 2014. Gross photosynthesis explains the 'artificial bias' of methane fluxes by static chamber (opaque versus transparent) at the hummocks in a boreal peatland. Environmental Research Letters 9, 105005. https://doi.org/10.1088/1748-9326/9/10/105005

Luan, J., Wu, J., Liu, S., Roulet, N., Wang, M., 2019. Soil nitrogen determines greenhouse gas emissions from northern peatlands under concurrent warming and vegetation shifting. Communications Biology 2, 1–10. https://doi.org/10.1038/s42003-019-0370-1

Lund, M., Christensen, T.R., Mastepanov, M., Lindroth, A., Ström, L., 2009. Effects of N and P fertilization on the greenhouse gas exchange in two northern peatlands with contrasting N deposition rates. Biogeosciences 6, 2135–2144. https://doi.org/10.5194/bg-6-2135-2009

Maasakkers, J.D., Varon, D.J., Elfarsdóttir, A., McKeever, J., Jervis, D., Mahapatra, G., Pandey, S., Lorente, A., Borsdorff, T., Foorthuis, L.R., Schuit, B.J., Tol, P., van Kempen, T.A., van Hees, R., Aben, I., 2022. Using satellites to uncover large methane emissions from landfills. Science Advances 8, eabn9683. https://doi.org/10.1126/sciadv.abn9683

MacKay, K., Lavoie, M., Bourlon, E., Atherton, E., O'Connell, E., Baillie, J., Fougère, C., Risk, D., 2021. Methane emissions from upstream oil and gas production in Canada are underestimated. Scientific Reports 11, 8041. https://doi.org/10.1038/s41598-021-87610-3

MacKay, K., Risk, D., Atherton, E., Fougére, C., Bourlon, E., O'Connell, E., Baillie, J., 2019. Fugitive and vented methane emissions surveying on the Weyburn CO2-EOR field in southeastern Saskatchewan, Canada. International Journal of Greenhouse Gas Control 88, 118–123. https://doi.org/10.1016/j.ijggc.2019.05.032

Maljanen, M., Hytönen, J., Martikainen, P.J., 2001. Fluxes of N_2O, CH_4 and CO_2 on afforested boreal agricultural soils. Plant and Soil 231, 113–121. https://doi.org/10.1023/A:1010372914805

Maljanen, M., Kohonen, A.-R., Virkajaärvi, P., Martikainen, P.J., 2007. Fluxes and production of N_2O, CO_2 and CH_4 in boreal agricultural soil during winter as affected by snow cover. Tellus B: Chemical and Physical Meteorology 59, 853–859. https://doi.org/10.1111/j.1600-0889.2007.00304.x

Maljanen, M., Liikanen, A., Silvola, J., Martikainen, P.J., 2003. Nitrous oxide emissions from boreal organic soil under different land-use. Soil Biology and Biochemistry 35, 689–700. https://doi.org/10.1016/S0038-0717(03)00085-3

Maljanen, M., Shurpali, N., Hytönen, J., Mäkiranta, P., Aro, L., Potila, H., Laine, J., Li, C., Martikainen, P.J., 2012. Afforestation does not necessarily reduce nitrous oxide emissions from managed boreal peat soils. Biogeochemistry 108, 199–218. https://doi.org/10.1007/s10533-011-9591-1

Maljanen, M., Sigurdsson, B.D., Guðmundsson, J., Óskarsson, H., Huttunen, J.T., Martikainen, P.J., 2010. Greenhouse gas balances of managed peatlands in the Nordic countries – present knowledge and gaps. Biogeosciences 7, 2711–2738. https://doi.org/10.5194/bg-7-2711-2010

Manning, C.C.M., Nicholson, D.P., 2022. dnicholson/gas_toolbox: MATLAB code for calculating gas fluxes. https://doi.org/10.5281/zenodo.6126685

Manning, C.C.M., Zheng, Z., Fenwick, L., McCulloch, R.D., Damm, E., Izett, R.W., Williams, W.J., Zimmermann, S., Vagle, S., Tortell, P.D., 2022. Interannual Variability in Methane and Nitrous Oxide Concentrations and Sea-Air Fluxes Across the North American Arctic Ocean (2015–2019). Global Biogeochemical Cycles 36, e2021GB007185. https://doi.org/10.1029/2021GB007185

Martikainen, P.J., Nykänen, H., Crill, P., Silvola, J., 1993. Effect of a lowered water table on nitrous oxide fluxes from northern peatlands. Nature 366, 51–53. https://doi.org/10.1038/366051a0

Marty, D., Nival, P., Yoon, W., 1997. Methanoarchaea associated with sinking particles and zooplankton collected in the Northeastern tropical Atlantic. Oceanologica Acta 20, 863–869.

Mau, S., Blees, J., Helmke, E., Niemann, H., Damm, E., 2013. Vertical distribution of methane oxidation and methanotrophic response to elevated methane concentrations in stratified waters of the Arctic fjord Storfjorden (Svalbard, Norway). Biogeosciences 10, 6267–6278. https://doi.org/10.5194/bg-10-6267-2013

Mau, S., Römer, M., Torres, M.E., Bussmann, I., Pape, T., Damm, E., Geprägs, P., Wintersteller, P., Hsu, C.-W., Loher, M., Bohrmann, G., 2017. Widespread methane seepage along the continental margin off Svalbard - from Bjørnøya to Kongsfjorden. Sci Rep 7, 42997. https://doi.org/10.1038/srep42997

McCarter, C.P.R., Wilkinson, S.L., Moore, P.A., Waddington, J.M., 2021. Ecohydrological trade-offs from multiple peatland disturbances: The interactive effects of drainage, harvesting, restoration and wildfire in a southern Ontario bog. Journal of Hydrology 601, 126793. https://doi.org/10.1016/j.jhydrol.2021.126793

McCaughey, W.P., Wittenberg, K., Corrigan, D., 1997. Methane production by steers on pasture. Can. J. Anim. Sci. 77, 519–524. https://doi.org/10.4141/A96-137

McGinn, S.M., Chung, Y.-H., Beauchemin, K.A., Iwaasa, A.D., Grainger, C., 2009. Use of corn distillers' dried grains to reduce enteric methane loss from beef cattle. Can. J. Anim. Sci. 89, 409–413. https://doi.org/10.4141/CJAS08133

McGinnis, D.F., Greinert, J., Artemov, Y., Beaubien, S.E., Wüest, A., 2006. Fate of rising methane bubbles in stratified waters: How much methane reaches the atmosphere? Journal of Geophysical Research: Oceans 111. https://doi.org/10.1029/2005JC003183

Melling, H., Gratton, Y., Ingram, G., 2001. Ocean circulation within the North Water polynya of Baffin Bay. Atmosphere-Ocean 39, 301–325. https://doi.org/10.1080/07055900.2001.9649683

Meredith, M., Sommerkorn, M., Cassotta, S., Derksen, C., Ekaykin, A., Hollowed, A., Kofinas, G., Mackintosh, A., Melbourne-Thomas, J., Muelbert, M.M.C., Ottersen, G., Pritchard, H., Schuur, E.A.G., 2019. Chapter 3: Polar regions, in: IPCC Special Report on the Ocean and Cryosphere in a Changing Climate. Cambridge University Press, Cambridge, UK and New York, USA, pp. 203–320.

Merrin, Z., Francisco, P.W., 2019. Unburned Methane Emissions from Residential Natural Gas Appliances. Environmental Science & Technology 53, 5473–5482. https://doi.org/10.1021/acs.est.8b05323

Millero, F.J., Poisson, A., 1981. International one-atmosphere equation of state of seawater. Deep Sea Research Part A. Oceanographic Research Papers 28, 625–629. https://doi.org/10.1016/0198-0149(81)90122-9

Miner, K.R., Turetsky, M.R., Malina, E., Bartsch, A., Tamminen, J., McGuire, A.D., Fix, A., Sweeney, C., Elder, C.D., Miller, C.E., 2022. Permafrost carbon emissions in a changing Arctic. Nature Reviews Earth & Environment 3, 55–67. https://doi.org/10.1038/s43017-021-00230-3

Ministry of Energy and Resources, Government of Saskatchewan, 2021. 2020 Natural Gas Volume and Value Summary.

Ministry of Energy and Resources, Government of Saskatchewan, 2020a. Temporary Regulatory Relief Measures.

Ministry of Energy and Resources, Government of Saskatchewan, 2020b. Crude Oil Volume and Value Summary.

Ministry of Energy and Resources, Government of Saskatchewan, 2020c. Saskatchewan Fuel, Flare and Vent.

Ministry of Energy and Resources, Government of Saskatchewan, 2019a. The Oil and Gas Emissions Management Regulations.

Ministry of Energy and Resources, Government of Saskatchewan, 2019b. Directive PNG015: Well Abandonment Requirements.

Ministry of Energy and Resources, Government of Saskatchewan, 2018. Directive PNG032: Volumetric, Valuation and Infrastructure Reporting in Petrinex.

Minkkinen, K., Ojanen, P., Koskinen, M., Penttilä, T., 2020. Nitrous oxide emissions of undrained, forestry-drained, and rewetted boreal peatlands. Forest Ecology and Management 478, 118494. https://doi.org/10.1016/j.foreco.2020.118494

Mitchell, A.L., Tkacik, D.S., Roscioli, J.R., Herndon, S.C., Yacovitch, T.I., Martinez, D.M., Vaughn, T.L., Williams, L.L., Sullivan, M.R., Floerchinger, C., Omara, M., Subramanian, R., Zimmerle, D., Marchese, A.J., Robinson, A.L., 2015. Measurements of Methane Emissions from Natural Gas Gathering Facilities and Processing Plants: Measurement Results. Environ. Sci. Technol. 49, 3219–3227. https://doi.org/10.1021/es5052809

Mønster, J., Kjeldsen, P., Scheutz, C., 2019. Methodologies for measuring fugitive methane emissions from landfills – A review. Waste Management 87, 835–859. https://doi.org/10.1016/j.wasman.2018.12.047

Moore, T.R., Clarkson, B.R., 2007. Dissolved organic carbon in New Zealand peatlands. New Zealand Journal of Marine and Freshwater Research 41, 137–141. https://doi.org/10.1080/00288330709509902

Morris, J.T., 1991. Effects of Nitrogen Loading on Wetland Ecosystems with Particular Reference to Atmospheric Deposition. Annual Review of Ecology and Systematics 22, 257–279. https://doi.org/10.1146/annurev.es.22.110191.001353

Mosher, B.W., Czepiel, P.M., Harriss, R.C., Shorter, J.H., Kolb, C.E., McManus, J.B., Allwine, E., Lamb, B.K., 1999. Methane Emissions at Nine Landfill Sites in the Northeastern United States. Environmental Science & Technology 33, 2088–2094. https://doi.org/10.1021/es981044z

Mustamo, P., Maljanen, M., Hyvärinen, M., Ronkanen, A.-K., Klöve, B., 2016. Respiration and emissions of methane and nitrous oxide from a boreal peatland complex comprising different land-use types. Boreal Environment Research 21, 405–426.

Myhre, G., Shindell, D., Bréon, F.-M., Collins, W., Fuglestvedt, J., Huang, J., Koch, D., Lamarque, J.-F., Lee, D., Mendoza, B., Nakajima, T., Robock, A., Stephens, G., Takemura, T., Zhang, H., 2013. Anthropogenic and Natural Radiative Forcing, in: Stocker, T.F., Qin, D., Plattner, G.-K., Tignor, M., Allen, S.K., Boschung, J., Nauels, A., Xia, Y., Bex, V., Midgley, P.M. (Eds.), Climate Change 2013: The Physical Science Basis. Contribution of Working Group I to the Fifth Assessment Report of the Intergovernmental Panel on Climate Change. Cambridge University Press, Cambridge, United Kingdom and New York, NY, USA, pp. 659--740.

Nanda, S., Berruti, F., 2021. Municipal solid waste management and landfilling technologies: a review. Environmental Chemistry Letters 19, 1433–1456. https://doi.org/10.1007/s10311-020-01100-y

Neill, C., Johnson, K.M., Lewis, E., Wallace, D.W.R., 1997. Accurate headspace analysis of *f*CO2 in discrete water samples using batch equilibration. Limnology and Oceanography 42, 1774–1783. https://doi.org/10.4319/lo.1997.42.8.1774

Nielsen, T., Laier, T., Kuijpers, A., Rasmussen, T.L., Mikkelsen, N.E., Nørgård-Pedersen, N., 2014. Fluid flow and methane occurrences in the Disko Bugt area offshore West Greenland: indications for gas hydrates? Geo-Marine Letters 34, 511–523. https://doi.org/10.1007/s00367-014-0382-2

Nieminen, M., Sallantaus, T., Ukonmaanaho, L., Nieminen, T.M., Sarkkola, S., 2017. Nitrogen and phosphorus concentrations in discharge from drained peatland forests are increasing. Science of The Total Environment 609, 974–981. https://doi.org/10.1016/j.scitotenv.2017.07.210

Niloofar, P., Francis, D.P., Lazarova-Molnar, S., Vulpe, A., Vochin, M.-C., Suciu, G., Balanescu, M., Anestis, V., Bartzanas, T., 2021. Data-driven decision support in livestock farming for improved animal health, welfare and greenhouse gas emissions: Overview and challenges. Computers and Electronics in Agriculture 190, 106406. https://doi.org/10.1016/j.compag.2021.106406

Nisbet, E.G., Dlugokencky, E.J., Fisher, R.E., France, J.L., Lowry, D., Manning, M.R., Michel, S.E., Warwick, N.J., 2021. Atmospheric methane and nitrous oxide: challenges along the path to Net Zero. Philosophical Transactions of the Royal Society A: Mathematical, Physical and Engineering Sciences 379, 20200457. https://doi.org/10.1098/rsta.2020.0457

Nisbet, E.G., Fisher, R.E., Lowry, D., France, J.L., Allen, G., Bakkaloglu, S., Broderick, T.J., Cain, M., Coleman, M., Fernandez, J., Forster, G., Griffiths, P.T., Iverach, C.P., Kelly, B.F.J., Manning, M.R., Nisbet-Jones, P.B.R., Pyle, J.A., Townsend-Small, A., al-Shalaan, A., Warwick, N., Zazzeri, G., 2020. Methane Mitigation: Methods to Reduce Emissions, on the Path to the Paris Agreement. Reviews of Geophysics 58, e2019RG000675. https://doi.org/10.1029/2019RG000675

Nisbet, E.G., Manning, M.R., Dlugokencky, E.J., Fisher, R.E., Lowry, D., Michel, S.E., Myhre, C.L., Platt, S.M., Allen, G., Bousquet, P., Brownlow, R., Cain, M., France, J.L., Hermansen, O., Hossaini, R., Jones, A.E., Levin, I., Manning, A.C., Myhre, G., Pyle, J.A., Vaughn, B.H., Warwick, N.J., White, J.W.C., 2019. Very Strong Atmospheric Methane Growth in the 4 Years 2014–2017: Implications for the Paris Agreement. Global Biogeochemical Cycles 33, 318–342. https://doi.org/10.1029/2018GB006009

Nordbakken, J.F., Ohlson, M., Högberg, P., 2003. Boreal Bog Plants: Nitrogen Sources and Uptake of Recently Deposited Nitrogen. Environmental Pollution 126, 191–200. https://doi.org/10.1016/S0269-7491(03)00194-5

Normandeau, A., MacKillop, K., Macquarrie, M., Richards, C., Bourgault, D., Campbell, D.C., Maselli, V., Philibert, G., Clarke, J.H., 2021. Submarine landslides triggered by iceberg collision with the seafloor. Nature Geoscience 14, 599–605. https://doi.org/10.1038/s41561-021-00767-4

Nykänen, H., Alm, J., Lång, K., Silvola, J., Martikainen, P.J., 1995. Emissions of CH_4, N_2O and CO_2 from a virgin fen and a fen drained for grassland in Finland. Journal of Biogeography 318, 351–357. https://doi.org/10.2307/2845930

Nykänen, H., Vasander, H., Huttunen, J.T., Martikainen, P.J., 2002. Effect of experimental nitrogen load on methane and nitrous oxide fluxes on ombrotrophic boreal peatland. Plant and Soil 242, 147–155. https://doi.org/10.1023/A:1019658428402

O'Connell, E., Risk, D., Atherton, E., Bourlon, E., Fougère, C., Baillie, J., Lowry, D., Johnson, J., 2019. Methane emissions from contrasting production regions within Alberta, Canada: Implications under incoming federal

methane regulations. Elementa: Science of the Anthropocene 7, 3. https://doi.org/doi.org/10.1525/elementa.341
Ominski, K.H., Boadi, D.A., Wittenberg, K.M., Fulawka, D.L., Basarab, J.A., 2007. Estimates of enteric methane emissions from cattle in Canada using the IPCC Tier-2 methodology. Canadian Journal of Animal Science 87. https://doi.org/10.4141/CJAS06034
Osterloh, K., Tauchnitz, N., Spott, O., Hepp, J., Bernsdorf, S., Meissner, R., 2017. Changes of methane and nitrous oxide emissions in a transition bog in central Germany (German National Park Harz Mountains) after rewetting. Wetlands Ecology and Management 1–16. https://doi.org/10.1007/s11273-017-9555-x
Pärn, J., Verhoeven, J., Butterbach-Bahl, K., Dise, N., Ullah, S., Egorov, S., Espenberg, M., Järveoja, J., Jauhiainen, J., Kasak, K., Klemedtsson, L., Kull, A., Laggoun-Défarge, F., Lapshina, E., Lohila, A., Lõhmus, K., Maddison, M., Mitsch, W., Müller, C., Mander, Ü., 2018. Nitrogen-rich organic soils under warm well-drained conditions are global nitrous oxide emission hotspots. Nature Communications 9. https://doi.org/10.1038/s41467-018-03540-1
Paull, C.K., Brewer, P.G., Ussler, W., Peltzer, E.T., Rehder, G., Clague, D., 2002. An experiment demonstrating that marine slumping is a mechanism to transfer methane from seafloor gas-hydrate deposits into the upper ocean and atmosphere. Geo-Mar Lett 22, 198–203. https://doi.org/10.1007/s00367-002-0113-y
Pearce, J.L., Beringer, J., Nicholls, N., Hyndman, R.J., Tapper, N.J., 2011. Quantifying the influence of local meteorology on air quality using generalized additive models. Atmospheric Environment 45, 1328–1336. https://doi.org/10.1016/j.atmosenv.2010.11.051
Peigné, J., Girardin, P., 2004. Environmental Impacts of Farm-Scale Composting Practices. Water, Air, and Soil Pollution 153, 45–68. https://doi.org/10.1023/B:WATE.0000019932.04020.b6
Pekney, N.J., Diehl, J.R., Ruehl, D., Sams, J., Veloski, G., Patel, A., Schmidt, C., Card, T., 2018. Measurement of methane emissions from abandoned oil and gas wells in Hillman State Park, Pennsylvania. Carbon Management 9, 165–175. https://doi.org/10.1080/17583004.2018.1443642
Peng, S., Lin, X., Thompson, R.L., Xi, Y., Liu, G., Hauglustaine, D., Lan, X., Poulter, B., Ramonet, M., Saunois, M., Yin, Y., Zhang, Z., Zheng, B., Ciais, P., 2022. Wetland emission and atmospheric sink changes explain methane growth in 2020. Nature 612, 477–482. https://doi.org/10.1038/s41586-022-05447-w
Penza, M., Suriano, D., Pfister, V., Prato, M., Cassano, G., 2017. Urban Air Quality Monitoring with Networked Low-Cost Sensor-Systems. Proceedings 1, 573. https://doi.org/10.3390/proceedings1040573
Pereira, D., Dias, E., Ponte, M., 2017. Investigating the internal structure of four Azorean Sphagnum bogs using ground-penetrating radar. Mires and Peat 19, 1–9. https://doi.org/10.19189/MaP.2016.OMB.259
Petroleum Technology Research Centre, 2020. CCS Potential in the Heavy Oil Regions of Saskatchewan and Alberta.
Platt, S.M., Eckhardt, S., Ferré, B., Fisher, R.E., Hermansen, O., Jansson, P., Lowry, D., Nisbet, E.G., Pisso, I., Schmidbauer, N., Silyakova, A., Stohl, A., Svendby, T.M., Vadakkepuliyambatta, S., Mienert, J., Lund Myhre, C., 2018. Methane at Svalbard and over the European Arctic Ocean. Atmospheric Chemistry and Physics 18, 17207–17224. https://doi.org/10.5194/acp-18-17207-2018
Punshon, S., Azetsu-Scott, K., Lee, C.M., 2014. On the distribution of dissolved methane in Davis Strait, North Atlantic Ocean. Marine Chemistry 161, 20–25. https://doi.org/10.1016/j.marchem.2014.02.004
Punshon, S., Azetsu-Scott, K., Sherwood, O., Edinger, E.N., 2019. Bottom water methane sources along the high latitude eastern Canadian continental shelf and their effects on the marine carbonate system. Marine Chemistry 212, 83–95. https://doi.org/10.1016/j.marchem.2019.04.004
Ray, R.L., Singh, V.P., Singh, S.K., Acharya, B.S., He, Y., 2022. What is the impact of COVID-19 pandemic on global carbon emissions? Science of The Total Environment 816, 151503. https://doi.org/10.1016/j.scitotenv.2021.151503
Reeburgh, W.S., 2007. Oceanic Methane Biogeochemistry. Chemical Reviews 107, 486–513. https://doi.org/10.1021/cr050362v
Rees, A.P., Bange, H.W., Arévalo-Martínez, D.L., Artioli, Y., Ashby, D.M., Brown, I., Campen, H.I., Clark, D.R., Kitidis, V., Lessin, G., Tarran, G.A., Turley, C., 2022. Nitrous oxide and methane in a changing Arctic Ocean. Ambio 51, 398–410. https://doi.org/10.1007/s13280-021-01633-8
Regina, K., Nykänen, H., Maljanen, M., Silvola, J., Martikainen, P., 1998. Emissions of N_2O and NO and net nitrogen mineralization in a boreal forested peatland treated with different nitrogen compounds. Canadian Journal of Forest Research 28, 132–140. https://doi.org/10.1139/x97-198
Regina, K., Nykänen, H., Silvola, J., Martikainen, P.J., 1996. Fluxes of nitrous oxide from boreal peatlands as affected by peatland type, water table level and nitrification capacity. Biogeochemistry 35, 401–418. https://doi.org/10.1007/BF02183033

Reisinger, A., Clark, H., Cowie, A.L., Emmet-Booth, J., Gonzalez Fischer, C., Herrero, M., Howden, M., Leahy, S., 2021. How necessary and feasible are reductions of methane emissions from livestock to support stringent temperature goals? Philosophical Transactions of the Royal Society A: Mathematical, Physical and Engineering Sciences 379, 20200452. https://doi.org/10.1098/rsta.2020.0452

Riddick, S.N., Mauzerall, D.L., Celia, M.A., Kang, M., Bressler, K., Chu, C., Gum, C.D., 2019. Measuring methane emissions from abandoned and active oil and gas wells in West Virginia. Science of The Total Environment 651, 1849–1856. https://doi.org/10.1016/j.scitotenv.2018.10.082

Robertson, A.M., Edie, R., Snare, D., Soltis, J., Field, R.A., Burkhart, M.D., Bell, C.S., Zimmerle, D., Murphy, S.M., 2017. Variation in Methane Emission Rates from Well Pads in Four Oil and Gas Basins with Contrasting Production Volumes and Compositions. Environmental Science & Technology 51, 8832–8840. https://doi.org/10.1021/acs.est.7b00571

Rolph, G., Stein, A., Stunder, B., 2017. Real-time Environmental Applications and Display sYstem: READY. Environmental Modelling & Software 95, 210–228. https://doi.org/10.1016/j.envsoft.2017.06.025

Rosa, E., Larocque, M., Pellerin, S., Gagné, S., Fournier, B., 2009. Determining the number of manual measurements required to improve peat thickness estimations by ground penetrating radar. Earth Surface Processes and Landforms 34, 377–383. https://doi.org/10.1002/esp.1741

Roscioli, J.R., Herndon, S.C., Yacovitch, T.I., Knighton, W.B., Zavala-Araiza, D., Johnson, M.R., Tyner, D.R., 2018. Characterization of methane emissions from five cold heavy oil production with sands (CHOPS) facilities. Journal of the Air & Waste Management Association 68, 671–684. https://doi.org/10.1080/10962247.2018.1436096

Roscioli, J.R., Yacovitch, T.I., Floerchinger, C., Mitchell, A.L., Tkacik, D.S., Subramanian, R., Martinez, D.M., Vaughn, T.L., Williams, L., Zimmerle, D., Robinson, A.L., Herndon, S.C., Marchese, A.J., 2015. Measurements of methane emissions from natural gas gathering facilities and processing plants: measurement methods. Atmospheric Measurement Techniques 8, 2017–2035. https://doi.org/10.5194/amt-8-2017-2015

Rosentreter, J.A., Borges, A.V., Deemer, B.R., Holgerson, M.A., Liu, S., Song, C., Melack, J., Raymond, P.A., Duarte, C.M., Allen, G.H., Olefeldt, D., Poulter, B., Battin, T.I., Eyre, B.D., 2021. Half of global methane emissions come from highly variable aquatic ecosystem sources. Nature Geoscience 14, 225–230. https://doi.org/10.1038/s41561-021-00715-2

Ruppel, C.D., Kessler, J.D., 2017. The interaction of climate change and methane hydrates. Reviews of Geophysics 55, 126–168. https://doi.org/10.1002/2016RG000534

Saint-Vincent, P.M.B., Sams, J.I., Reeder, M.D., Mundia-Howe, M., Veloski, G.A., Pekney, N.J., 2021. Historic and modern approaches for discovery of abandoned wells for methane emissions mitigation in Oil Creek State Park, Pennsylvania. Journal of Environmental Management 280, 111856. https://doi.org/10.1016/j.jenvman.2020.111856

Salm, J.-O., Kimmel, K., Uri, V., Mander, Ü., 2009. Global warming potential of drained and undrained peatlands in Estonia: A synthesis. Wetlands 29, 1081–1092. https://doi.org/10.1672/08-206.1

Salm, J.-O., Maddison, M., Tammik, S., Soosaar, K., Truu, J., Mander, Ü., 2012. Emissions of CO_2, CH_4 and N_2O from undisturbed, drained and mined peatlands in Estonia. Hydrobiologia 692, 41–55. https://doi.org/10.1007/s10750-011-0934-7

Saunois, M., Jackson, R.B., Bousquet, P., Poulter, B., Canadell, J.G., 2016. The growing role of methane in anthropogenic climate change. Environmental Research Letters 11, 120207. https://doi.org/10.1088/1748-9326/11/12/120207

Saunois, M., Stavert, A.R., Poulter, B., Bousquet, P., Canadell, J.G., Jackson, R.B., Raymond, P.A., Dlugokencky, E.J., Houweling, S., Patra, P.K., Ciais, P., Arora, V.K., Bastviken, D., Bergamaschi, P., Blake, D.R., Brailsford, G., Bruhwiler, L., Carlson, K.M., Carrol, M., Castaldi, S., Chandra, N., Crevoisier, C., Crill, P.M., Covey, K., Curry, C.L., Etiope, G., Frankenberg, C., Gedney, N., Hegglin, M.I., Höglund-Isaksson, L., Hugelius, G., Ishizawa, M., Ito, A., Janssens-Maenhout, G., Jensen, K.M., Joos, F., Kleinen, T., Krummel, P.B., Langenfelds, R.L., Laruelle, G.G., Liu, L., Machida, T., Maksyutov, S., McDonald, K.C., McNorton, J., Miller, P.A., Melton, J.R., Morino, I., Müller, J., Murguia-Flores, F., Naik, V., Niwa, Y., Noce, S., O'Doherty, S., Parker, R.J., Peng, C., Peng, S., Peters, G.P., Prigent, C., Prinn, R., Ramonet, M., Regnier, P., Riley, W.J., Rosentreter, J.A., Segers, A., Simpson, I.J., Shi, H., Smith, S.J., Steele, L.P., Thornton, B.F., Tian, H., Tohjima, Y., Tubiello, F.N., Tsuruta, A., Viovy, N., Voulgarakis, A., Weber, T.S., van Weele, M., van der Werf, G.R., Weiss, R.F., Worthy, D., Wunch, D., Yin, Y., Yoshida, Y., Zhang, W., Zhang, Z., Zhao, Y., Zheng, B., Zhu, Qing, Zhu, Qiuan, Zhuang, Q., 2020. The Global Methane Budget 2000–2017. Earth System Science Data 12, 1561–1623. https://doi.org/10.5194/essd-12-1561-2020

Savitzky, Abraham., Golay, M.J.E., 1964. Smoothing and Differentiation of Data by Simplified Least Squares Procedures. Analytical Chemistry 36, 1627–1639. https://doi.org/10.1021/ac60214a047
Scarpelli, T.R., Jacob, D.J., Maasakkers, J.D., Sulprizio, M.P., Sheng, J.-X., Rose, K., Romeo, L., Worden, J.R., Janssens-Maenhout, G., 2020. A global gridded (0.1° × 0.1°) inventory of methane emissions from oil, gas, and coal exploitation based on national reports to the United Nations Framework Convention on Climate Change. Earth System Science Data 12, 563–575. https://doi.org/10.5194/essd-12-563-2020
Scarpelli, T.R., Jacob, D.J., Moran, M., Reuland, F., Gordon, D., 2021. A gridded inventory of Canada's anthropogenic methane emissions. Environmental Research Letters 17, 014007. https://doi.org/10.1088/1748-9326/ac40b1
Scheutz, C., Kjeldsen, P., 2019. Guidelines for landfill gas emission monitoring using the tracer gas dispersion method. Waste Management 85, 351–360. https://doi.org/10.1016/j.wasman.2018.12.048
Schlesinger, W.H., 2013. An estimate of the global sink for nitrous oxide in soils. Global Change Biology 19, 2929–2931. https://doi.org/10.1111/gcb.12239
Schroth, M.H., Eugster, W., Gómez, K.E., Gonzalez-Gil, G., Niklaus, P.A., Oester, P., 2012. Above- and below-ground methane fluxes and methanotrophic activity in a landfill-cover soil. Waste Management 32, 879–889. https://doi.org/10.1016/j.wasman.2011.11.003
Schwietzke, S., Pétron, G., Conley, S., Pickering, C., Mielke-Maday, I., Dlugokencky, E.J., Tans, P.P., Vaughn, T., Bell, C., Zimmerle, D., Wolter, S., King, C.W., White, A.B., Coleman, T., Bianco, L., Schnell, R.C., 2017. Improved Mechanistic Understanding of Natural Gas Methane Emissions from Spatially Resolved Aircraft Measurements. Environ. Sci. Technol. 51, 7286–7294. https://doi.org/10.1021/acs.est.7b01810
Sejian, V., Lal, R., Lakritz, J., Ezeji, T., 2011. Measurement and prediction of enteric methane emission. International Journal of Biometeorology 55, 1–16. https://doi.org/10.1007/s00484-010-0356-7
Sentio Engineering, 2015. Technology for Emissions Reductions: Cold Heavy Oil Production with Sand (CHOPS) Methods for Reduction of Methane Venting. Petroleum Technology Alliance of Canada (PTAC).
Shakhova, N., Semiletov, I., Leifer, I., Sergienko, V., Salyuk, A., Kosmach, D., Chernykh, D., Stubbs, C., Nicolsky, D., Tumskoy, V., Gustafsson, Ö., 2014. Ebullition and storm-induced methane release from the East Siberian Arctic Shelf. Nature Geoscience 7, 64–70. https://doi.org/10.1038/ngeo2007
Shakhova, N., Semiletov, I., Salyuk, A., Yusupov, V., Kosmach, D., Gustafsson, Ö., 2010. Extensive Methane Venting to the Atmosphere from Sediments of the East Siberian Arctic Shelf. Science 327, 1246–1250. https://doi.org/10.1126/science.1182221
Shaw, J.T., Shah, A., Yong, H., Allen, G., 2021. Methods for quantifying methane emissions using unmanned aerial vehicles: a review. Philosophical Transactions of the Royal Society A: Mathematical, Physical and Engineering Sciences 379, 20200450. https://doi.org/10.1098/rsta.2020.0450
Shen, J., Melaku, N.D., Treu, R., Wang, J., 2019. Inventories of methane and nitrous oxide emissions from animal and crop farms of 69 municipalities in Alberta, Canada. Journal of Cleaner Production 234, 895–911. https://doi.org/10.1016/j.jclepro.2019.06.270
Sherwood, O.A., Davin, S.H., Lehmann, N., Buchwald, C., Edinger, E.N., Lehmann, M.F., Kienast, M., 2021. Stable isotope ratios in seawater nitrate reflect the influence of Pacific water along the northwest Atlantic margin. Biogeosciences 18, 4491–4510. https://doi.org/10.5194/bg-18-4491-2021
Shipham, M.C., Bartlett, K.B., Crill, P.M., Harriss, R.C., Blaha, D., 1998. Atmospheric methane measurements in central New England: An analysis of the long-term trend and the seasonal and diurnal cycles. Journal of Geophysical Research: Atmospheres 103, 10621–10630. https://doi.org/10.1029/98JD00106
Silvan, N., Tuittila, E.-S., Kitunen, V., Vasander, H., Laine, J., 2005. Nitrate uptake by *Eriophorum vaginatum* controls N_2O production in a restored peatland. Soil Biology and Biochemistry 37, 1519–1526. https://doi.org/10.1016/j.soilbio.2005.01.006
Silyakova, A., Jansson, P., Serov, P., Ferré, B., Pavlov, A.K., Hattermann, T., Graves, C.A., Platt, S.M., Myhre, C.L., Gründger, F., Niemann, H., 2020. Physical controls of dynamics of methane venting from a shallow seep area west of Svalbard. Continental Shelf Research 194, 104030. https://doi.org/10.1016/j.csr.2019.104030
Smith, P., Reay, D., Smith, J., 2021. Agricultural methane emissions and the potential formitigation. Philosophical Transactions of the Royal Society A: Mathematical, Physical and Engineering Sciences 379, 20200451. https://doi.org/10.1098/rsta.2020.0451
Stein, A.F., Draxler, R.R., Rolph, G.D., Stunder, B.J.B., Cohen, M.D., Ngan, F., 2015. NOAA's HYSPLIT Atmospheric Transport and Dispersion Modeling System. Bulletin of the American Meteorological Society 96, 2059–2077. https://doi.org/10.1175/BAMS-D-14-00110.1
Storm, I.M.L.D., Hellwing, A.L.F., Nielsen, N.I., Madsen, J., 2012. Methods for Measuring and Estimating Methane Emission from Ruminants. Animals 2, 160–183. https://doi.org/10.3390/ani2020160

Stramma, L., Kieke, D., Rhein, M., Schott, F., Yashayaev, I., Koltermann, K.P., 2004. Deep water changes at the western boundary of the subpolar North Atlantic during 1996 to 2001. Deep Sea Research Part I: Oceanographic Research Papers 51, 1033–1056. https://doi.org/10.1016/j.dsr.2004.04.001

Streletskaya, I.D., Vasiliev, A.A., Oblogov, G.E., Streletskiy, D.A., 2018. Methane Content in Ground Ice and Sediments of the Kara Sea Coast. Geosciences 8, 434. https://doi.org/10.3390/geosciences8120434

Subke, J.-A., Kutzbach, L., Risk, D., 2021. Soil Chamber Measurements, in: Foken, T. (Ed.), Springer Handbook of Atmospheric Measurements, Springer Handbooks. Springer International Publishing, Cham, pp. 1603–1624. https://doi.org/10.1007/978-3-030-52171-4_60

Suess, E., 2014. Marine cold seeps and their manifestations: geological control, biogeochemical criteria and environmental conditions. International Journal of Earth Sciences 103, 1889–1916. https://doi.org/10.1007/s00531-014-1010-0

Sun, T., Ocko, I.B., Sturcken, E., Hamburg, S.P., 2021. Path to net zero is critical to climate outcome. Sci Rep 11, 22173. https://doi.org/10.1038/s41598-021-01639-y

Tang, C.C.L., Ross, C.K., Yao, T., Petrie, B., DeTracey, B.M., Dunlap, E., 2004. The circulation, water masses and sea-ice of Baffin Bay. Progress in Oceanography 63, 183–228. https://doi.org/10.1016/j.pocean.2004.09.005

Tauchnitz, N., Brumme, R., Bernsdorf, S., Meissner, R., 2007. Nitrous oxide and methane fluxes of a pristine slope mire in the German National Park Harz Mountains. Plant and Soil 303, 131–138. https://doi.org/10.1007/s11104-007-9493-0

Thonat, T., Saunois, M., Bousquet, P., Pison, I., Tan, Z., Zhuang, Q., Crill, P.M., Thornton, B.F., Bastviken, D., Dlugokencky, E.J., Zimov, N., Laurila, T., Hatakka, J., Hermansen, O., Worthy, D.E.J., 2017. Detectability of Arctic methane sources at six sites performing continuous atmospheric measurements. Atmospheric Chemistry and Physics 17, 8371–8394. https://doi.org/10.5194/acp-17-8371-2017

Thornton, B.F., Geibel, M.C., Crill, P.M., Humborg, C., Mörth, C.-M., 2016. Methane fluxes from the sea to the atmosphere across the Siberian shelf seas. Geophysical Research Letters 43, 5869–5877. https://doi.org/10.1002/2016GL068977

Thornton, B.F., Prytherch, J., Andersson, K., Brooks, I.M., Salisbury, D., Tjernström, M., Crill, P.M., 2020. Shipborne eddy covariance observations of methane fluxes constrain Arctic sea emissions. Science Advances 6. https://doi.org/10.1126/sciadv.aay7934

Tian, H., Xu, R., Canadell, J.G., Thompson, R.L., Winiwarter, W., Suntharalingam, P., Davidson, E.A., Ciais, P., Jackson, R.B., Janssens-Maenhout, G., Prather, M.J., Regnier, P., Pan, N., Pan, S., Peters, G.P., Shi, H., Tubiello, F.N., Zaehle, S., Zhou, F., Arneth, A., Battaglia, G., Berthet, S., Bopp, L., Bouwman, A.F., Buitenhuis, E.T., Chang, J., Chipperfield, M.P., Dangal, S.R.S., Dlugokencky, E., Elkins, J.W., Eyre, B.D., Fu, B., Hall, B., Ito, A., Joos, F., Krummel, P.B., Landolfi, A., Laruelle, G.G., Lauerwald, R., Li, W., Lienert, S., Maavara, T., MacLeod, M., Millet, D.B., Olin, S., Patra, P.K., Prinn, R.G., Raymond, P.A., Ruiz, D.J., van der Werf, G.R., Vuichard, N., Wang, J., Weiss, R.F., Wells, K.C., Wilson, C., Yang, J., Yao, Y., 2020. A comprehensive quantification of global nitrous oxide sources and sinks. Nature 586, 248–256. https://doi.org/10.1038/s41586-020-2780-0

Tiemeyer, B., Albiac Borraz, E., Augustin, J., Bechtold, M., Beetz, S., Beyer, C., Drösler, M., Ebli, M., Eickenscheidt, T., Fiedler, S., Förster, C., Freibauer, A., Giebels, M., Glatzel, S., Heinichen, J., Hoffmann, M., Höper, H., Jurasinski, G., Leiber-Sauheitl, K., Peichl-Brak, M., Roßkopf, N., Sommer, M., Zeitz, J., 2016. High emissions of greenhouse gases from grasslands on peat and other organic soils. Global Change Biology 22, 4134–4149. https://doi.org/10.1111/gcb.13303

Townsend-Small, A., Ferrara, T.W., Lyon, D.R., Fries, A.E., Lamb, B.K., 2016. Emissions of coalbed and natural gas methane from abandoned oil and gas wells in the United States. Geophysical Research Letters 43, 2283–2290. https://doi.org/10.1002/2015GL067623

Townsend-Small, A., Hoschouer, J., 2021. Direct measurements from shut-in and other abandoned wells in the Permian Basin of Texas indicate some wells are a major source of methane emissions and produced water. Environmental Research Letters. https://doi.org/10.1088/1748-9326/abf06f

Turner, D.B., 1970. Workbook of Atmospheric Dispersion Estimates. Environmental Protection Agency, Office of Air Programs, Research Triangle Park, North Carolina, USA.

Tyner, D.R., Johnson, M.R., 2021. Where the Methane Is – Insights from Novel Airborne LiDAR Measurements Combined with Ground Survey Data. Environmental Science & Technology 55, 9773–9783. https://doi.org/10.1021/acs.est.1c01572

Tyner, D.R., Johnson, M.R., 2018. A Techno-Economic Analysis of Methane Mitigation Potential from Reported Venting at Oil Production Sites in Alberta. Environmental Science & Technology 52, 12877–12885. https://doi.org/10.1021/acs.est.8b01345

Ugbogu, E.A., Elghandour, M.M.M.Y., Ikpeazu, V.O., Buendía, G.R., Molina, O.M., Arunsi, U.O., Emmanuel, O., Salem, A.Z.M., 2019. The potential impacts of dietary plant natural products on the sustainable mitigation of methane emission from livestock farming. Journal of Cleaner Production 213, 915–925. https://doi.org/10.1016/j.jclepro.2018.12.233

UK Government, 2021. COP26: The Negotiations Explained. UN Climate Change Conference UK 2021.

Van Beek, C.L., Pleijter, M., Jacobs, C.M.J., Velthof, G.L., van Groenigen, J.W., Kuikman, P.J., 2010. Emissions of N_2O from fertilized and grazed grassland on organic soil in relation to groundwater level. Nutrient Cycling in Agroecosystems 86, 331–340. https://doi.org/10.1007/s10705-009-9295-2

Van Beek, C.L., Pleijter, M., Kuikman, P.J., 2011. Nitrous oxide emissions from fertilized and unfertilized grasslands on peat soil. Nutrient Cycling in Agroecosystems 89, 453–461. https://doi.org/10.1007/s10705-010-9408-y

Van Houtan, K.S., Tanaka, K.R., Gagné, T.O., Becker, S.L., 2021. The geographic disparity of historical greenhouse emissions and projected climate change. Science Advances 7, eabe4342. https://doi.org/10.1126/sciadv.abe4342

Vogt, J., Laforest, J., Argento, M., Kennedy, S., Bourlon, E., Lavoie, M., Risk, D., 2022. Active and inactive oil and gas sites contribute to methane emissions in western Saskatchewan, Canada. Elementa: Science of the Anthropocene 10, 00014. https://doi.org/10.1525/elementa.2022.00014

von Fischer, J.C., Cooley, D., Chamberlain, S., Gaylord, A., Griebenow, C.J., Hamburg, S.P., Salo, J., Schumacher, R., Theobald, D., Ham, J., 2017. Rapid, Vehicle-Based Identification of Location and Magnitude of Urban Natural Gas Pipeline Leaks. Environ. Sci. Technol. 51, 4091–4099. https://doi.org/10.1021/acs.est.6b06095

Waddington, J.M., Morris, P.J., Kettridge, N., Granath, G., Thompson, D.K., Moore, P.A., 2015. Hydrological feedbacks in northern peatlands. Ecohydrology 8, 113–127. https://doi.org/10.1002/eco.1493

Wallage, Z.E., Holden, J., McDonald, A.T., 2006. Drain blocking: An effective treatment for reducing dissolved organic carbon loss and water discolouration in a drained peatland. Science of The Total Environment 367, 811–821. https://doi.org/10.1016/j.scitotenv.2006.02.010

Wang, M., Wu, J., Lafleur, P.M., Luan, J., 2019. Investigation of the climatological impacts of agricultural management and abandonment on a boreal bog in western Newfoundland, Canada. Science of The Total Environment. https://doi.org/10.1016/j.scitotenv.2019.134632

Wang, M., Wu, J., Lafleur, P.M., Luan, J., Chen, H., Zhu, X., 2018. Can abandoned peatland pasture sequestrate more carbon dioxide from the atmosphere than an adjacent pristine bog in Newfoundland, Canada? Agricultural and Forest Meteorology 248, 91–108. https://doi.org/10.1016/j.agrformet.2017.09.010

Wanninkhof, R., 2014. Relationship between wind speed and gas exchange over the ocean revisited. Limnology and Oceanography: Methods 12, 351–362. https://doi.org/10.4319/lom.2014.12.351

Warner, B.G., Nobes, D.C., Theimer, B.D., 1990. An application of ground penetrating radar to peat stratigraphy of Ellice Swamp, southwestern Ontario. Canadian Journal of Earth Sciences 27, 932–938. https://doi.org/10.1139/e90-096

Wiesenburg, D.A., Guinasso, N.L.Jr., 1979. Equilibrium Solubilities of Methane, Carbon Monoxide, and Hydrogen in Water and Sea Water. Journal of Chemical and Engineering Data 24. https://doi.org/10.1021/je60083a006

Williams, J.P., Regehr, A., Kang, M., 2021. Methane Emissions from Abandoned Oil and Gas Wells in Canada and the United States. Environmental Science & Technology 55, 563–570. https://doi.org/10.1021/acs.est.0c04265

Williams, J.P., Risk, D., Marshall, A., Nickerson, N., Martell, A., Creelman, C., Grace, M., Wach, G., 2019. Methane emissions from abandoned coal and oil and gas developments in New Brunswick and Nova Scotia. Environmental Monitoring and Assessment 191, 1–12. https://doi.org/10.1007/s10661-019-7602-1

Wood, J.M., Euzen, T., Sharp, L., Leroux, S., 2021. Phase separation and secondary migration of methane-rich gas accompanying uplift of an unconventional tight-hydrocarbon system, Montney Formation, western Canada. Marine and Petroleum Geology 124, 104808. https://doi.org/10.1016/j.marpetgeo.2020.104808

Wood, S.N., 2011. Fast stable restricted maximum likelihood and marginal likelihood estimation of semiparametric generalized linear models. Journal of the Royal Statistical Society 73, 3–36.

Wösten, J.H.M., Ismail, A.B., Wijk, A.L.M.V., 1997. Peat subsidence and its practical implications: a case study in Malaysia. Geoderma 78, 25–36. https://doi.org/10.1016/S0016-7061(97)00013-X

Wu, Y.S., Hannah, C.G., Petrie, B., Pettipas, R., Peterson, I., Prinsenberg, S., Lee, C., Moritz, R., 2013. Ocean current and sea ice statistics for Davis Strait. Fisheries and Oceans Canada.

Xia, T., Catalan, J., Hu, C., Batterman, S., 2020. Development of a mobile platform for monitoring gaseous, particulate, and greenhouse gas (GHG) pollutants. Environ Monit Assess 193, 7. https://doi.org/10.1007/s10661-020-08769-2

Xu, L., Lin, X., Amen, J., Welding, K., McDermitt, D., 2014. Impact of changes in barometric pressure on landfill methane emission. Global Biogeochemical Cycles 28, 679–695. https://doi.org/10.1002/2013GB004571

Yacovitch, T.I., Herndon, S.C., Pétron, G., Kofler, J., Lyon, D., Zahniser, M.S., Kolb, C.E., 2015. Mobile Laboratory Observations of Methane Emissions in the Barnett Shale Region. Environmental Science & Technology 49, 7889–7895. https://doi.org/10.1021/es506352j

Zaman, M., Kleineidam, K., Bakken, L., Berendt, J., Bracken, C., Butterbach-Bahl, K., Cai, Z., Chang, S.X., Clough, T., Dawar, K., Ding, W.X., Dörsch, P., dos Reis Martins, M., Eckhardt, C., Fiedler, S., Frosch, T., Goopy, J., Görres, C.-M., Gupta, A., Henjes, S., Hofmann, M.E.G., Horn, M.A., Jahangir, M.M.R., Jansen-Willems, A., Lenhart, K., Heng, L., Lewicka-Szczebak, D., Lucic, G., Merbold, L., Mohn, J., Molstad, L., Moser, G., Murphy, P., Sanz-Cobena, A., Šimek, M., Urquiaga, S., Well, R., Wrage-Mönnig, N., Zaman, S., Zhang, J., Müller, C., 2021. Micrometeorological Methods for Greenhouse Gas Measurement, in: Zaman, Mohammad, Heng, Lee, Müller, Christoph (Eds.), Measuring Emission of Agricultural Greenhouse Gases and Developing Mitigation Options Using Nuclear and Related Techniques: Applications of Nuclear Techniques for GHGs. Springer International Publishing, Cham, pp. 141–150. https://doi.org/10.1007/978-3-030-55396-8_4

Zavala-Araiza, D., Herndon, S.C., Roscioli, J.R., Yacovitch, T.I., Johnson, M.R., Tyner, D.R., Omara, M., Knighton, B., 2018. Methane emissions from oil and gas production sites in Alberta, Canada. Elementa: Science of the Anthropocene 6, 27. https://doi.org/10.1525/elementa.284

Zeiss, C.A., 2006. Accelerated methane oxidation cover system to reduce greenhouse gas emissions from MSW landfills in cold, semi-arid regions. Water, Air, and Soil Pollution 176, 285–306. https://doi.org/10.1007/s11270-006-9169-z

Zhao, Y., Booge, D., Marandino, C.A., Schlundt, C., Bracher, A., Atlas, E.L., Williams, J., Bange, H.W., 2022. Dimethylated sulfur compounds in the Peruvian upwelling system. Biogeosciences 19, 701–714. https://doi.org/10.5194/bg-19-701-2022

Appendix A: Sea-air methane flux estimates derived from marine surface observations and instantaneous atmospheric measurements in the northern Labrador Sea and Baffin Bay

A.1 Figures

Figure 30: The measurement tower at the bow of the ship with anemometer, temperature sensor, and air inlet mounted on the truss approximately where the arrow is pointing. The GPS was fixed at the lower end of the truss. Photo credit to David Cote (DFO, Canada).

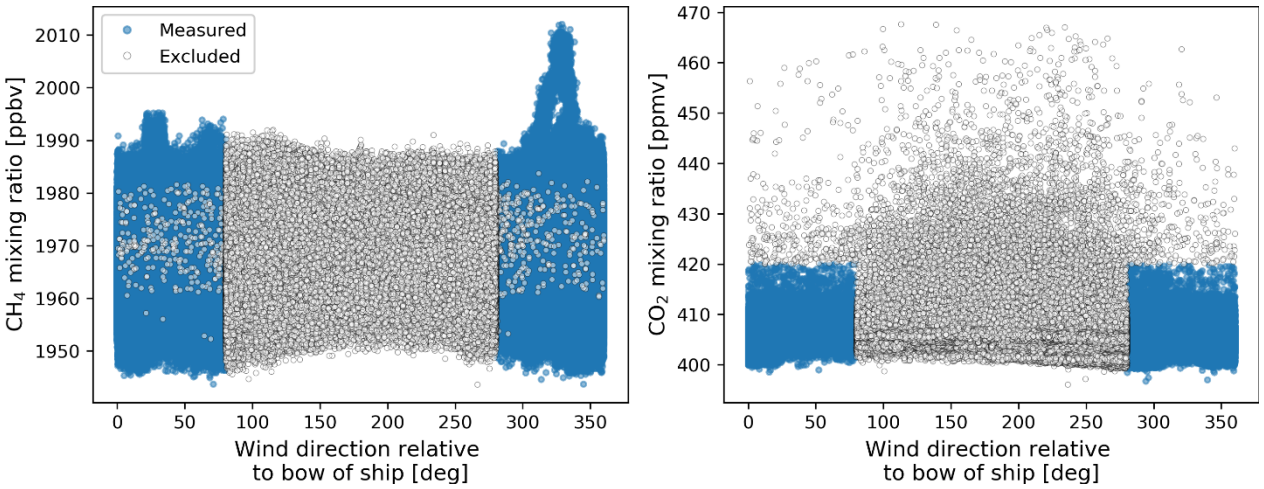

Figure 31: Gas mixing ratios throughout the cruise for wind directions relative to the bow of the ship are shown. All data represented by open circles fulfil the criterion for measurements potentially contaminated by the ship's exhaust (wind directions between 80−280° or CO_2 mixing ratios < 420 ppm) amounting to 26 % of all measured 1 Hz data.

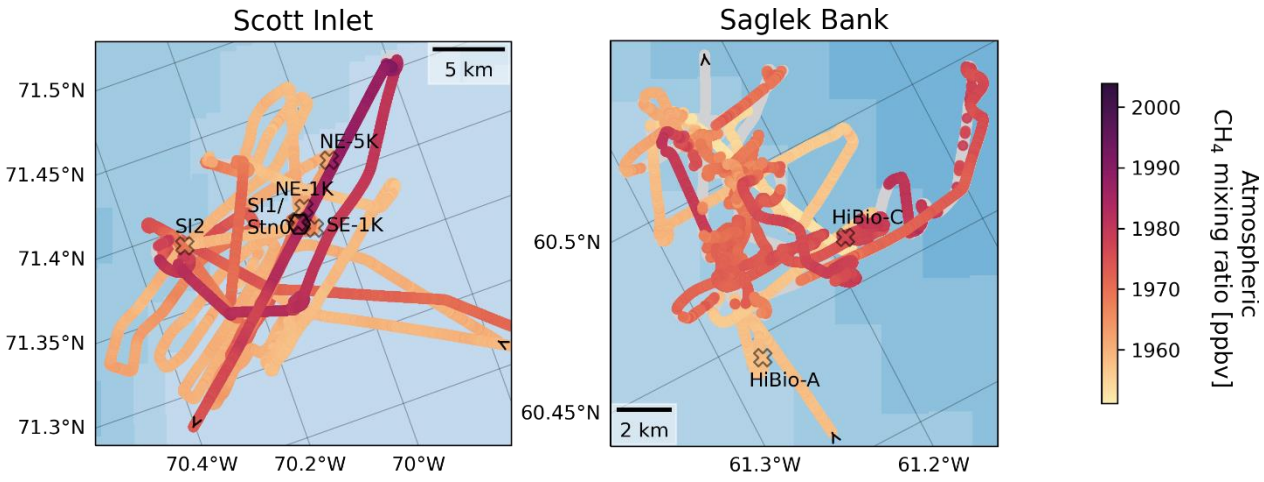

Figure 32: Close-up of Scott Inlet and Saglek Bank, where multiple water measurements were taken. The locations of CTD-Rosette sampling are indicated together with the respective names of stations. The arrows indicate the direction where the ship was heading. Stations SI1 and Stn0 were co-located at the Scott Inlet seep (black hexagon, left panel). Gray circles indicate measurements excluded due to the ship's contamination.

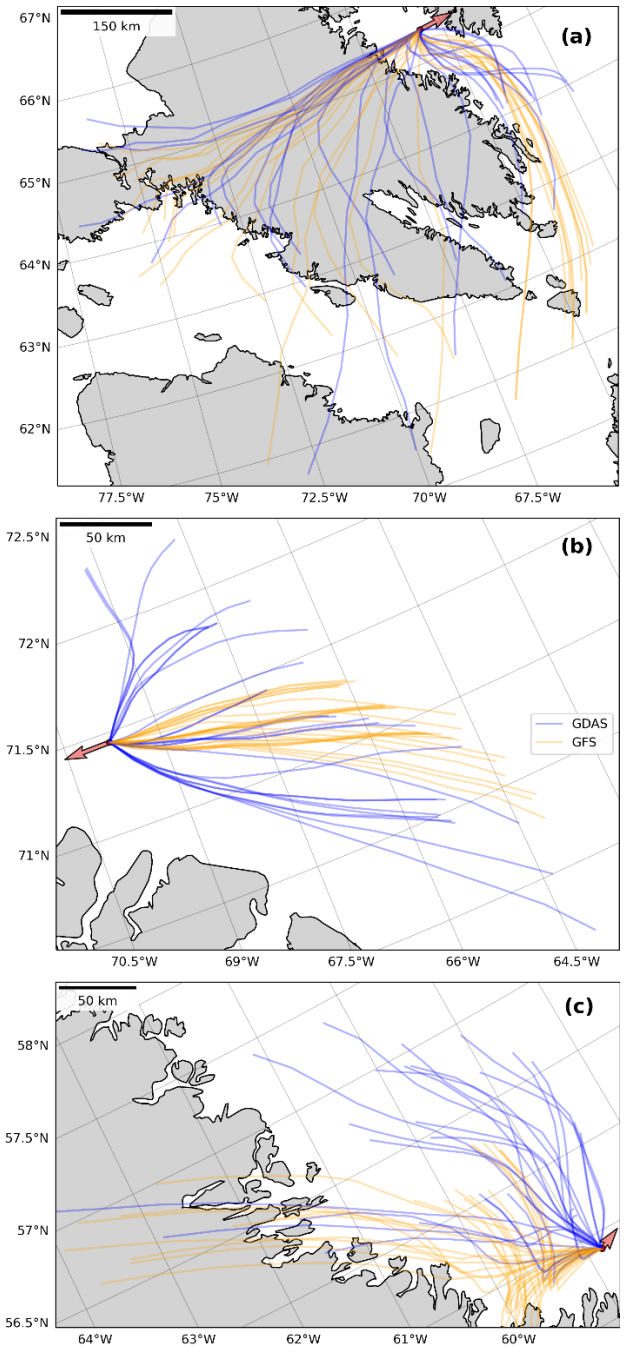

Figure 33: Back-trajectories of air masses approaching the locations where highest atmospheric CH_4 levels were measured in the Cumberland Sound (a), at Scott Inlet (b) and in the Labrador Sea (c). Orange lines represent trajectories using the GFS archive and blue lines show trajectories with the GDAS meteorological model. Red arrows indicate the direction of air movement averaged over five minutes before and after the time of sampling, pointing in the direction the wind is blowing to.

A.2 Flux estimates

To determine the sea-air fluxes, the wind profile power law following Hsu et al. (1994) was used to correct wind speeds in m s^{-1} from the anemometer at 14.1 m height above sea level to 10 m height:

$$u_{10} = u_{14.1} \frac{10}{14.1}^{0.11}.$$

Furthermore, the Schmidt number for CH_4 in sea water following the example of Manning and Nicholson (2022) based on Jähne et al. (1987) was incorporated:

$$Sc = \frac{\mu_w}{D_w},$$

with the kinematic viscosity of seawater (Manning and Nicholson, 2022):

$$\mu_w = 0.0001 \cdot (17.91 - 0.5381 \cdot T_w + 0.00694 \cdot {T_w}^2 + 0.02305 \cdot S_w) \cdot \frac{1}{\rho_w},$$

the water temperature (T_w) in °C, salinity (S_w) in psu as measured by the CTD, and density at atmospheric pressure (ρ_w) in kg m^{-3} (Fofonoff and Millard, 1983; Millero and Poisson, 1981).

The diffusion coefficient (D_w) in m^2/s was determined following Manning and Nicholson (2022) and based on Jähne et al. (1987):

$$D_w = 3.0470 \cdot 10^{-6} \cdot e^{\frac{-18360}{R \cdot (T_w + 273.15)}} \cdot (1 - 0.049 \cdot S_w / 35.5),$$

using the ideal gas constant $R = 8.314510 \frac{kg\ m^2}{s^2\ K\ mol}$.

Appendix B: Active and inactive oil and gas sites contribute to methane emissions in western Saskatchewan, Canada

B.1 Setup and instrument details

The inlet for the gas analyzer was located on the top of the roof, 2.55 m above the ground mounted on a fixed mast, together with the anemometer and compass (Figure 34). The anemometer and compass were both oriented facing the front of the truck. The motion-induced wind was removed using compass and GPS data to obtain true wind parameters. The compass was calibrated for local conditions each day as soon as all instruments were running to eliminate magnetic interference. The gas analyzer was calibrated in January 2020 and benchmarked daily. The gas samples were pumped through sample tubing from the inlet to the analyzer. In order to account for the time lag, we conducted a breath test on a daily basis and recorded the time the gas sample took from the inlet to the analyzer (approx. 10 s).

Figure 34: The mobile laboratory. Snapshot of the truck during a stationary measurement in the Kindersley area.

B.2 Geolocations of oil and gas infrastructure

The three surveyed areas were each composed of thousands of single pieces of infrastructure. Geolocations, stati and production type of respective oil and gas wells were retrieved from AccuMap®, an IHS Markit product. Locations of facilities like storage tanks, pneumatic sheds etc. were extracted from a GIS database provided by IHS Markit. Since measured emissions were attributed to local oil and gas infrastructure, the accuracy of their geolocations was important for our approach. Geolocations of wells and facilities were provided by different vendors, and after visual inspection we deemed well geolocations accurate, while some provided facility geolocations deviated from actual locations. Thus, we improved geolocations of single-well batteries within the same dominion land survey as the associated oil or gas well by attributing the well geolocation to the facility geolocation. Upon subsequent visual inspection, we confirmed that the reattributed geolocations were improved.

Since we observed several unlit flare stacks as emitting culprits in the field, we also complemented our infrastructure database with flare stack positions from provincial emission reports associated with flaring, and attributed respective geolocations of facilities to the flare stacks. That way, we carefully assembled a comprehensive infrastructure database from different sources with improved geolocations.

B.3 Surveyed routes and areas with enriched CH_4 concentrations

In the Swift Current area, we surveyed 438 km, 835 km in Kindersley and 718 km in Lloydminster. The driven routes and obtained excess CH_4 concentrations (above background) are shown in Figure 35 and Figure 36. Excess CH_4 concentrations reached a maximum of 3.4 ppmv in Swift Current, 9.3 ppmv in Kindersley and 5.6 ppmv in Lloydminster.

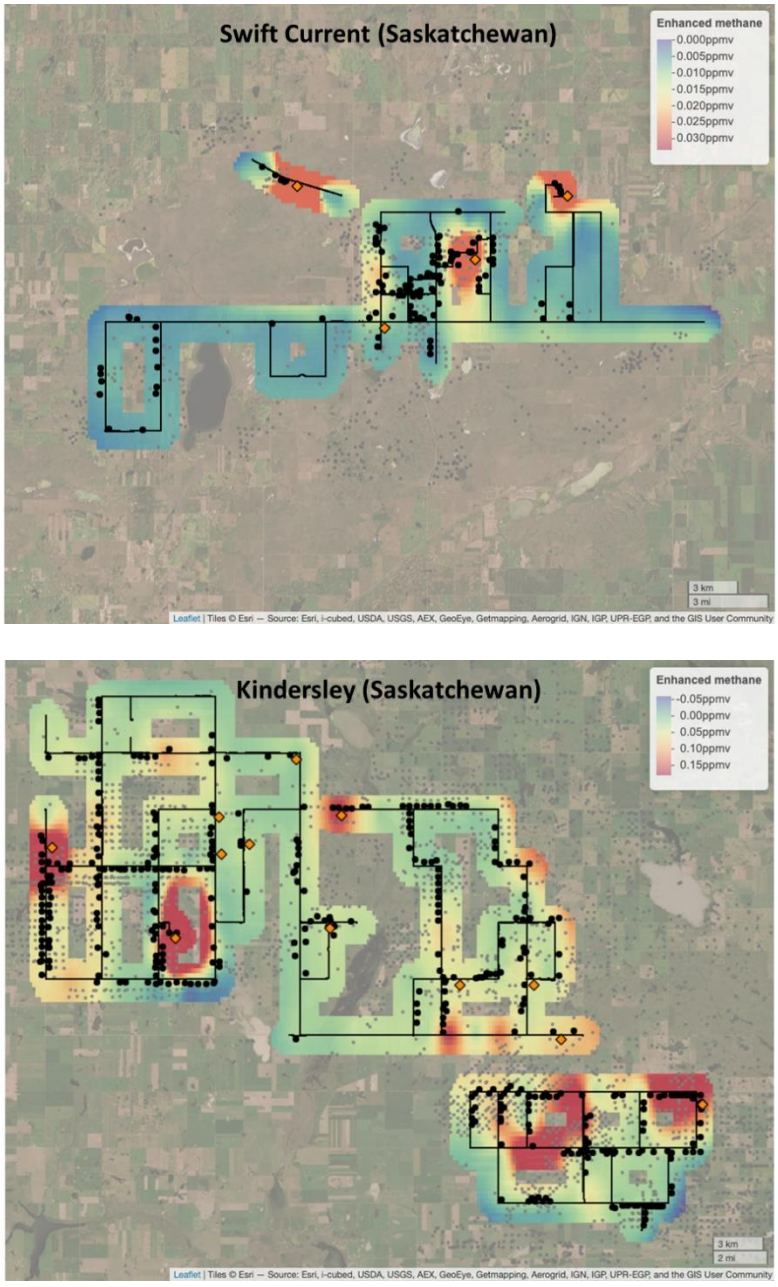

Figure 35: Surveyed routes in the studied areas. Driven routes (black lines) in the Swift Current and Kindersley area in Saskatchewan, Canada. Gray dots represent present oil and gas infrastructure, black dots sampled infrastructure. Orange diamonds show the location of the truck during stationary CH_4 measurements (Other Test Method 33A, short: OTM). Elevated atmospheric CH_4 concentrations in ppmv above background (eCH_4) as shown in the maps were interpolated via averaging eCH_4 over 0.02 x 0.02° grids and resampling over 0.0025°.

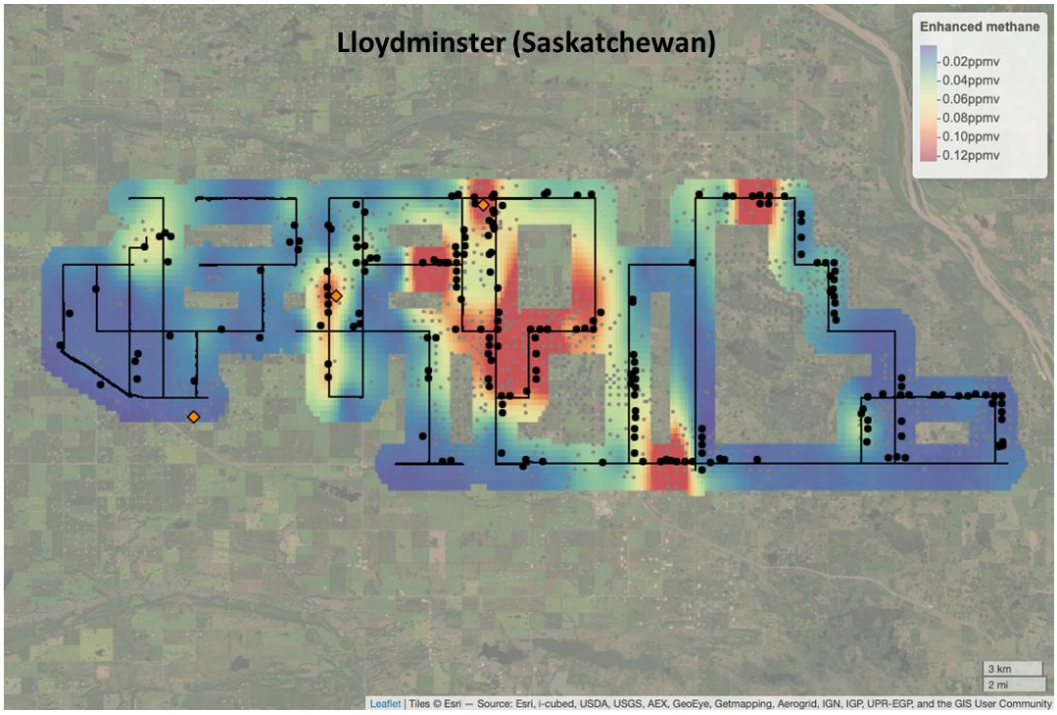

Figure 36: Surveyed routes in Lloydminster, Saskatchewan. Same as for Figure 35.

B.4 *In situ* evidence of CH_4 leaks and vents

In order to confirm high emitters during mobile surveys and to find a suitable location for stationary CH_4 measurements (OTMs), we took optical gas images of the emitting infrastructure as evidence for CH_4 leaks and vents (Figure 37).

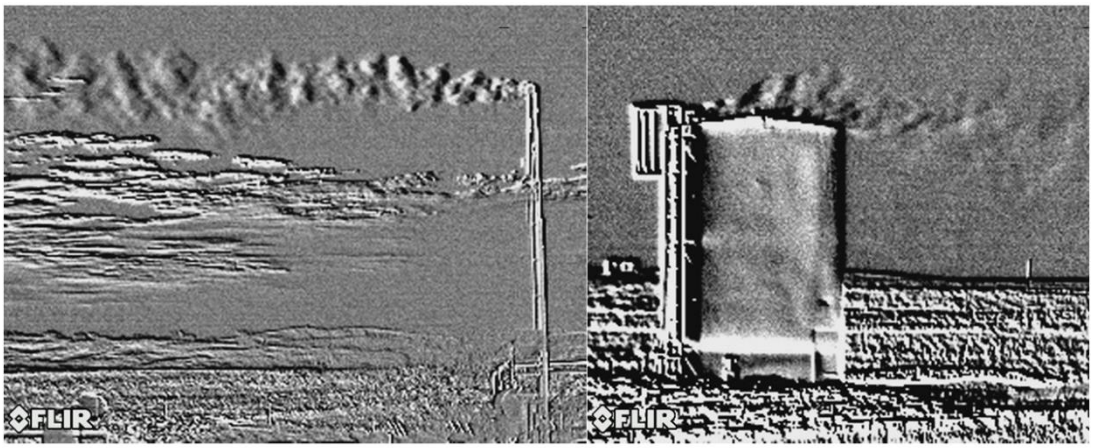

Figure 37: Optical gas images taken with a forward-looking infrared camera. The images show CH_4 plumes from an unlit flare in Swift Current and a venting tank in Kindersley (also shown in Figure 34).

B.5 Oil and gas production history

The oil and gas production in the surveyed areas in the past years has partially experienced a slightly decreasing trend and was substantially affected by the COVID-19 pandemic in early 2020. By the time we surveyed the three regions, the oil and gas production rates had mostly recovered from impacts of the pandemic. The number of producing wells has been diminishing particularly in Kindersley and Lloydminster since 2018 (Figure 38).

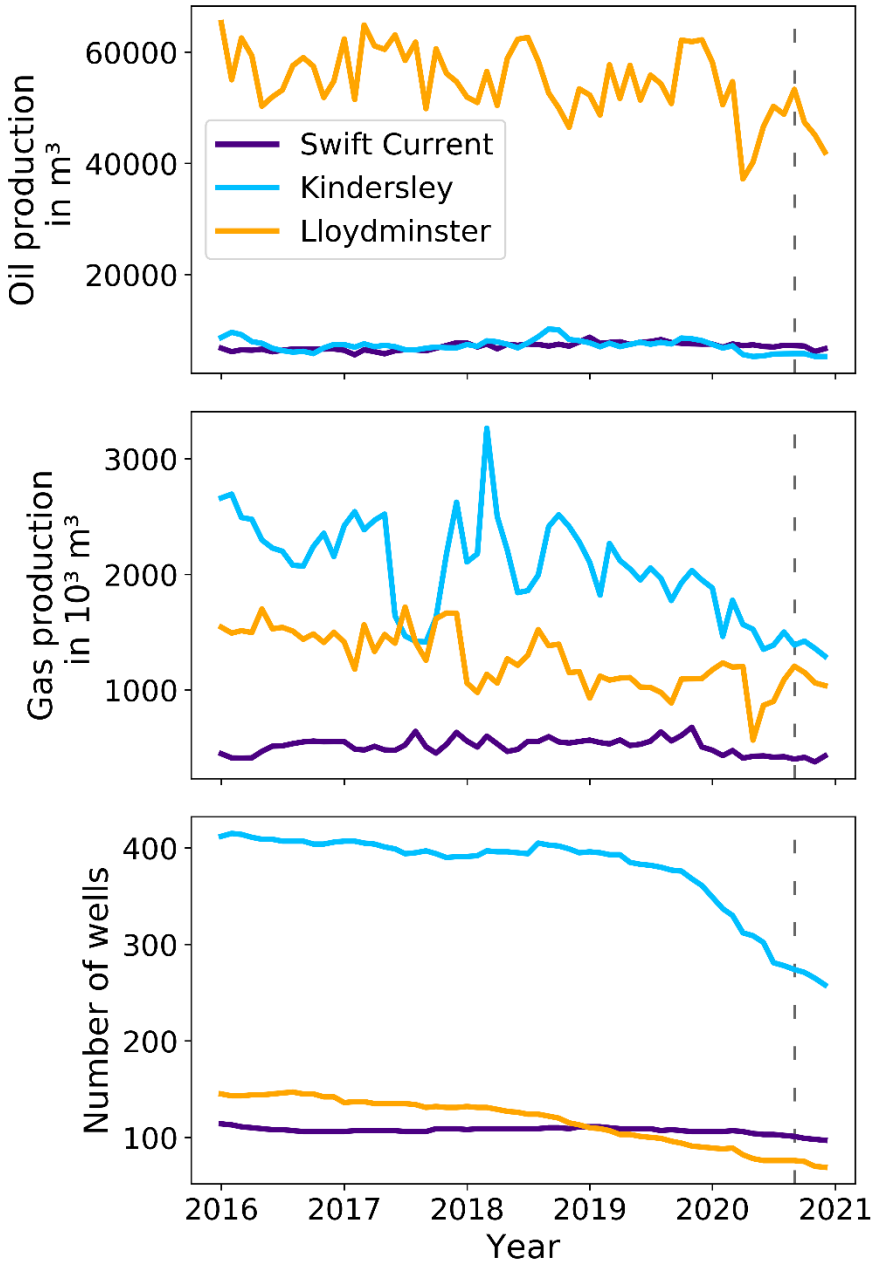

Figure 38: Production history of wells. Total monthly oil and gas production history of wells that were sampled during mobile surveys, and the number of producing wells in Swift Current, Kindersley and Lloydminster from 2016 to 2020. The dashed vertical line shows the month we conducted measurements in the studied areas in September 2020.

B.6 Infrastructure types of sampled and emitting sites

CH_4 emissions can vary by fluid produced and by region (MacKay et al., 2021). Generally, most wells we surveyed produced oil, and accordingly most emitting wells were oil wells (Figure 39). The majority of sampled and emitting facilities were crude oil single-well batteries (in Swift Current and Kindersley) and heavy crude oil single-well batteries (in Lloydminster). Figure 41 shows per-facility emission factors based on the September 2020 report obtained from the Government of Saskatchewan. In Swift Current, highest emissions originated from gas plants and gas single well batteries, which we did not sample in Swift Current (Figure 40). Likewise, we sampled little to no crude oil multiwell proration or thermal in-situ batteries in Kindersley, which showed highest emissions according to the provincial report. However, in Lloydminster, we were able to capture a few of the highest emitting facilities, namely heavy crude oil paper, thermal in-situ and heavy crude oil multiwell proration batteries during surveys. This partially explains the deviation of our measured CH_4 emission rate estimates and reported emissions. Nonetheless, heavy crude oil single-well batteries, the facility type sampled most during our surveys in Lloydminster were among the highest emitters according to emission reports, as well as crude oil single-well batteries which were most abundant in our Kindersley and Swift Current surveys.

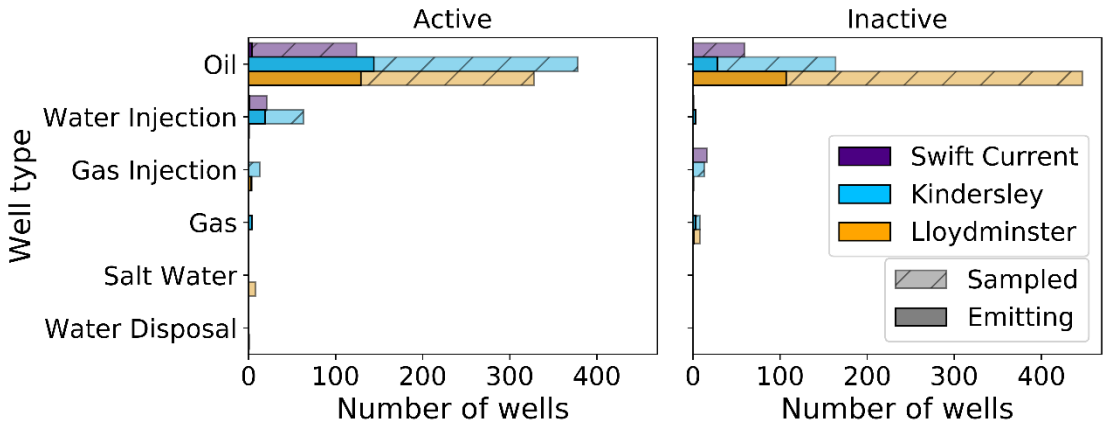

Figure 39: Well characteristics. Number of sampled and emitting wells associated with different types of fluids in each region divided into active and inactive infrastructure groups.

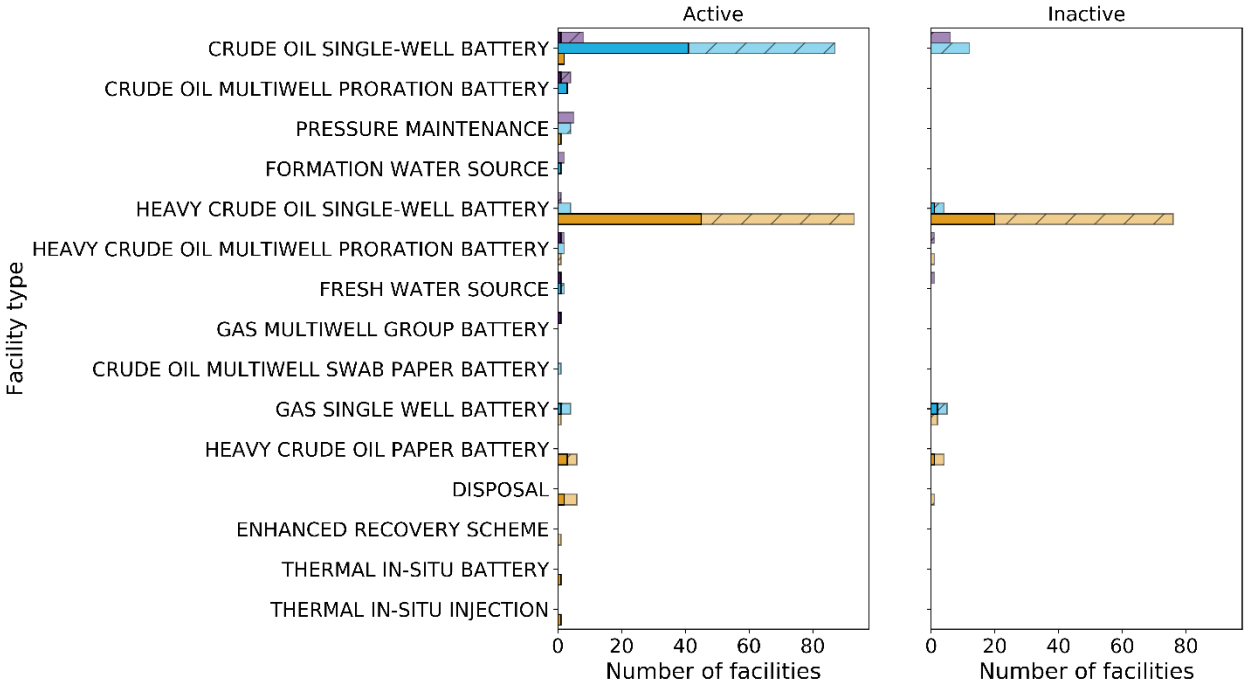

Figure 40: Facility characteristics. Type and number of sampled and emitting facilities in each region divided into active and inactive infrastructure groups. The same legend as in Figure 39 applies.

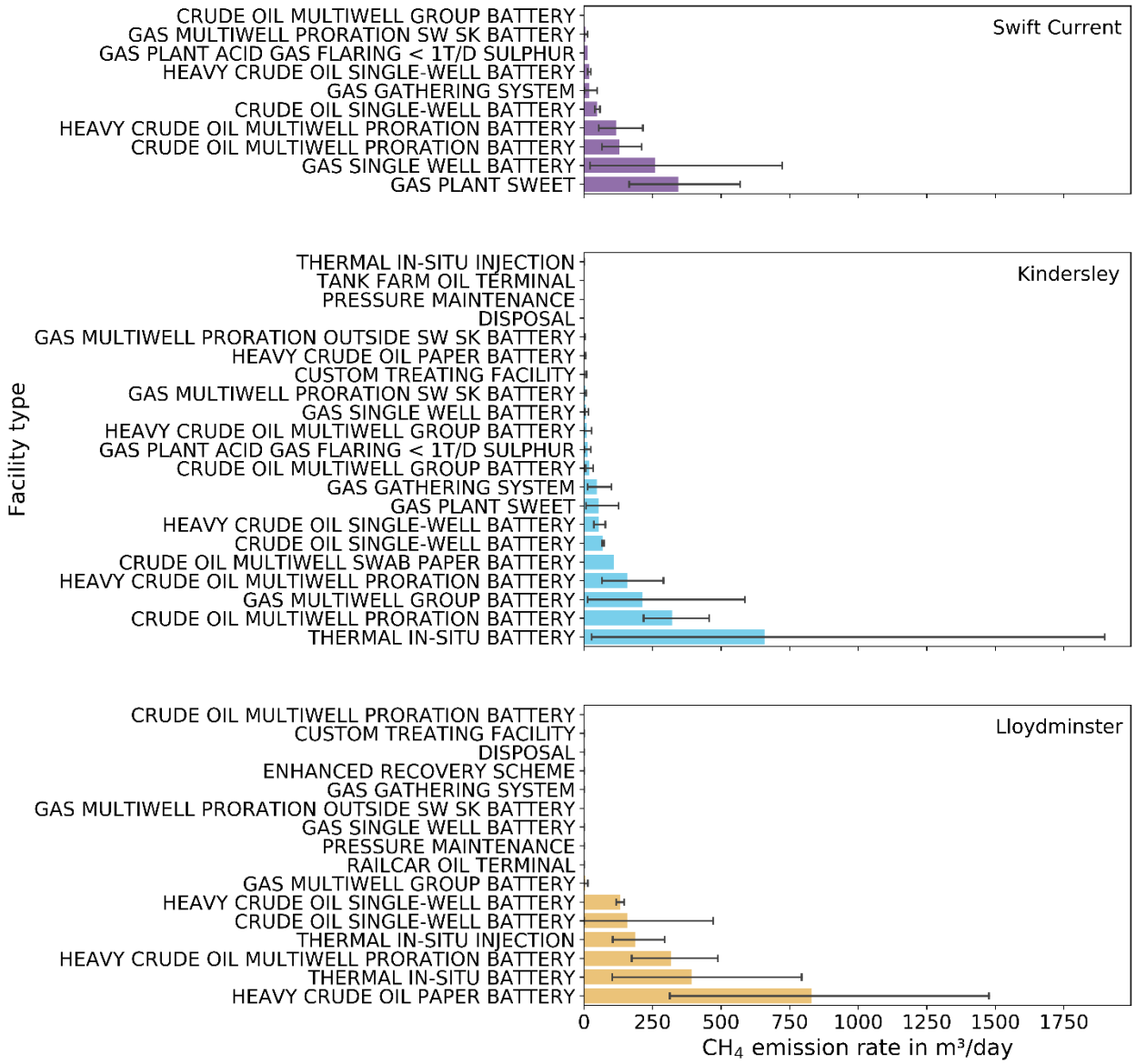

Figure 41: Emission factors of facility types. Reported CH_4 emissions per facility type in each area based on the monthly report of September 2020. The bars show mean per-facility emissions with errorbars representing the 95% confidence interval. Some facility types did not emit CH_4 following the provincial report.

Appendix C: Cross-sector comparison of methane emissions from anthropogenic sources: A case study in Canada

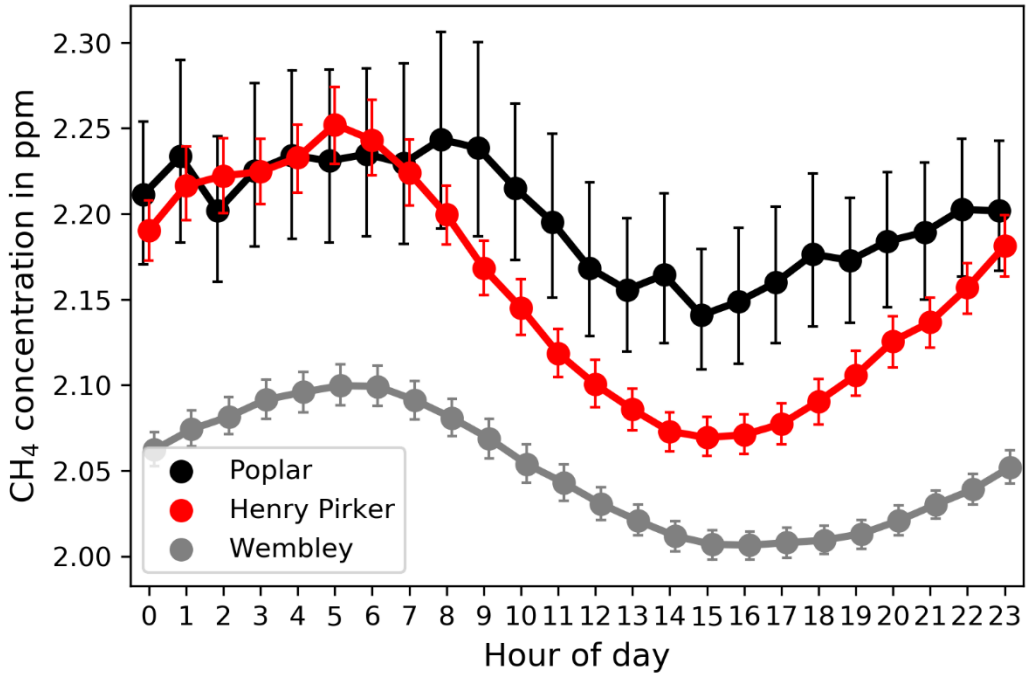

Figure 42: Daily variation of hourly averaged CH_4 concentrations at three airshed stations in the Grande Prairie region, Alberta, Canada. Averages were taken over different periods for each station (Poplar: October 2021−January 2022, Henry Pirker: October 2018−October 2021, Wembley: October 2018−September 2021). The points indicate mean concentrations, error bars show the bootstrapped 95% confidence interval. Note that measurements were taken at different times and cannot be directly compared among stations based on this figure.

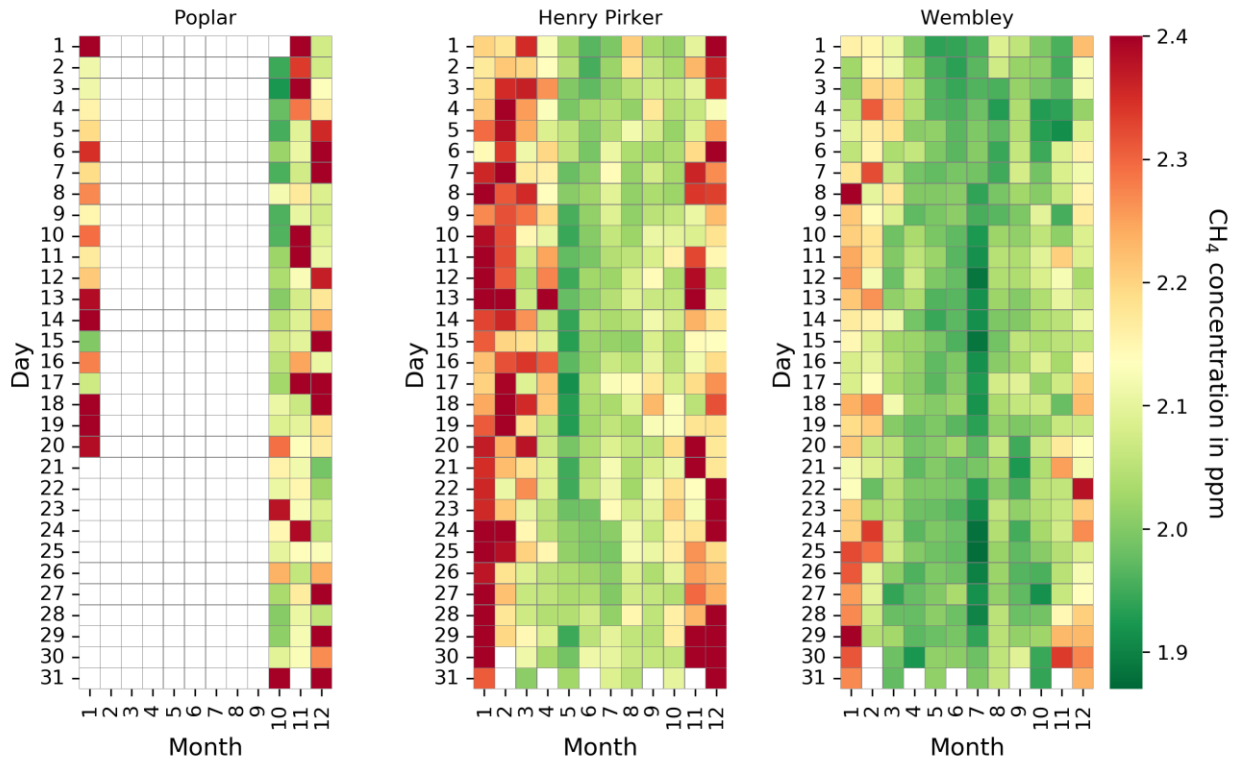

Figure 43: Daily mean CH_4 concentrations at three airshed stations in the Grande Prairie region, Alberta, Canada throughout the year. Wherever several years of data were available (Poplar: October 2021−January 2022, Henry Pirker: October 2018−October 2021, Wembley: October 2018−September 2021), daily data was averaged over years (for Henry Pirker and Wembley). White squares indicate missing data (or months with less than 31 days).